# JRC TECHNICAL REPORTS

# JRC - Ispra
# Atmosphere – Biosphere – Climate
# Integrated monitoring Station

*2016 Report*

J.P. Putaud, P. Bergamaschi, F. Cavalli, A. Dell'Acqua, K. Douglas, I. Goded, F. Grassi, C. Gruening, N.R. Jensen, F. Lagler, G. Manca, S. Martins Dos Santos, M. Matteucci, R. Passarella, V. Pedroni, O. Pokorska.

2018

EUR 28974 EN

How to cite this report: Putaud, J.P., Bergamaschi, P., Cavalli, F., Dell'Acqua, A., Douglas, K., Goded, I., Grassi, F., Gruening, C., Jensen, N.R., Lagler, F., Manca, G., Martins Dos Santos, S., Matteucci, M., Passarella, R., Pedroni, V., Pokorska, O., *JRC-Ispra Atmosphere – Biosphere – Climate Integrated monitoring Station: 2016 report*, EUR 28974 EN, Publications Office of the European Union, Luxembourg, 2018, ISBN 978-92-79-77198-9, doi:10.2760/453600, JRC109424.


All images © European Union 2018, except: *Fig. 1 (background from Google Earth), Fig. 14 (EMEP), Fig. 18 (Thermo Scientific), Fig. 55 (Gill Instruments), Fig. 56 (LI-COR), Fig. 57 (Wikipedia), and Fig. 58 (*Schlumberger Water Services*).*

# Contents

# Abstract

A comprehensive set of essential atmospheric variables have been measured at the JRC-Ispra Atmosphere - Biosphere - Climate Integrated monitoring Station (ABC-IS) for several years to assess the impact of European policies and international conventions on air pollution and climate forcing. The variables we measure at the Atmospheric Observatory in Ispra include greenhouse gas concentrations ($CO_2$, $CH_4$, $N_2O$, $SF_6$), radon ($^{222}Rn$) activity concentration, short-lived gaseous and particulate pollutant (CO, $SO_2$, NO, $NO_2$, $O_3$, $PM_{2.5}$ and its main ionic and carbonaceous constituents) concentrations, atmospheric particle micro-physical characteristics (number concentration and size distribution) and optical properties (light scattering and absorption in-situ, light scattering and extinction vertical profiles remotely), eutrophying and acidifying species ($SO_4^{2-}$, $NO_3^-$, $NH_4^+$) wet deposition. On-line measurements data are available in real time at http://abc-is.jrc.ec.europa.eu/. Vegetation ⇆ atmosphere exchanges ($CO_2$, $O_3$, $H_2O$ and heat) are measured at our Forest Flux Station of San Rossore, backed up by meteorological and pedological measurements. All the measurements performed at ABC-IS are made under international projects and programs including ICOS (Integrated Carbon Observation System), ACTRIS (Aerosols, Clouds and Trace gases Research Infra-Structure), EMEP (co-operative Program for Monitoring and Evaluation of the long range transmission of air pollutants in Europe) and GAW (Global Atmosphere Watch), which implies the use of standard methods and scales, and the participation in quality assurance activities. The JRC has a leading role in ACTRIS and EMEP regarding the quality assurance for carbonaceous aerosol measurements. All the data obtained at ABC-IS are submitted to international open data bases (www.europe-fluxdata.eu, fluxnet.ornl.gov, www.ingos-infrastructure.eu, ebas.nilu.no) and can be freely downloaded from these web sites. The data we produce are used in European wide assessments, for model inputs and validation, and for calibrating satellite airborne sensors. The ABC-IS 2016 report presents the data produced during the past year in the context of the previous years of measurements.

All the essential in-situ and remote sensing measurements scheduled for 2016 were regularly performed across the year, except for short periods of calibration, preventive and corrective maintenance.

Greenhouse gas (GHG) measurements have been performed at the JRC Ispra site since October 2007. Minimum values of $CH_4$, $N_2O$ and $SF_6$ measured in Ispra under clean air conditions are close to marine background values, while $CO_2$ mixing ratios can even be lower than the Mace Head baseline due to the continental biospheric $CO_2$ sink. Deviations from baseline concentrations provide information about regional and larger scale European greenhouse gas sources. From our daytime measurements, we derived increasing trends in $CO_2$ ($+0.9\%$ $yr^{-1}$) and $CH_4$ ($+0.4\%$ $yr^{-1}$) over the past 9 years, and in $N_2O$ ($+0.3\%$ $yr^{-1}$) over the past 6 years. GHG measurements from the 100 m high tower of our new Atmospheric Observatory in Ispra started in December 2016.

The concentrations of most short-lived pollutants monitored at the JRC-Ispra station (CO, $NO_2$, $O_3$, atmospheric particulate matter) have decreased in 2016 compared to 2015 by about 10 to 15%. This can be at least in part explained by the weather conditions, 2016 being normally wet (except in January and December), while 2015 was exceptionally dry. Only $SO_2$ concentrations increased slightly ($\sim$+10%), but still remained far below limit values. In contrast, $SO_4^{2-}$ wet deposition decreased (-25%), while wet deposition of $NH_4^+$ increased (+10%), giving rise to a very limited number (3) of acid rain events in 2016. In general, 2016 did not break the general decreasing trend in atmospheric pollution observed in Ispra since 1986. A noticeable exception regards ozone ($O_3$), whose concentrations have remained relatively high in 2016. The indicators for health and ecosystem safeguard have deteriorated since 2012 (2014 excluded) compared to the 2000's. It would be worth studying the geographical extent of this tendency across Europe to understand its origin.

The decreasing trend in particulate matter mass concentrations observed over the past 3 decades have been accompanied with a decrease in ultra-fine particle number between 2004 and 2013, but no longer since then. It has also led to a decrease in visible light scattering by the atmospheric particles, but not that much in light absorption. This implies that the negative radiative forcing (climate cooling) of atmospheric particles is getting smaller and smaller in our area. Determining the climate effect of the aerosol remains a big challenge and further investment would be needed in this field.

The atmosphere $\leftrightarrows$ vegetation exchange measurements at our forest flux station of San Rossore show that the pine tree forest is a net sink for $CO_2$ (530 gC/m² absorbed in 2016). The different meteorological conditions prevailing in 2016 (wetter) compared to 2015 (dryer) allowed us to observe that the carbon sequestration by this Mediterranean forest was 5% greater during the dryer year than the wetter year.

# 1 Introduction

The mission of the Atmosphere-Biosphere-Climate Integrated monitoring Station (ABC-IS) is to measure changes in atmospheric variables to obtain data that are essential for the conception, development, implementation and monitoring of the impact of European policies and International conventions on air pollution and climate change. Measurements include greenhouse gas concentrations, forest ⇆ atmosphere fluxes, and concentrations of pollutants in the gas phase, particulate matter and precipitations, as well as aerosol micro-physical and optical characteristics. Most measurements are performed at the JRC-Ispra site (Fig. 1), and some at the typical Mediterranean site of San Rossore site (Fig. 51). The goal of ABC-IS is to establish real world interactions between air pollution, climate change and the biosphere, highlighting possible trade-offs and synergies between air pollution and climate change policies. Possible interactions include the role of pollutants in climate forcing and $CO_2$ uptake by vegetation, the impact of climate change and air pollution on $CO_2$ uptake by vegetation, the effect of biogenic emission on air pollution and climate forcing, etc…
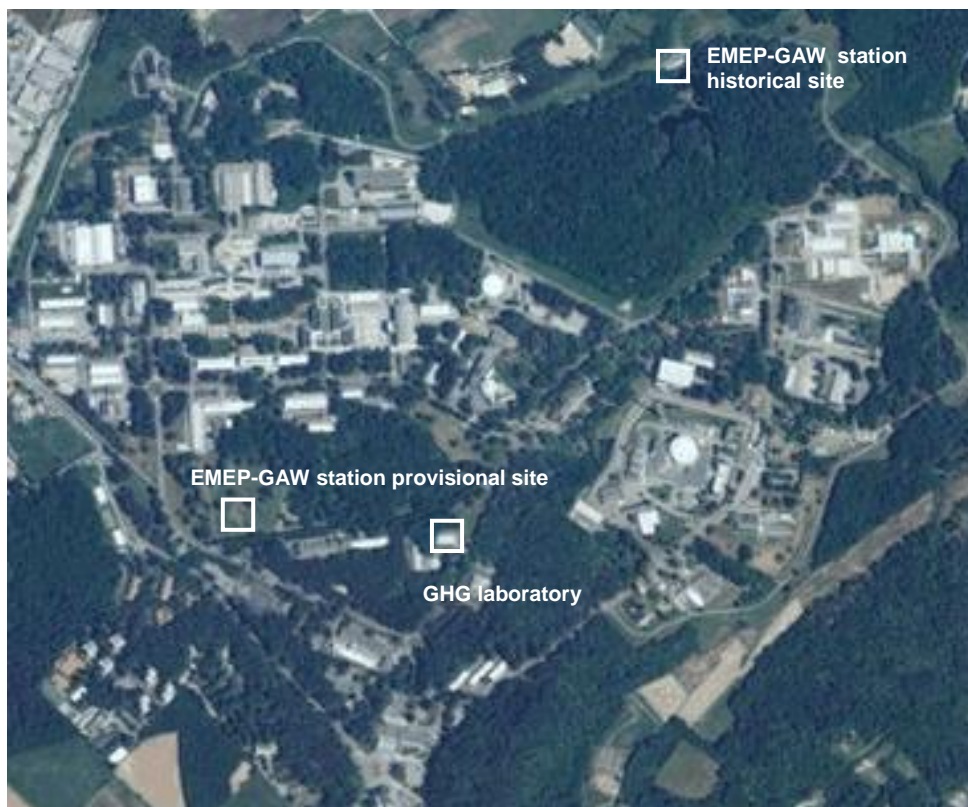


*Fig. 1: The JRC-Ispra site and the location of the laboratory for greenhouse gas measurements, the historical and the provisional EMEP-GAW station sites.*

Measurements are performed in the framework of international monitoring programs like the European Research Infrastructure Consortium project ICOS (Integrated Carbon Observation System), EMEP (Co-operative program for monitoring and evaluation of the long range transmission of air pollutants in Europe of the UN-ECE *Convention on Long-Range Transboundary Air Pollution* CLRTAP) and GAW (the Global Atmosphere Watch program of the World Meteorological Organization). The ABC-IS infrastructure has also been used in competitive projects (e.g. ACTRIS, InGOS).

Through the participation of ABC-IS in international networks, inter-laboratory comparisons are conducted and standard methods are developed within the European Reference Laboratory for Air Pollution of the JRC Air and Climate Unit.

## 2  Quality management system

ABC-IS is a research infrastructure of JRC's *Directorate for Energy, Transport and Climate*.

We achieved ISO 9001 re-certification in June 2013, which is also valid for the year 2016 (ISO 9001 is mainly about "project management"). In addition, external and internal ISO 9001 audits were also performed successfully in 2016.

In addition, JRC Ispra also achieved in Nov. 2010 the ISO 14001 certificate (ISO 14001 is mainly about "environmental issues"), which is valid for several years. An audit also took place in 2015.

For information (the links below being accessible to JRC staff only), the "quality management system (QMS) for the ABC-IS regional station" includes server space at the following links:

\\ies.jrc.it\H02\H02QMS\_year_2016_

\\ies.jrc.it\H02\LargeFacilities\ABC-IS\

\\ies.jrc.it\H02\Laboratories

\\ies.jrc.it\H02\Laboratories\LifeCycleSheets

where the following information can be found: list of instruments; information about calibrations; standards used and maintenance; standard operational procedures (SOP's); instrument lifecycle sheets and log-books; manuals for the instruments; *etc.* For additional specific details about QMS, for the year 2016 and the ABC-IS station, see e.g. the file 2016_Instruments'_calibration_&_standards_&_maintenance.xls, that can be found under \\ies.jrc.it\H02\LargeFacilities\ABC-IS\Quality_management.

More QMS information/details can also be found in the sections "Measurement techniques" in this report.

More general QMS information/documentations about how the AC Unit (H02/C5) was run in 2016, the management of all of the projects within the Unit and the running of the ABC-IS station can also be found at

\\ies.jrc.it\h02\H02QMS\_year_2016_\1_UNIT\QMS_info\QMS_documents_H02

\\ies.jrc.it\h02\H02QMS\_year_2017_\1_Unit\QMS_info\QMS_documents_and_Unit

and especially in the seven C5 Unit QMS documents listed here (latest versions):

QMS_DIR_C_C5_Quality_Unit_Management_Manual_v12_0.pdf

QMS_C5_MANPROJ_PROJ_Laboratory_Management_v11_0.pdf

QMS_C5_MANPROJ_PROJ_Model_Management_v11_0.pdf

QMS_C5_MANPROJ_PROJ_Informatics_Management_v11_0.pdf

QMS_C5_MANPROJ_PROJ_Knowledge_Management_v11_0.pdf

QMS_C5_MANPROJ_PROJ_Review_Verification_Validation_Approval_v7_0.pdf

QMS_C5_MANPROJ_PROJ_Administration_Implementation_v6_0.pdf

The latest versions of these documents are available at:

\\ies.jrc.it\H02\H02QMS\_year_2017_\1_UNIT\QMS_info\QMS_documents_and_Unit.

*Fig. 2: (a) Laboratory for atmospheric GHG measurements at Building 5 with 15m mast, (b) new JRC Atmospheric Observatory with 100m tower (Building 77r)*
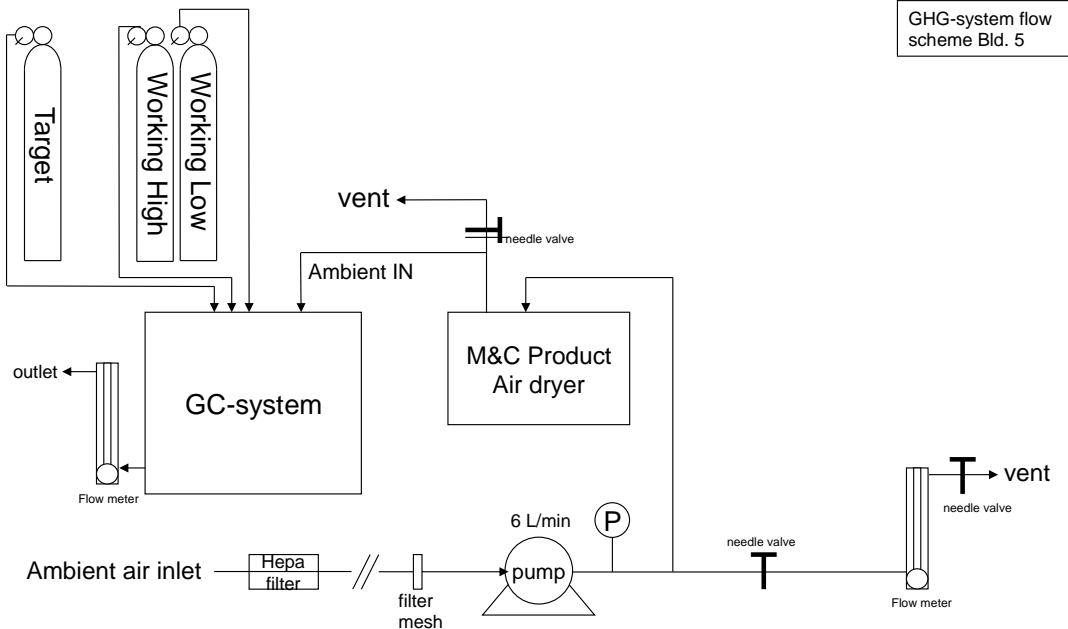


*Fig. 3: Bd 5 GHG-system flow scheme*

# 3  Greenhouse gas concentration monitoring at the JRC-Ispra site

## 3.1  Location

The JRC monitoring station at Ispra is currently the only low altitude measurement site for greenhouse gases (GHGs) near the Po Valley. The unique location of the station at the South-Eastern border of Lake Maggiore in a semi-rural area at the North-Western edge of the Po Valley allows sampling of highly polluted air masses from the Po Valley during meteorological conditions with southerly flow, contrasted by situations with northerly winds bringing relatively clean air to the site. A high-resolution modelling study analysed in detail the sensitivity of the atmospheric concentrations at the monitoring station (*Bergamaschi and Brunner, 2015*). The sensitivity usually shows a significant diurnal cycle. At night, measurements are dominated by the area 40-60 km around the station, while daytime footprints are much larger, typically dominated by distances beyond 60 km. During summer daytime, the radius $\tau_{s50}$ (at which the cumulative surface sensitivity reaches 50% of the total sensitivity) is on average 187 km. Furthermore, the diurnal cycle in local wind direction due to the regional mountain - lake/valley wind system leads to a significant diurnal cycle of the sensitivity (north-west vs. south-east), that is strongest during the summer.

The main urban areas around the station are Varese, 20 km east of the station, Novara, 40 km south, Gallarate - Busto Arsizio, about 20 km southeast, and Milan, 60 km south-east of the station. The JRC GHG station was setup in 2007 at Building 5 (Fig. 2a) of the JRC Ispra site (45.807°N, 8.631°E, 223 m asl) and has been operated continuously since the end of 2007. In 2016 a new station building inside the JRC premises (Building 77r, 45.8147°N, 8.6360°E, 210 m asl) was completed. The new station includes a 100m tower on top of the station building (Fig. 2b), with platforms every 20 m. By the end of 2016 the new station had been equipped with a new GHG instrument and sampling system, with multiple sampling lines at 40, 60, and 100m. The new GHG station is currently integrated into the European Integrated Carbon Observation System (ICOS) network (https://www.icos-ri.eu/).

## 3.2  Measurement programme

The GHG monitoring station in Building 5 has been in operation since October 2007, complementary to the JRC-Ispra EMEP-GAW station, which started in 1985 (*Putaud et al., 2017*), and to the flux measurement tower in the forest of San Rossore.  GHG measurements at the new Atmospheric Observatory started at the end of November 2016. In October 2017, the new GHG station successfully passed the first step of the official ICOS labelling procedure. The station is planned as "ICOS class-2" atmospheric station, which requires continuous $CO_2$, $CH_4$ and meteorological measurements, following ICOS guidelines (which includes rigorous standardisation of instrumentation, sampling, calibration, QA/QC and centralised data processing).

The GHG station in Building 5 will be run until the end of 2017, to give one year of overlapping measurements from both stations.
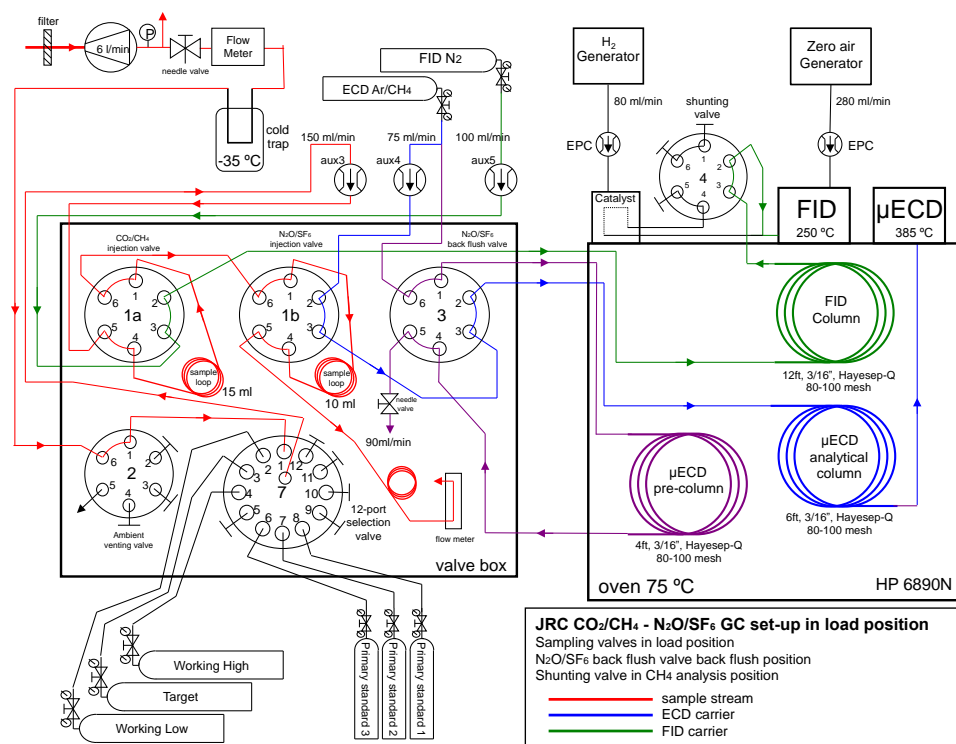
Data File C:\CHEM32\1\DATA\ISPRA\AMBIENT_20150807 2016-10-19 16-11-58\SIG10017.D
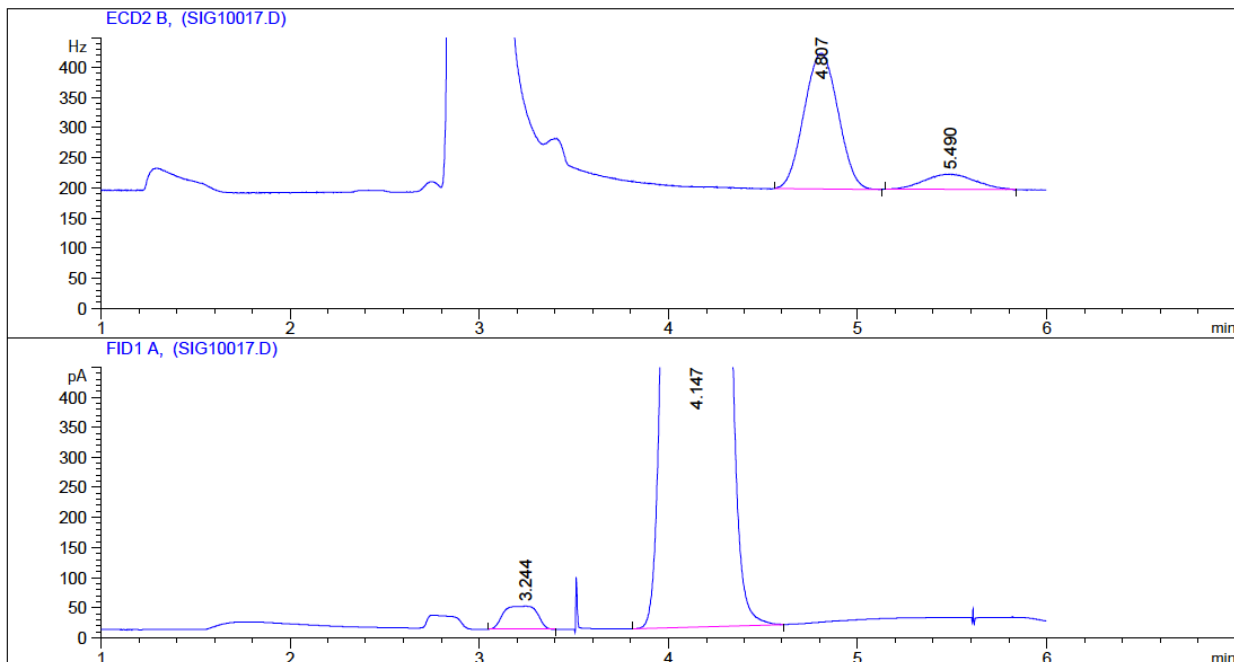Sample Name: AMBIENT



*Fig. 4: The top panel shows a schematic of the GC-system set-up while typical chromatograms are shown in the lower panels.*

## 3.3    Instrumentation in Building 5

### 3.3.1    Sampling

Air samples in Building 5 are collected from the top of a 15 m high mast using a 50 m ½" Teflon tube at a flow rate of ~6 L /min using a KNF membrane pump (KNF N811KT.18). The sampled air is filtered for aerosols by a Pall Hepa filter (model PN12144) positioned 10 m downstream of the inlet and dried cryogenically by a commercial system from M&C TechGroup (model EC30 FD) down to a water vapour content of <0.015%v before being directed to the analyser. The remaining water vapour is equivalent to a maximum 'volumetric error' of <0.06 ppmv of $CO_2$ or <0.3 ppbv of $CH_4$ or <0.05 ppbv $N_2O$. A schematic overview of the sample flow set-up is shown in Fig. 3.

### 3.3.2    Analyses

#### 3.3.2.1 Gas Chromatograph Agilent 6890N (S/N US10701038)

Continuous monitoring at 6 minute time resolution of $CO_2$, $CH_4$, $N_2O$, and $SF_6$ is performed with an Agilent 6890N gas chromatograph equipped with a Flame Ionization Detector (FID) and micro-Electron Capture Detector ($\mu$ECD) using a set-up described by *Worthy el al.* (1998). The calibration strategy has been adopted from *Pepin et al.* (2001) and is based on a Working High (WH) and Working Low (WL) standard (namely bracketing standards), which are calibrated regularly using NOAA primary standards. The WH and WL are both measured 2 times per hour for calculating ambient mixing ratios, and a target (TG) sample is measured every 6 hours for quality control. The working standards and target cylinders are filled with synthetic air, while NOAA primary standards are filled with real air.

$N_2O$ concentrations were also calculated using a second calibration strategy that is based on the one-point-reference method with a correction for non-linearity of $\mu$ECD. The non-linear response of the $\mu$ ECD was estimated using NOAA primary standards and then it was applied to the entire time series. This second method improves the quality of the time series when the bracketing standards do not cover the range for $N_2O$ ambient concentrations (i.e. range too large or range that does not include the ambient concentration). GHG measurements are reported as dry air mole fractions (mixing ratios) using the WMO NOAA2004 scale for $CH_4$, the WMOX2007 for $CO_2$ and the NOAA2006A scale for $N_2O$ and $SF_6$. We use a suite of five NOAA tanks ranging from 369-523 ppm for $CO_2$, 1782-2397 ppb for $CH_4$, 318-341 ppb for $N_2O$, and 6.1-14.3 ppt for $SF_6$ as primary standards. The GC control and peak integration runs on *ChemStation* commercial software. Further processing of the raw data is based on custom built software developed in C language and named GC_6890N_Pro. A schematic of the GC-system set-up and typical chromatograms are shown in Fig. 4.

In March all the GC columns were replaced with new ones. The new columns have the same properties as the old columns. The nickel catalyst used to convert $CO_2$ to $CH_4$ was replaced during the same intervention.

*Fig. 5: Sampling, conditioning and distribution system diagram for the GHG measurements at the new Atmospheric Observatory (Building 77r).*

### *3.3.2.2 Radon analyser ANSTO (custom built)*

[222]Radon activity concentrations in Bq m[-3] have been semi-continuously monitored (30 minute time integration) applying an ANSTO dual-flow loop two-filter detector (Zahorowski et al., 2004) since October of 2008. The detector stopped working in July 2016 following a major problem in the calibration unit. In December 2016 the problem was fixed and the detector was moved to the new GHG station (Building 77r) and a separate sampling line installed, collecting air at 100m height.

While the [222]Rn monitor was close to Building 5, the air sample was taken from a separate inlet positioned at 3.5 m above the ground. A 500 L decay tank was placed in the inlet line to allow for the decay of Thoron ([220]Rn with a half-life of 55.6 s) before reaching the [222]Radon monitor. The ANSTO [222]Radon monitor was calibrated once a month using a commercial passive [226]Radium source from Pylon Electronic Inc. (Canada) inside the calibration unit with an activity of 21.99 kBq, which corresponds to a [222]Radon delivery rate of 2.77 Bq min^{-1}. The lower limit of detection is 0.02 Bq m[-3] for a 30% precision (relative counting error). The total measurement uncertainty is estimated to be <5% for ambient [222]Radon activities at Ispra.

## 3.4     Instrumentation in the new Atmospheric Observatory (Bd 77R)

### 3.4.1     Air sampling

Air samples are collected at the different levels on the tower using ½" Synflex tubes at a flow rate of ~9 L min^{-1}. Each sampling line is provided with a KNF diaphragm pump (KNF N89 KTE) and three different particulate filters: a Pall Hepa Capsule Versapor filter at the inlet, and two filters with nominal pore size of 40 $\mu$ m and 7 $\mu$ m (model Swagelok SS-8TF-40 and SS-8TF-7, respectively). A small air flow (around 0.2 L min^{-1}) is diverted from the main line toward the Picarro G2401 by using a dedicated vacuum pump (model Vacuubrand, MD1) located downstream of the analyser. This flow is partially dried by a chiller (M&C Techground, model ECS) at a dew point of 5 °C. A water alarm is located downstream of the chiller to avoid that any liquid water reaches the analyser.

### 3.4.2     Analyses

### *3.4.2.2 Cavity Ring-Down Spectrometer Picarro G2401 (S/N 2326-CFKADS2193)*

The new atmospheric station (Building 77r) is equipped with a Picarro G2401 Cavity Ring-Down Spectrometer that measures the concentration of $CO_2$, $CH_4$, CO and $H_2O$ with a time resolution of 5 seconds. Concentrations are measured at three levels on the tower: 40 m, 60 m and 100 m above ground level (Fig. 5). A rotary valve, model Valvo Vici EMT2SD16MWE, allows the selection of the tower level to be analysed. The Picarro G2401 directly controls this valve and each tower level is analysed for 20 minutes (first five minutes are rejected as stabilisation time).

The calibration strategy for the Picarro G2401 is based on four gas tanks provided by the ICOS CAL laboratory that must be analysed at least once a month. These cylinders were not yet available at the end of 2016 and the analyser was calibrated using the NOAA standards used for the calibration of the GC working standards. Moreover, the performance of the Picarro G2401 must be evaluated using a long-term and a short-term target cylinder that are also provided by the ICOS-CAL laboratory. The short-term target should be measured at least two times per day, while the long-term target once a month. The target cylinders were not yet available at the end of 2016.

### *3.3.2.3 Radon analyser ANSTO (custom built)*

Measurement of [222]Rn in Building 77r started in December 2016, after moving the ANSTO radon monitor from Building 5 to Building 77r. The calibration unit of the detector was replaced with a new one that allows for the removal of water vapour from the air that flows through the radioactive source. The air sample is taken from a separate inlet at 100 m above ground by using a blower (Becker, model SV 8.130/1-01). The thoron decay volume and the radioactive source used for calibration were the same as those deployed in Building 5.

## 3.5 Measurement uncertainties

The different types of uncertainties affecting the GC measurements have been estimated using the algorithms developed in the InGOS ("Integrated non-CO2 Greenhouse gas Observing System") project (http://www.ingos-infrastructure.eu/). These uncertainties are defined as follows:

- 'Working standard repeatability' is calculated as the 24-hours centred moving, $1\sigma$ standard deviation of the bracketing standards (or reference standard in case of the one-point-reference method).

- 'Laboratory internal scale consistency uncertainty' (LISC) is the median of the difference between measured and assigned values of the target gas. The median is calculated for different time periods where GC settings were constant (including the used working standards and target gas).

- 'Monthly reproducibility' represents the values of the smoothed target residuals. Smoothing is performed with a centred running median with a window length of 30 days.

- 'Scale transfer and non-linearity uncertainty' is based on the uncertainty of the assigned working standard concentration and it accounts for the uncertainty introduced by scale transfer from NOAA standards to the working standards.
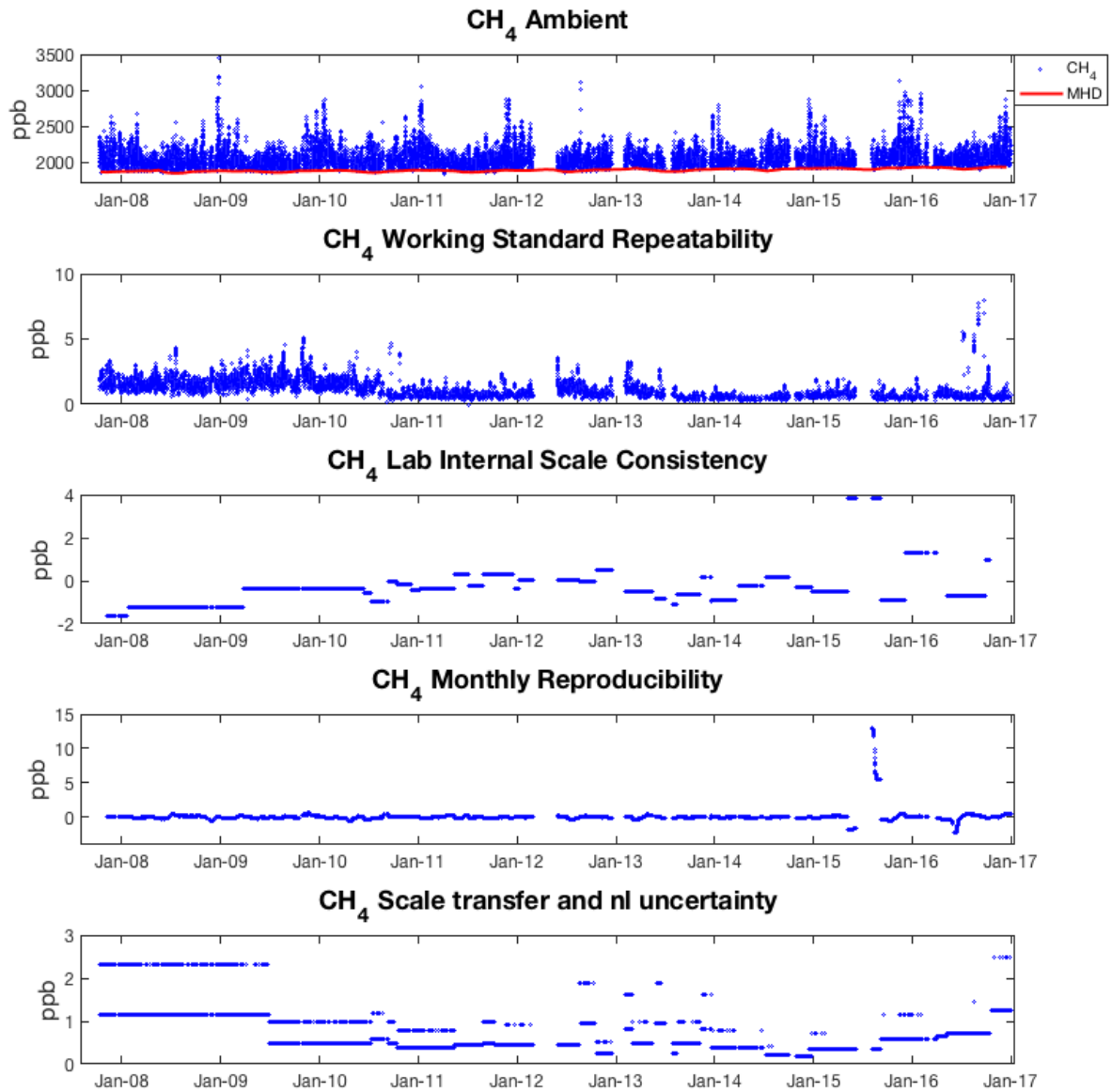
*Fig. 6: Time series of continuous CH₄ ambient measurements at Ispra (Building 5) between October 2007 and December 2016 with associated uncertainties. CH₄ ambient concentrations are reported as hourly mean values of dry air mole fractions. Furthermore, monthly mean concentrations from the background station Mace Head (MHD) on the West coast of Ireland are also included (Mace Head data from Simon O'Doherty, University of Bristol).*

## 3.6 Overview of measurement results

Fig. 6, 8, 9 and 10 give an overview of the GC greenhouse gas measurements in Building 5 since the start of the measurements in October 2007 until December 2016. These figures show also the uncertainties of the ambient concentrations; the 'scale transfer and non-linearity' uncertainty has been calculated only for $CH_4$ and $N_2O$. For $N_2O$ and $SF_6$ only data since 15/09/2010 are shown. Before this date there was a dilution problem with the sample loop connected to the column of the µECD detector. The flushing of the sample loop during ambient measurement was not sufficient to remove completely the carrier gas used in the previous analysis. The $N_2O$ data shown in Fig. 9 are calculated using the one-point-reference method (see above).

Measurements collected in Building 5 are plotted together with the monthly mean baseline data from the Mace Head (Ireland) station to illustrate the Atlantic background mixing ratios. Minimum values of $CH_4$, $N_2O$ and $SF_6$ measured at the JRC-Ispra site are close to the Mace Head baseline, while $CO_2$ mixing ratios can be lower than the Mace Head baseline due to the continental biospheric $CO_2$ sink.

During summer 2015 the GC underwent a significant maintenance in which the jet of the FID detector, the multi-position rotary valve and the nickel catalyser were replaced. After the maintenance, the precision of $CO_2$ measurements was worse than before because of the continuous decrease in the efficiency of the new nickel catalyst used to convert the $CO_2$ into methane. This catalyser has been replaced in March 2016. Afterward, the precision of $CO_2$ measurements has returned to typical values observed before summer 2015.

Fig. 7 shows hourly mean $^{222}$Radon activities from October 2008 till July 2016. The time series shows large diurnal and seasonal variations, mainly due to the diurnal and seasonal variations of the boundary layer height.
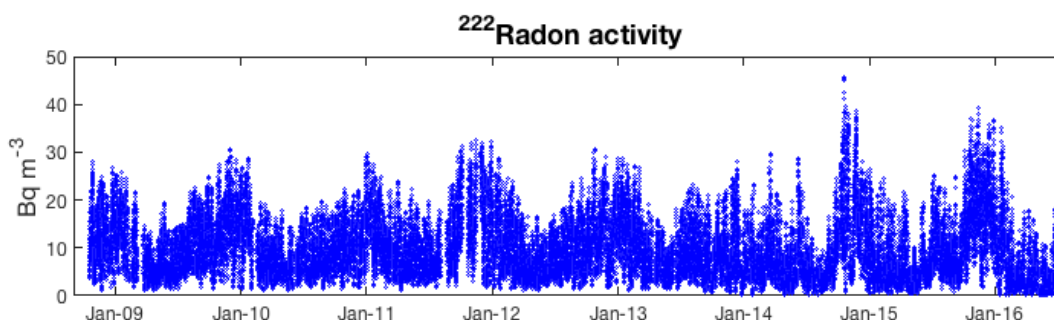


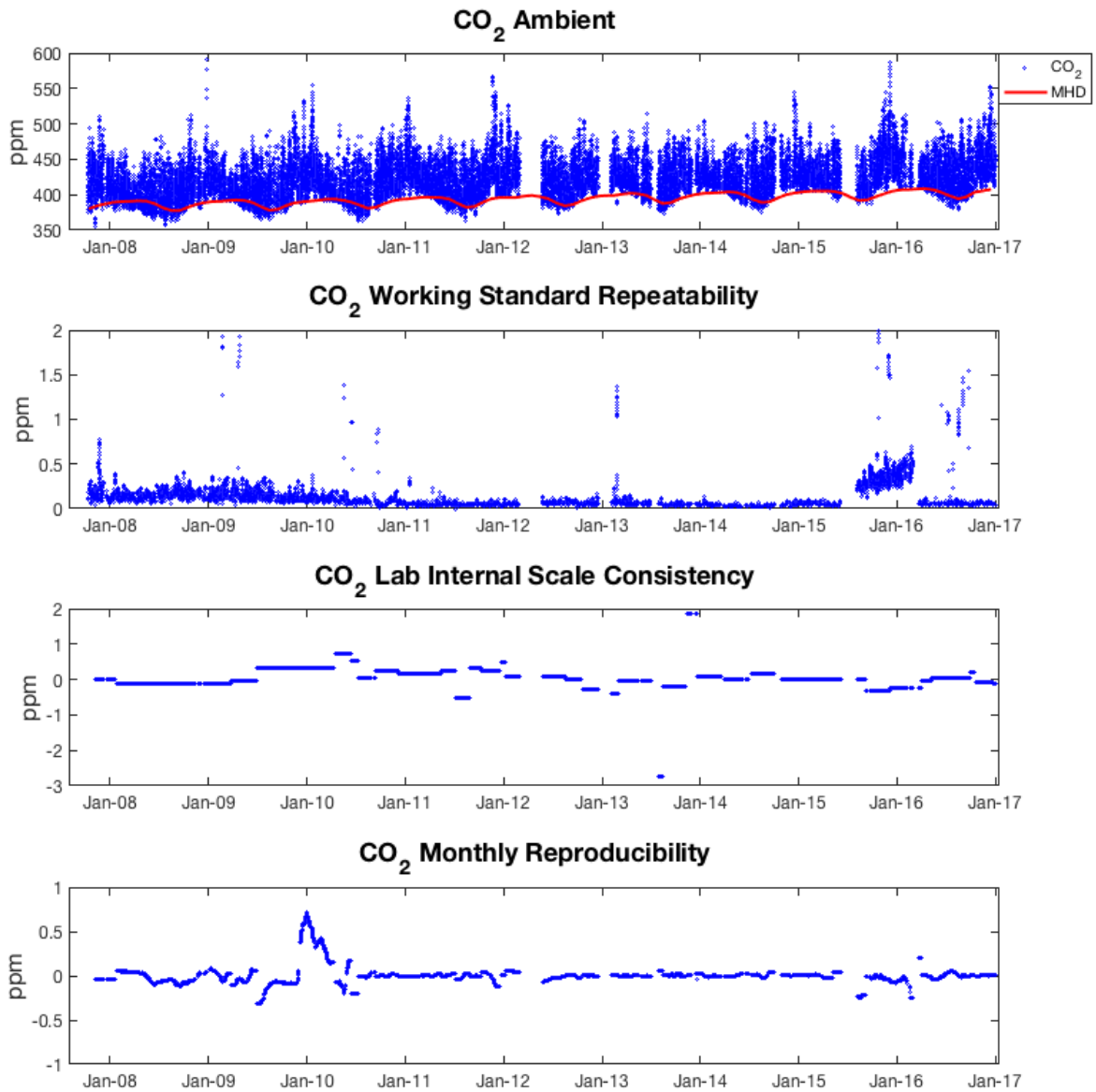*Fig. 7: Time series of hourly mean 222Radon activity from Oct. 2008 to Dec. 2016.*

*Fig. 8: Time series of continuous CO₂ ambient measurements at Ispra (Building 5) between October 2007 and December 2016 with associated uncertainties. CO₂ ambient concentrations are reported as hourly mean values of dry air mole fractions. Furthermore, flask measurements from the background station Mace Head (MHD) on the West coast of Ireland are also included (Dlugokencky, et al., 2017).*
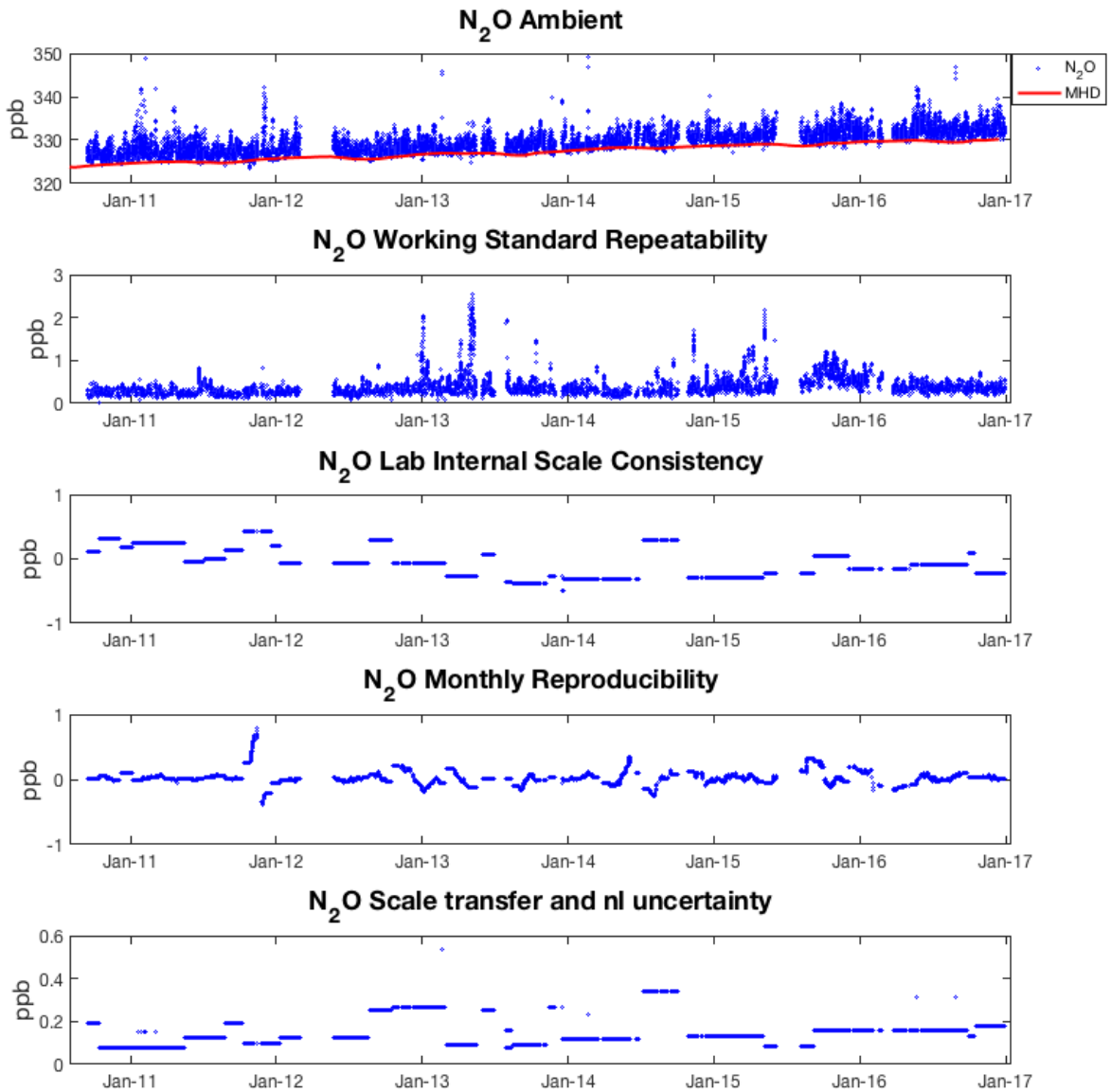
*Fig. 9: Time series of continuous N2O ambient measurements at Ispra (Building 5) between September 2010 and December 2016 with associated uncertainties. N2O ambient concentrations are reported as hourly mean values of dry air mole fractions. Furthermore, monthly mean concentrations from the background station Mace Head (MHD) on the West coast of Ireland are also included (Mace Head data from Simon O'Doherty, University of Bristol).*

*Fig. 10: Time series of continuous SF₆ ambient measurements at Ispra (Building 5) between September 2010 and December 2016 with associated uncertainties. SF₆ ambient concentrations are reported as hourly mean values of dry air mole fractions. Furthermore, monthly mean concentrations from the background station Mace Head (MHD) on the West coast of Ireland are also included (Mace Head data from Simon O'Doherty, University of Bristol).*
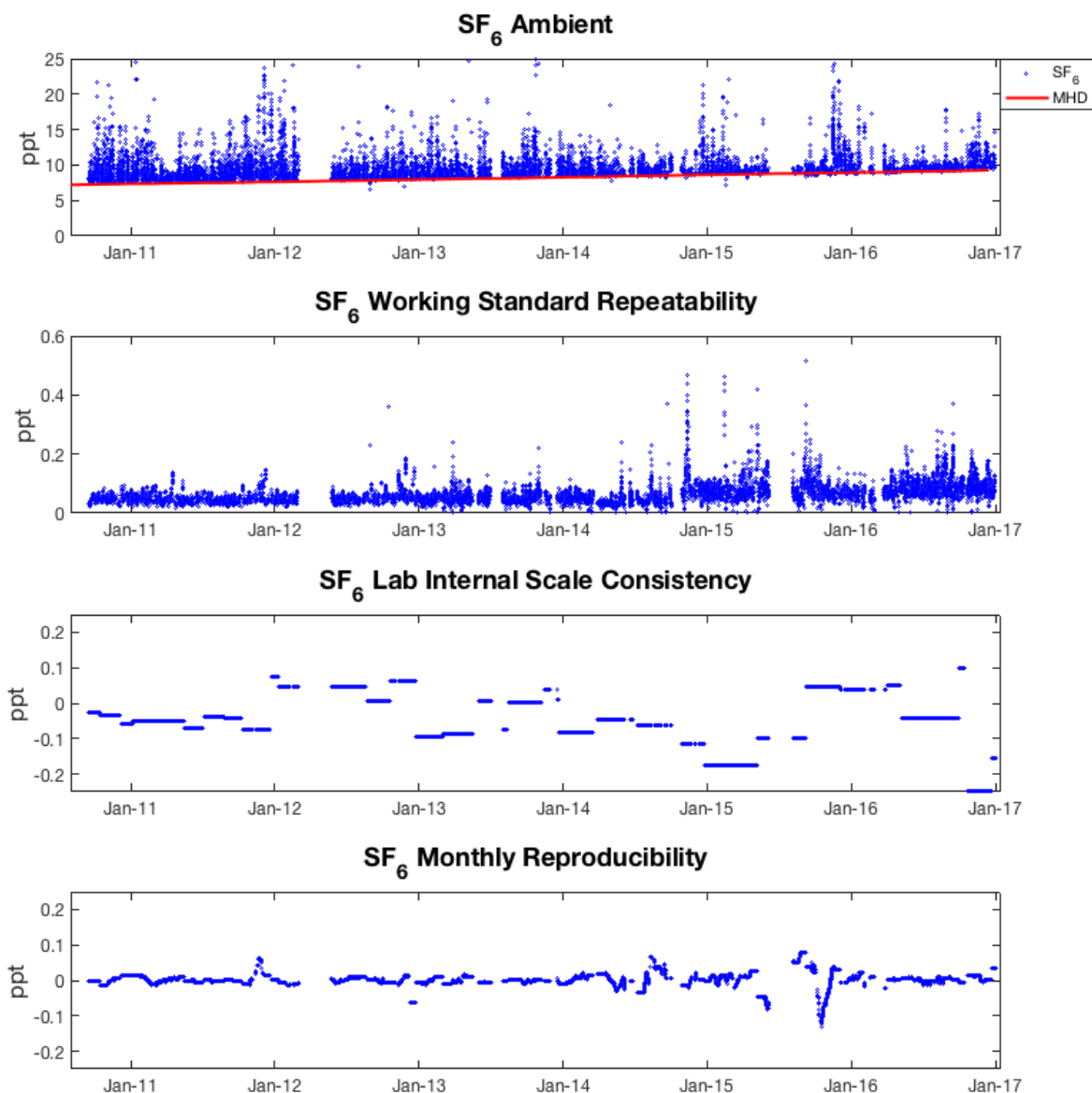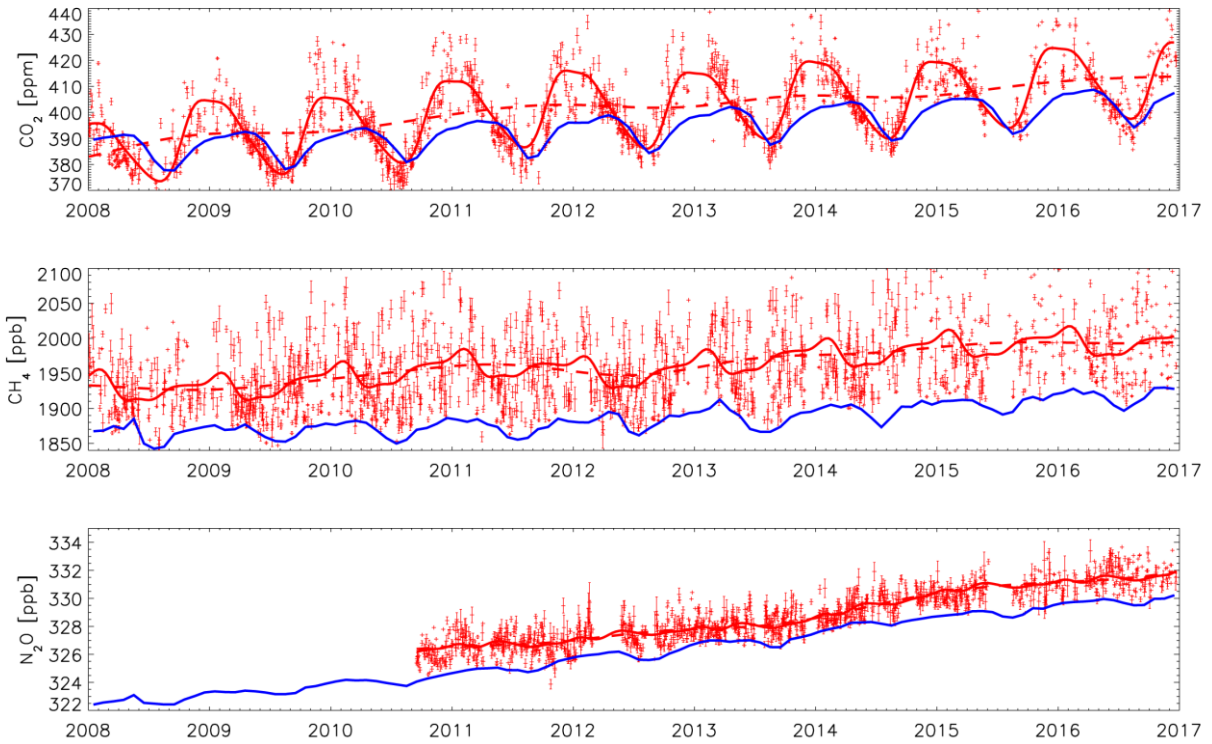
*Fig. 11: Trends in atmospheric GHG concentrations. Top panel: CO₂; middle panel: CH₄; lower panel: N₂O. The figure show daily average values, using only daytime measurements (between 12:00 and 15:00 LT) and excluding GHG measurements under stagnant meteorological conditions (with wind speed below 0.5 ms⁻¹). Solid red line: Fit to daily data (based on NOAA fitting procedure [Thoning et al., 1989]); dashed red line: trend derived from fitting procedure; blue solid line: baseline concentrations at Mace Head.*
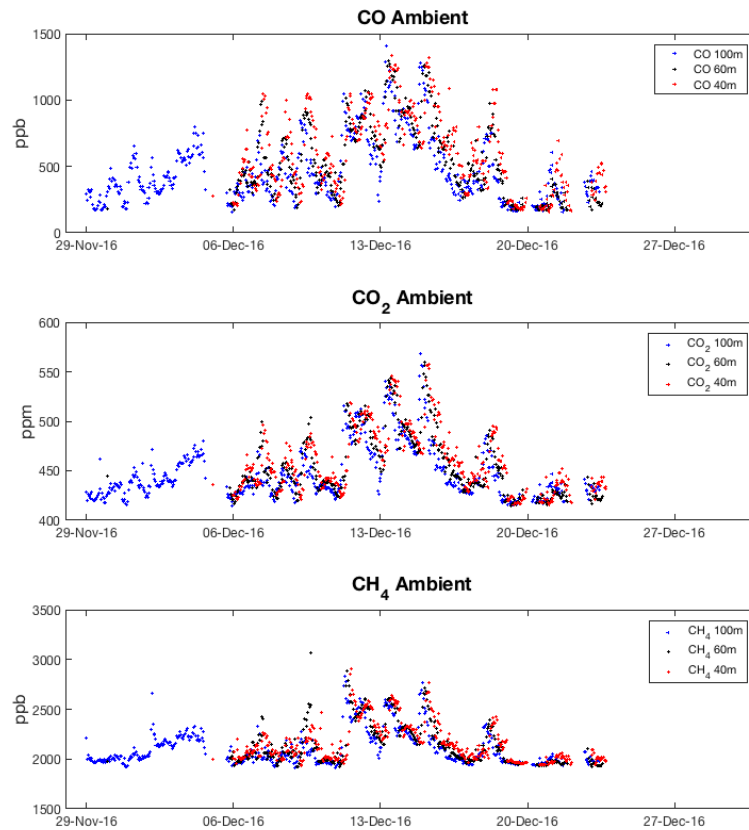


*Fig. 12: First measurements of CO, CO₂ and CH₄ at new Atmospheric Observatory (Building 77r), sampled at three different heights from the tower (40, 60, 100m), from November 29ᵗʰ till December 24ᵗʰ, 2016. Concentrations are reported as hourly mean values of dry air mole fractions.*

Fig. 11 shows the time series of daily average $CO_2$, $CH_4$, and $N_2O$ values, using only daytime measurements (between 12:00 and 15:00 LT) and excluding GHG measurements under stagnant meteorological conditions (with wind speeds below 0.5 ms$^{-1}$). In order to further analyse the trends and seasonal variations we applied the NOAA fitting procedure [*Thoning et al.*, 1989]. For $CH_4$ we derive an average trend of 6.9 ppb yr$^{-1}$ between 2008 and 2016, which is very close to the observed global $CH_4$ trend of 7.0 ± 2.7 ppb yr$^{-1}$ during this period (www.esrl.noaa.gov/gmd/ccgg/trends_ch4/). Also for $N_2O$, the derived trend at Ispra of 0.9 ppb yr$^{-1}$ is identical to the global trend of 0.9 ppb yr$^{-1}$ during the last 10 years [WMO, 2017]. The very close correspondence of the trends in $CH_4$ and $N_2O$ at Ispra with the global trends is also reflected in the almost constant offset between the average concentrations at Ispra and the Mace Head baseline. This suggests that the regional $CH_4$ and $N_2O$ emissions in the catchment area of the Ispra station were effectively constant during the analysis period 2008-2016.

For $CO_2$, we derive an average trend of 3.4 ppm yr$^{-1}$ between 2008 and 2016, compared to a global trend of 2.2 ± 0.5 ppm yr$^{-1}$ (https://www.esrl.noaa.gov/gmd/ccgg/trends/). The interpretation of the $CO_2$ trends at Ispra, is however complicated by the large seasonal variation of the biospheric $CO_2$ fluxes. The larger $CO_2$ trend derived from the data at Ispra is largely driven by the relatively low summertime $CO_2$ values during 2008-2010, indicating a relatively strong biospheric $CO_2$ uptake in the catchment area of the Ispra station during these years.

Finally, Fig. 13 shows hourly mean $^{222}$Radon activities measured in Building 77r at 100m level. These concentrations are significantly lower than the previously observed values in Building 5, mainly because of the different sampling height of the two sites.
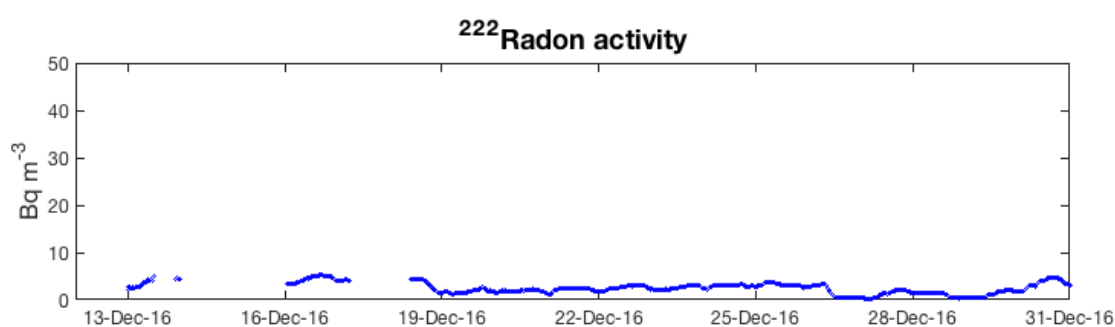


*Fig. 13: First $^{222}$Rn measurements at new Atmospheric Observatory (Building 77r). The figure shows the time series of hourly mean $^{222}$Radon activity, collected at 100m height, from November 29th till December 24th, 2016.*
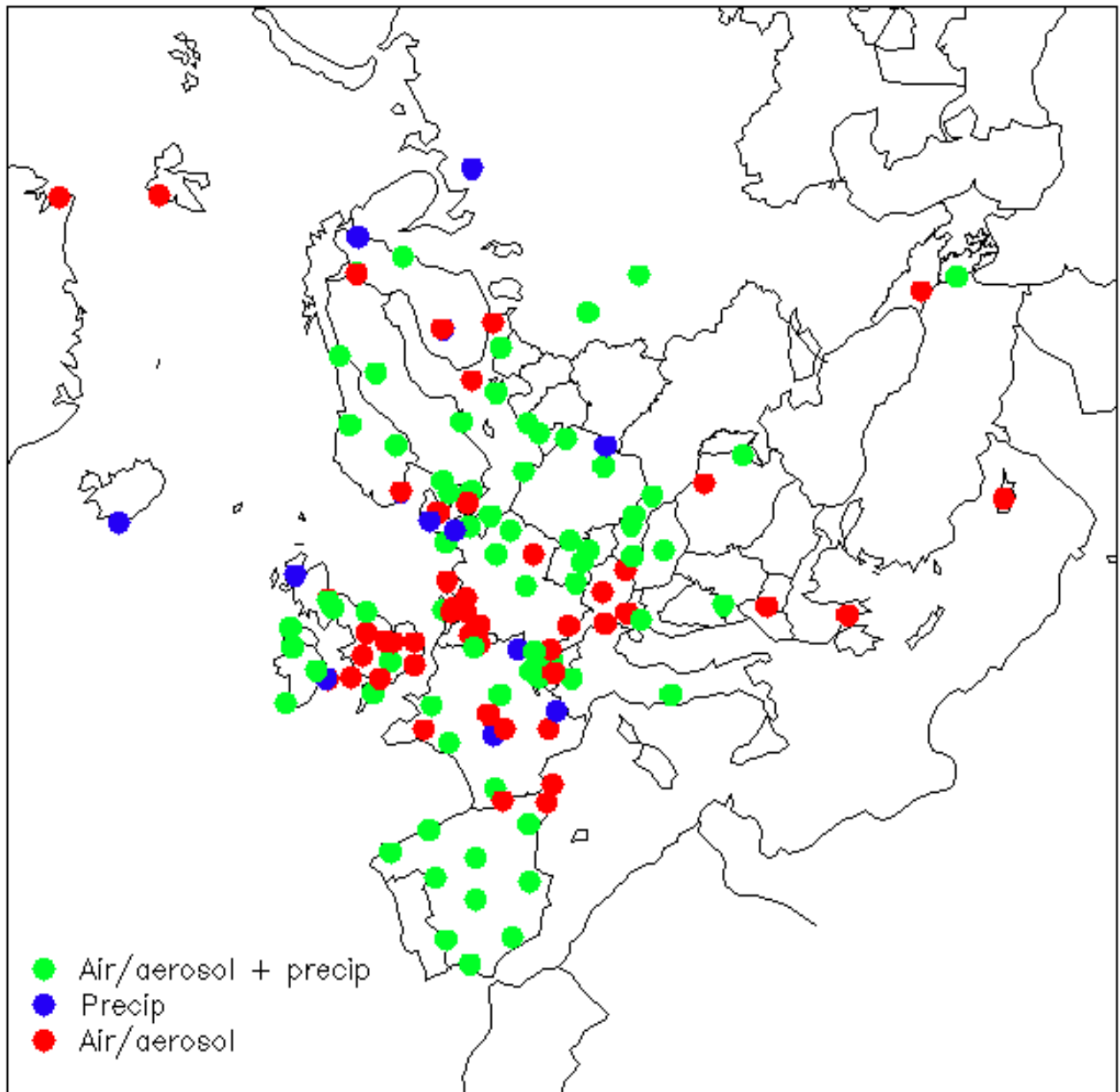
Fig. 14: most recent map of the EMEP stations across Europe (2014) made available by the
Chemical co-ordinating Centre (CCC).

# 4 Short-lived atmospheric species at the JRC-Ispra site

## 4.1 Introduction

### 4.1.1 Location

Air pollution has been monitored since 1985 at the EMEP and regional GAW station for atmospheric research (45°48.881'N, 8°38.165'E, 209 m a.s.l.) located by the Northern fence of the JRC-Ispra site (see Fig. 1), situated in a semi-rural area at the NW edge of the Po valley in Italy. From the end of March 2013, the measurement of short-lived atmospheric species (Table 2) has been performed at a provisional site (45°48.438'N, 8°37.582'E, 217 m a.s.l.), due to the reconstruction of the laboratory at the historical site (Fig. 1). The main cities around are Varese (20 km east), Novara (40 km south), Gallarate – Busto Arsizio (about 20 km south-east) and the Milan conurbation (60 km to the south-east). Busy roads and highways link these urban centres. Emissions of pollutants reported for the four industrial large point sources ($CO_2$ emissions > 1500 tons $d^{-1}$) located between 5 and 45 km NE to SE from Ispra also include 2 and 3 tons of CO per day, plus 3 and 5 tons of NOx (as $NO_2$) per day for the 2 closest ones (**PRTR emissions**, 2010).

### 4.1.2 Underpinning programmes

#### 4.1.2.1 The EMEP programme (*http://www.emep.int/*)

Currently, about 50 countries and the European Community have ratified the **CLRTAP**. Lists of participating institutions and monitoring stations (Fig. 14) can be found at: ***http://www.nilu.no/projects/ccc/network/index.html***

The set-up and running of the JRC-Ispra EMEP station resulted from a proposal of the Directorate General for Environment of the European Commission in Brussels, in agreement with the Joint Research Centre, following the Council Resolution **N° 81/462/EEC**, article 9, to support the implementation of the EMEP programme.

The JRC-Ispra station has operated on a regular basis in the extended EMEP measurement program since November 1985. Data are transmitted yearly to the EMEP Chemical Co-ordinating Centre (CCC) for data control and statistical evaluation, and available from the EBAS data bank (Emep Database, ***http://ebas.nilu.no/***).

#### 4.1.2.2. The GAW programme (*http://www.wmo.int/web/arep/gaw/gaw_home.html*)

WMO's Global Atmosphere Watch (GAW) was established in 1989 with the scope of providing information on the physico-chemical composition of the atmosphere. These data provide a basis to improve our understanding of both atmospheric changes and atmosphere-biosphere interactions. GAW is one of WMO's most important contributions to the study of environmental issues, with about 80 member countries participating in GAW's measurement programme. Since December 1999, the JRC-Ispra station is also part of the GAW coordinated network of regional stations. Data contributing to the GAW programme are also available via EBAS.

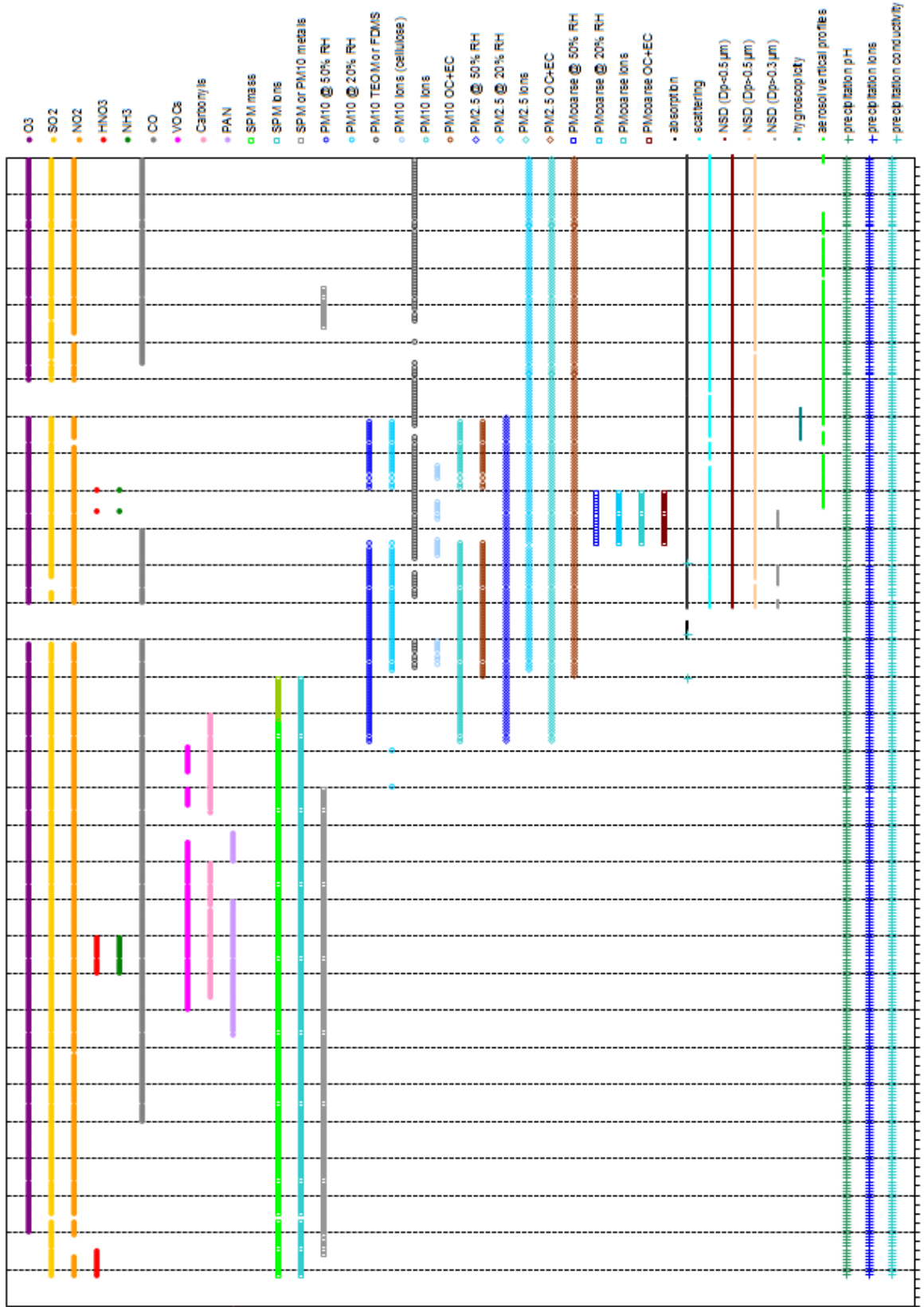*Fig. 15: Atmospheric short-lived species measurements performed at the JRC-Ispra station for atmospheric research since 1985.*

### *4.1.2.3. The institutional programme (http:/ec.europa.eu/jrc/en/research-topic/air-quality)*

Since 2002, the measurement programme of the air pollution monitoring station of JRC-Ispra has gradually been focused on short-lived climate forcers such as tropospheric ozone and aerosols, and their precursors (Fig. 15). Concretely, more sensitive gas monitors were introduced, as well as a set of new measurements providing aerosol characteristics that are linked to radiative forcing. The station contributed to the impact category "implementation, monitoring and evaluation of EU policies" as listed in the JRC institutional project work plan 2017 (Deliverable 201702).

The site is also being used for research and development purposes. Regarding particulate organic and elemental carbon, techniques developed by the Air and Climate unit in Ispra have been implemented and validated by international atmospheric research networks (EUSAAR, ACTRIS), recommended in the EMEP sampling and analytical procedure manual, and adopted by the European Committee for Standardisation (CEN) as a standard method (EN16909).

Currently, preliminary air pollution data obtained at the JRC-Ispra are visible and downloadable in real time from http://abc-is.jrc.ec.europa.eu. All validated data obtained at the JRC-Ispra station under the EMEP and the GAW program, and other past and current international projects (EUSAAR, ACTRIS) can be retrieved from the EBAS database (*http://ebas.nilu.no/*), selecting Ispra as station of interest.

Additional information about the JRC-Ispra air monitoring station and other stations from the EMEP network can also be found in the following papers: Van Dingenen et al., 2004; Putaud et al., 2004; Mira-Salama et al., 2008; Putaud et al., 2010; Putaud et al., 2014.

*Table 1: Variables related to short-lived pollutants and radiative forcers measured in 2016*

| METEOROLOGY | Pressure, temperature, humidity, wind, solar radiation |
|---|---|
| GAS PHASE | $SO_2$, NO, $NO_X$, $O_3$, CO |
| PARTICULATE PHASE | $PM_{2.5}$ mass, $Cl^-$, $NO_3^-$, $SO_4^{2-}$, $C_2O_4^{2-}$, $Na^+$, $NH_4^+$, $K^+$, $Mg^{2+}$, $Ca^{2+}$, OC, and EC contents<br>Number size distribution (10 nm - 10 µm)<br>Aerosol light absorption, scattering and back-scattering coefficients<br>Altitude-resolved aerosol light back-scattering and extinction |
| WET DEPOSITION | $Cl^-$, $NO_3^-$, $SO_4^{2-}$, $C_2O_4^{2-}$, $Na^+$, $NH_4^+$, $K^+$, $Mg^{2+}$, $Ca^{2+}$<br>pH, conductivity |
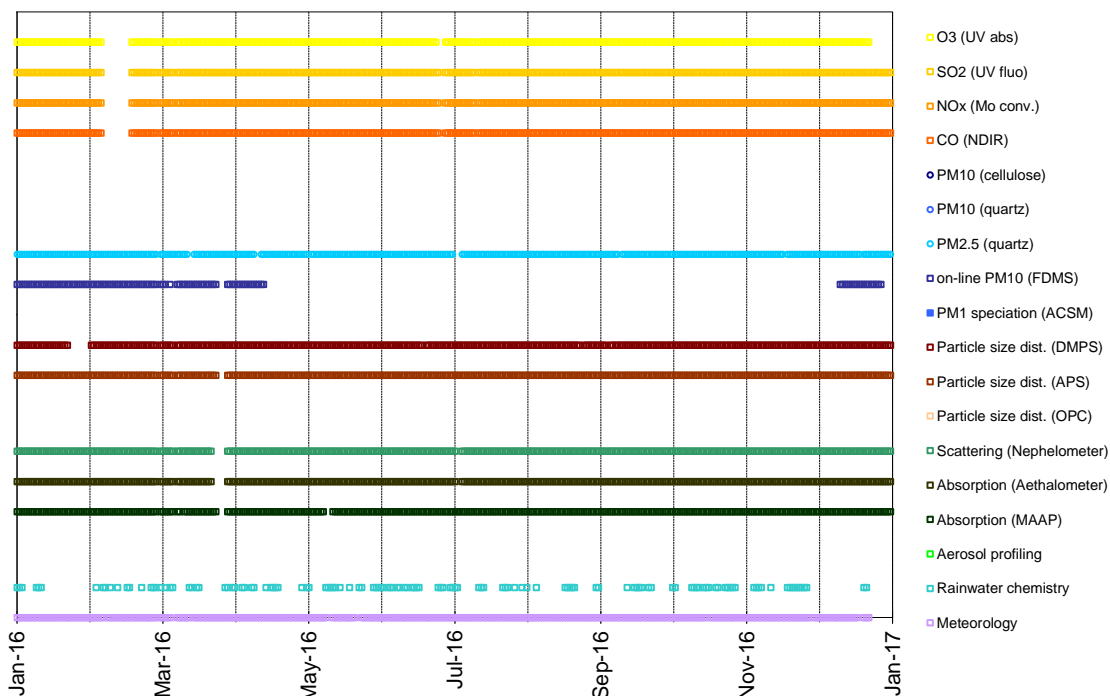


Fig. 16. Year 2016 data coverage at the JRC EMEP-GAW station.

## 4.2    Measurements and data processing

### 4.2.1    Air pollutant and short-lived radiative forcer measurements at the JRC- Ispra station in 2016

Since 1985, the JRC-Ispra air monitoring station program evolved significantly (Fig. 15). The measurements performed at the JRC-Ispra EMEP-GAW station in 2016 are listed in Table 1, and Fig. 16 shows the data coverage.

Meteorological variables were measured continuously, except from Dec. 23rd to 31st (technical problem). The values measured by the JRC Radioactivity Alarm and Meteorological Network (Bd 51) were used for gap filling.

$SO_2$, $O_3$, NOx and CO were measured almost continuously during the year 2016, except for the period 6 – 17 Feb. due to annual revision of the mobile laboratory and maintenance/linearity checks of all analysers, and for three 1 - 2 day gaps in March, June and July, due to power fails. In addition, $O_3$ measurements are missing from Dec. 23rd to 31st, due to data acquisition problems.

Particulate matter ($PM_{2.5}$) samples were collected daily and analysed for $PM_{2.5}$ mass (at 20% RH), main ions, OC (organic carbon) and EC (elemental carbon), for the whole of 2016, except for 11 days (sampler breakdowns).

On-line $PM_{10}$ measurements (FDMS-TEOM, Filter Dynamics Measurement System - Tapered Element Oscillating Microbalance) were carried out only from Jan. 1st to Apr. 13th and from Dec. 9th to Dec. 27th due to a major breakdown (the instrument was sent to the manufacturer's).

Particle number size distributions (10 nm < Dp < 10 μm), aerosol light scattering and aerosol light absorption coefficients were measured almost continuously (96 to 99% coverage) in 2016. The main gap in submicrometer number size distribution measurements (Jan 24th to 31st) coincide with the calibration workshop at the WCCAP in Leipzig.

The Raymetrics Raman LiDAR was operated according to the EARLINET schedule (Mon. at solar noon ±1 hr, at sunset -2,+3hr, Thu. at sunset -2,+3hr, and during Calipso overpasses ± 1hr), weather and staff availability permitting.

Precipitation was collected throughout the year and analysed for pH, conductivity, and main ions (collected water volume permitting). Only a few major precipitation events were missed.

### 4.2.2 Measurement techniques

#### 4.2.2.1 On-line monitoring

<u>Meteorological Variables</u>

Meteorological data and solar radiation were measured directly at the EMEP station with the instrumentation described below.

*WXT510 (S/N: A1410009, A1410010 & A1410011)*

Two WXT510 weather transmitters from Vaisala recorded simultaneously the six weather variables temperature, pressure, relative humidity, precipitation and wind speed and direction from the top of a 10 m high mast.

The wind data measurements utilise three equally spaced ultrasonic transducers that determine the wind speed and direction from the time it takes for ultrasound to travel from one transducer to the two others. Precipitation rate is measured with a piezoelectric sensor that detects the impact of individual raindrops and thus infers the accumulated rainfall. For the pressure, temperature and humidity measurements, separate sensors employing high precision RC oscillators are used.

*Kipp and Zonen CMP 11 (S/N: 070289)*

To determine the total solar radiation, a Kipp and Zonen CMP11 Pyranometer have been installed in 2015, which measures the irradiance (in $W/m^2$) on a plane surface from direct solar radiation and diffuse radiation incident from the hemisphere above the device. The CMP11 S/N 070289 only is installed on the top of the container (3 m above ground). The measurement principle is based on a thermal detector. The radiant energy is absorbed by a black disc and the heat generated flows through a thermal resistance to a heat sink. The temperature difference across the thermal resistance is then converted into a voltage and precisely measured. The CMP11 features a fast response time of 12 s, a small non stability of +/-0.5 % and a small non linearity of +/-0.2 %.

<u>Gas Phase Air Pollutants</u>

*Sampling*

$SO_2$, NO, $NO_x$, $O_3$ and CO were measured from the mobile laboratory (plates number CM328CN), parked at the EMEP/GAW provisional station at JRC-Ispra (see Fig. 1) about 500 meters from the historical site.

The sampling line at the mobile lab. (inlet about 3.5 m above ground) consists of an inlet made of a stainless steel cylindrical cap (to prevent rain and bugs to enter the line), outside a stainless steel tube (diameter = about 4 cm), inside a Teflon tube (d = about 2.7 cm) and a "multi-channel distributor" tube, with ten ¼" connectors. This inlet is flushed by an about 45 L min$^{-1}$ flow with a fan-coil (*measured with a gas-counter made by RITTER, sn. 11456*). Each instrument samples from the tube with its own pump through a 0.25 inch Teflon line and a 5 μm pore size 47 mm diameter Teflon filter (to eliminate particles from the sampled air). See also Fig. 17.

More details about the mobile lab and instruments (where exactly they were measuring and when) can be found in sections below.

*$SO_2$: UV Fluorescent $SO_2$ Analyser*

*Thermo 43iTLE (S/N 1021443379): 01.01-31.12.2016: Provisional station, mobile lab.*

At first, the air flow is scrubbed to eliminate aromatic hydrocarbons. The sample is then directed to a chamber where it is irradiated at 214 nm (UV), a wavelength where $SO_2$ molecules absorb. The fluorescence signal emitted by the excited $SO_2$ molecules going back

to the ground state is filtered between 300 and 400 nm (specific of $SO_2$) and amplified by a photomultiplier tube. A microprocessor receives the electrical zero and fluorescence reaction intensity signals and calculates $SO_2$ based on a linear calibration curve.

Calibration was performed with a certified $SO_2$ standard at a known concentration in air (44 ppb, Air Liquide). Zero check was done, using a zero air gas cylinder from Air Liquide, Alphagaz 1, CnHm < 0.5 ppm).

The specificity of the trace level Thermo instrument (TEI 43i-TLE) is that it uses a pulsed lamp. The 43i-TLE's detection limit is 0.05 ppb (about 0.13 µg m$^{-3}$) over 300 second averaging time, according to the technical specifications.

For more details about the instruments, manuals are available at \\ies.jrc.it\H02\lLargefacilities\ABC-IS\Quality_management\Manuals



Inlet head with a grid to prevent rain/insects entering.

Sampling line, length = about 2 meter.
Inside: Teflon tube, d = about 2.7 cm.
Outside: Stainless steel, d = about 4 cm.

1/4" Teflon tube connections.
Length = about 0.5 meter.

10 connections for analyzers/ instruments.

Teflon tube with connections, d = about 6 cm, Length = about 20 cm.

Flexible tube, d = about 4 cm.
Length = about 1.5 meter.

Fan coil flow (pump)
Flow about 50 L min$^{-1}$.

Fig. 17. Sampling inlet system for the gaseous air pollutant at the mobile lab. Inlet for the measurements is about 3.5 m above ground

NO + NO$_X$: Chemiluminescent Nitrogen Oxides Analyser (NO$_2$=NO$_X$-NO)

Thermo 42iTL (S/N 936539473): 01.01-31.12.2016: Provisional station, mobile lab.

This nitrogen oxide analyser is based on the principle that nitric oxide (NO) and ozone react to produce excited $NO_2$ molecules, which emit infrared photons when going back to lower energy states:

$$NO + O_3 \rightarrow [NO_2]^* + O_2 \rightarrow NO_2 + O_2 + h\nu$$
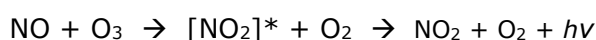
A stream of purified air (dried with a Nafion Dryer for 42iTL) passing through a silent discharge ozonator generates the ozone concentration needed for the chemiluminescent reaction. The specific luminescence signal intensity is therefore proportional to the NO concentration. A photomultiplier tube amplifies this signal.

$NO_2$ is detected as NO after reduction in a Mo converter heated at about 325 °C.

The ambient air sample is drawn into the analyser, flows through a capillary, and then to a valve, which routes the sample either straight to the reaction chamber (NO detection), or through the converter and then to the reaction chamber ($NO_X$ detection). The calculated NO and $NO_X$ concentrations are stored and used to calculate $NO_2$ concentrations ($NO_2 = NO_x - NO$), assuming that only $NO_2$ is reduced in the Mo converter.

Calibration was performed using a zero air gas cylinder (Air Liquide, Alphagaz 1, CnHm<0.5 ppm) and a NO span gas (85 ppb, Air Liquide). Calibration with a span gas was performed with a certified NO standard at a known concentration in $N_2$.

For more details about the instruments, the manuals are available on \\ies.jrc.it\H02\LargeFacilities\ABC-IS\Quality_management\Manuals

*$O_3$: UV Photometric Ambient Analyser*

*Thermo 49C (S/N 0503110398): 01.01-31.12.2016: Provisional station, mobile lab.*

The UV photometer determines ozone concentrations by measuring the absorption of $O_3$ molecules at a wavelength of 254 nm (UV light) in the absorption cell, followed by the use of Beer-Lambert law. The concentration of ozone is related to the magnitude of the absorption. The reference gas, generated by scrubbing ambient air, passes into one of the two absorption cells to establish a zero light intensity reading, $I_0$. Then the sample passes through the other absorption cell to establish a sample light intensity reading, I. This cycle is reproduced with inverted cells. The average ratio $R=I/I_0$ between 4 consecutive readings is directly related to the ozone concentration in the air sample through the Beer-Lambert law. Calibration is performed using externally generated zero air and external span gas. Zero air is taken from a gas cylinder (Air Liquide, Alphagaz 1, CnHm < 0.5 ppm). Span gas normally in the range 50 - 100 ppb is generated by a TEI 49C-PS transportable primary standard ozone generator (S/N 0503110396) calibrated/check by ERLAP (European Reference Laboratory of Air Pollution). A Nafion Dryer system is connected to the $O_3$ instrument.

For more details about the instruments, the manual is available on \\ies.jrc.it\H02\LargeFacilities\ABC-IS\Quality_management\Manuals

*CO:        Non-Dispersive Infrared Absorption CO Analyser*

*Horiba AMPA-370 (S/N WYHEOKSN) from 01.01 to 31.12.2016: Provisional station, mobile lab.*

In 2016, carbon monoxide (CO) has been continuously monitored using a commercial Horiba AMPA-370 CO monitor based on the principle of non-dispersive infrared absorption (NDIR). The Horiba APMA-370 uses solenoid valve cross flow modulation applying the same air for both the sample and the reference, instead of the conventional technique to apply an optical chopper to obtain modulation signals. With this method the reference air is generated by passing the sample air over a heated oxidation catalyst to selectively remove CO which is then directly compared to the signal of the untreated sample air at a 1 Hz frequency. The result is a very low zero-drift and stable signal over long periods of time.

To reduce the interference from water vapour to about 1% the sample air was dried to a constant low relative humidity level of around 30% applying a Nafion dryer (Permapure MD-070-24P) in the inlet stream. The detection limit of the Horiba AMPA-370 is ~20 ppbv for a one minute sampling interval. The overall measurement uncertainty is estimated to be ± 7%.

For more details about the instrument, see the manual available from \\ies.jrc.it\H02\LargeFacilities\ABC-IS\Quality_management\Manuals

In 2016, the gas phase monitors were calibrated eleven times with suitable span gas cylinders and zero air (see text for more details). Sampling flow rates are as follow:

| Compounds | Flow rates (L min$^{-1}$) |
|---|---|
| SO$_2$ | 0.5 |
| NO, NO$_x$ | 1.0/1.3 |
| O$_3$ | 0.7 |
| CO | 1.5 |

Atmospheric Particles

Sampling Conditions

Since 2008, all instruments for the physical characterisation of aerosols (Multi-Angle Absorption Photometer, Aethalometer, Nephelometer, Aerodynamic Particle Sizer, Differential Mobility Particle Sizer) sample isokinetically from an Aluminium inlet pipe (diameter = 15 cm, length of horizontal part ~280 cm and vertical part ~220 cm) described in Jensen et al., 2010. The Tapered Element Oscillating Micro-balances (FDMS-TEOMs) used their own inlet systems. The MAAP sampled from the main inlet through Nafion dryers at a flow rate of 1000 L hr$^{-1}$ from Jun. 23$^{rd}$ to Nov. 23$^{rd}$, and 480 L hr$^{-1}$ for the remainder of 2016.

The size dependent particle losses along the pipe radius were determined by measuring the ambient aerosol size distribution with two DMPS at the sampling points P0 and P2 for different radial positions relative to the tube centre (0, 40 and 52 mm) at P2 (Gruening et al., 2009). Data show a small loss of particles towards the rim of the tube can be observed, but it stays below 15 %. The bigger deviation for particles smaller than 20 nm is again a result of very small particle number concentrations in this diameter range and thus rather big counting errors.

*PM$_{10}$ Mass Concentration: Tapered Element Oscillating Mass balance (TEOM), Series 1400a*

*Thermo FDMS – TEOM (S/N 140AB233870012 & 140AB253620409)*

The Series 1400a TEOM® monitor incorporates an inertial balance patented by Rupprecht & Patashnick, now Thermo Scientific. It measures the mass collected on an exchangeable filter cartridge by monitoring the frequency changes of a tapered element. The sample flow passes through the filter, where particulate matter is collected, and then continues through the hollow tapered element on its way to an electronic flow control system and vacuum pump. As more mass collects on the exchangeable filter, the tube's natural frequency of oscillation decreases. A *direct* relationship exists between the tube's change in frequency and mass on the filter. The TEOM mass transducer does not require recalibration because it is designed and constructed from non-fatiguing materials. However, calibration was verified twice in 2016 using a filter of known mass.

The instrument set-up includes a Sampling Equilibration System (SES) that allows a water strip-out without sample warm up by means of Nafion Dryers. In this way the air flow RH is reduced to < 30%, when TEOM® operates at 30°C only. The Filter Dynamic Measurement System (FDMS) is based on measuring changes of the TEOM filter mass when sampling alternatively ambient and filtered air. The changes in the TEOM filter mass while sampling filtered air is attributed to sampling (positive or negative) artefacts, and is used to correct changes in the TEOM filter mass observed while sampling ambient air.

*Particle Number Size Distribution: Differential Mobility Particle Sizer (DMPS)*

*DMPS "B, DMA serial no. 158", CPC TSI 3772 (S/N 70847419 and 3772133103), neutraliser $^{85}Kr$ 10 mCi (2007)*

The Differential Mobility Particle Sizer consists of a home-made medium size (inner diameter 50 mm, outer diameter 67 mm and length 280 mm) Vienna-type Differential Mobility Analyser (DMA) and a Condensation Particle Counter (CPC), TSI 3772. Its setup follows the ACTRIS specifications for DMPS systems.

DMAs use the fact that electrically charged particles move in an electric field according to their electrical mobility. Electrical mobility depends mainly on particle size and electrical charge. Atmospheric particles are brought in the bipolar charge equilibrium in the bipolar diffusion charger (Eckert & Ziegler neutralizer with 370 MBq): a radioactive source ($^{85}$Kr) ionises the surrounding atmosphere into positive and negative ions. Particles carrying a high charge can discharge by capturing ions of opposite polarity. After a very short time, particles reach a charged equilibrium such that the aerosol carries the bipolar Fuchs-Boltzman charge distribution. A computer program sets stepwise the voltage between the 2 DMA's electrodes (from 10 to 11500 V). Negatively charged particles are so selected according to their mobility. After a certain waiting time, the CPC measures the number concentration for each mobility bin. The result is a particle mobility distribution. The number size distribution is calculated from the mobility distribution by an inversion routine (from Stratmann and Wiedensohler, 1996) based on the bipolar charge distribution and the size dependent DMA transfer function. The DMPS measures aerosol particles in the range 10 - 800 nm with a 12 minute cycle. It records data using 45 size channels for high-resolution size information. This submicrometer particle sizer is capable of measuring concentrations in the range from 1 to $2.4 \times 10^6$ particles $cm^{-3}$. Instrumental parameters that are necessary for data evaluation such as flow rates, relative humidity, ambient pressure and temperature are measured and saved as well.

The CPC detection efficiency curve and the particle diffusion losses in the system are taken into account at the data processing stage.

Accessories include:

- FUG High voltage cassette power supplies Series HCN7E – 12500 Volts.

- Rotary vacuum pump vane-type (sampling aerosol at 1 LPM)

- Controlled blower (circulating dry sheath air)

- Nafion dryers for the sheath and sample air streams, implemented since October 2009.

- Mass flow meter and pressure transducer (to measure sheath air and sample flows).

*Particle Number Size Distribution: Aerodynamic Particle Sizer (APS)*

*APS TSI 3321 (S/N 70535014 & S/N 1243)*

The APS 3321 is a time-of-flight spectrometer that measures the velocity of particles in an accelerating air flow through a nozzle.

Ambient air is sampled at 1 L $min^{-1}$, sheath air (from the room) at 4 L $min^{-1}$. In the instrument, particles are confined to the centre-line of an accelerating flow by sheath air. They then pass through two broadly focused laser beams, scattering light as they do so. Side-scattered light is collected by an elliptical mirror that focuses the collected light onto a solid-state photodetector, which converts the light pulses to electrical pulses. By electronically timing the gap between the peaks of the pulses, the velocity can be calculated for each individual particle.

Velocity information is stored in 1024 time-of-flight bins. Using a polystyrene latex (PSL) sphere calibration, which is stored in non-volatile memory, the APS Model 3321 converts each time-of-flight measurement to an aerodynamic particle diameter. For convenience, this particle size is binned into 52 channels (on a logarithmic scale).

The particle range spanned by the APS is 0.5 - 20 $\mu$m in both aerodynamic size and light-scattering signal. Particles are also detected in the 0.3 to 0.5 $\mu$m range using light-scattering alone, and are binned together in one channel. The APS is also capable of storing correlated light-scattering-signal. *dN/dLogDp* data are averaged over 10 min.

*Particle Scattering and Backscattering Coefficient*

*Integrating Nephelometer TSI 3563 (S/N 1081 & S/N 142101)*

The integrating nephelometer is a high-sensitivity device capable of measuring the scattering properties of aerosol particles. The nephelometer measures the light scattered by the aerosol and then subtracts the light scattered by the walls of the measurement chamber, light scattered by the gas, and electronic noise inherent in the detectors.

Dried ambient air (since 18.11.2009) was sampled at 5.1 L min$^{-1}$ (12 L min$^{-1}$ from Dec. 14th) from a PM10 inlet. .

The three-color detection version of TSI nephelometer detects scattered light intensity at three wavelengths (450, 550, and 700 nm). Normally the scattered light is integrated over an angular range of 7–170° from the forward direction, but with the addition of the backscatter shutter feature to the Nephelometer, this range can be adjusted to either 7–170° or 90–170° to give total scatter and backscatter signals. A 75 Watt quartz-halogen white lamp, with a built-in elliptical reflector, provides illumination for the aerosol. The reflector focuses the light onto one end of an optical pipe where the light is carried into the internal cavity of the instrument. The optical pipe is used to thermally isolate the lamp from the sensing volume. The output end of the optical light pipe is an opal glass diffuser that acts as a *quasi*-cosine (Lambertian) light source. Within the measuring volume, the first aperture on the detection side of the instrument limits the light integration to angles greater than 7°, measured from the horizontal at the opal glass. On the other side, a shadow plate limits the light to angles less than 170°. The measurement volume is defined by the intersection of this light with a viewing volume cone defined by the second and fourth aperture plates on the detection side of the instrument. The fourth aperture plate incorporates a lens to collimate the light scattered by aerosol particles so that it can be split into separate wavelengths. The nephelometer uses a reference chopper to calibrate scattered signals. The chopper makes a full rotation 23 times per second. The chopper consists of three separate areas labelled "signal", "dark", and "calibrate". The "signal" section simply allows all light to pass through unaltered. The "dark" section is a very black background that blocks all light. This section provides a measurement of the photomultiplier tube (PMT) background noise. The third section is directly illuminated to provide a measure of lamp stability over time. To reduce the lamp intensity to a level that will not saturate the photomultiplier tubes, the "calibrate" section incorporates a neutral density filter that blocks approximately 99.9 % of the incident light. To subtract the light scattered by the gas portion of the aerosol, a high-efficiency particulate air (HEPA) filter is switched in line with the inlet for 300 s every day at 08:00 UTC. This allows compensation for changes in the background scattering of the nephelometer, and in gas composition that will affect Rayleigh scattering of air molecules with time. When the HEPA filter is not in line with the inlet, a small amount of filtered air leaks through the light trap to keep the apertures and light trap free of particles. A smaller HEPA filter allows a small amount of clean air to leak into the sensor end of the chamber between the lens and second aperture. This keeps the lens clean and confines the aerosol light scatter to the measurement volume only.

Nephelometer data are corrected for angular non idealities and truncation errors according to Anderson and Ogren, 1998. A Nafion dryer has been installed (18.11.2009) at the inlet to measure light scattering by dry aerosols. Internal RH generally ranges from 0 to 40 % (average 21%, 90$^{th}$ percentile 42% in 2016). At 40% RH, aerosol scattering would be on average increased by about 15% compared to 0% RH in Ispra (Adam et al., 2012). However, aerosol particle scattering coefficients presented in this report are **not** corrected for RH effects, except when specified.

*Particle Absorption Coefficient*

*Aethalometer Magee AE-31 ('A' S/N 408:0303 & 'B' S/N 740:0609)*

The principle of the Aethalometer is to measure the attenuation of a beam of light transmitted through a filter, while the filter is continuously collecting an aerosol sample. Suction is provided by an internally-mounted pump. Attenuation measurements are made at successive regular intervals of a time-base period. The objectives of the Aethalometer hardware and software systems are as follows:

(a) to collect the aerosol sample with as few losses as possible on a suitable filter material;

(b) to measure the optical attenuation of the collected aerosol deposit as accurately as possible;

(c) to calculate the rate of increase of the equivalent black carbon (EBC) component of the aerosol deposit and to interpret this as an EBC concentration in the air stream;

(d) to display and record the data, and to perform necessary instrument control and diagnostic functions.


The optical attenuation of the aerosol deposit on the filter is measured by detecting the intensity of light transmitted through the spot on the filter. In the AE-31, light sources emitting at different wavelengths (370, 470, 520, 590, 660, 880 and 950 nm) are also installed in the source assembly. The light shines through the lucite aerosol inlet onto the aerosol deposit spot on the filter. The filter rests on a stainless steel mesh grid, through which the pumping suction is applied. Light penetrating the diffuse mat of filter fibres can also pass through the spaces in the support mesh. This light is then detected by a photodiode placed directly underneath the filter support mesh. As the EBC content of the aerosol spot increases, the amount of light detected by the photodiode will diminish.

For better accuracy, additional measurements are necessary: the amount of light penetrating the combination of filter and support mesh is relatively small, and a correction is needed for the 'dark response signal' of the overall system. This is the electronics' output when the lamps are off: typically, it may be a fraction of a percent of the response when the lamps are on. To eliminate the effect of the dark response, we take 'zero' readings of the system response with the lamps turned off, and subtract this 'zero' level from the response when the lamps are on.

The other measurement necessary is a 'reference beam' measurement to correct for any small changes in the light intensity output of the source. This is achieved by a second photodiode placed under a different portion of the filter that is not collecting the aerosol, on the left-hand side where the fresh tape enters. This area is illuminated by the same lamps. If the light intensity output of the lamps changes slightly, the response of this detector is used to correct mathematically the 'sensing' signal. The reference signal is also corrected for the dark response 'zero' as described above.

The algorithm in the computer program (see below) can account for changes in the lamp intensity output by always using the ratio quantity [Sensing]/[Reference]. As the filter deposit accumulates EBC, this ratio will diminish.

In practice, the algorithm can account for lamp intensity fluctuations to first order, but we find a residual effect when operating at the highest sensitivities. To minimize this effect and to realize the full potential of the instrument, it is desirable for the lamps' light output intensity to remain as constant as possible from one cycle to the next, even though the lamps are turned on and off again. The computer program monitors the repeatability of the reference signal, and issues a warning message if the fluctuations are considered unacceptable. When operating properly, the system can achieve a reference beam repeatability of better than 1 part in 10000 from one cycle to the next. The electronics circuit board converts the optical signals directly from small photocurrents into digital data, and passes it to the computer for calculation. A mass flow meter monitors the sampled air flow rate. These data and the result of the EBC calculation are written to disk and displayed on the front panel of the instrument.

Aethalometer data can be corrected for the shadowing effect and for multiple-scattering in the filter to derive the aerosol absorption coefficient (Arnott et al., 2005) with a correction factor C = 3.60, 3.65, and 3.95 for 470, 520 and 660 nm, respectively. Note that ACTRIS provisionally recommends the use of a constant conversion factor $C_0$ = 3.5 for all wavelengths (Mueller, 2015).

*Multi Angle Absorption Photometer (S/N 4254515)*

A Multi Angle Absorption Photometer (MAAP) model 5012 from Thermo Scientific was installed at the EMEP station in September 2008 and provides equivalent black carbon concentrations (EBC) and aerosol absorption ($\alpha$) data at a nominal wavelength of 670 nm. Note that during a EUSAAR workshop (www.eusaar.org) in 2007 it has been observed that the operating wavelength of all MAAP instruments present at that workshop was 637 nm with a line width of 18 nm (full width at half maximum). The operating wavelength of this MAAP instrument has not been measured yet, therefore it is assumed to work at 670 nm as stated by the manufacturer.

The MAAP is based on the principle of aerosol-related light absorption and the corresponding atmospheric equivalent black carbon (EBC) mass concentration. Model 5012 uses a multi angle absorption photometer to analyse the modification of scattering and absorption in the forward and backward hemisphere of a glass-fibre filter caused by deposited particles. The internal data inversion algorithm of the instrument is based on a radiation transfer model and explicitly takes into account multiple scattering processes inside the deposited aerosol and between the aerosol layer and the filter matrix (see Petzold et al., 2004).

The sample air is drawn into the MAAP and aerosols are deposited onto the glass fibre filter tape. The filter tape accumulates the aerosol sample until a threshold value is reached, then the tape is automatically advanced. Inside the detection chamber (Fig. 18), a 670-nanometer light emitting diode is aimed towards the deposited aerosol and filter tape matrix. The light transmitted into the forward hemisphere and reflected into the back hemisphere is measured by a total of five photo-detectors. During sample accumulation, the light intensities at the different photo-detectors change compared to a clean filter spot. The reduction of light transmission, change in reflection intensities under different angles and the air sample volume are continuously measured during the sample period. With these data and using its proprietary radiation transfer scheme, the MAAP calculates the equivalent black carbon concentration (EBC) as the instruments measurement result.

Using the specific absorption cross section $\sigma_{BC}$ = 6.6 m$^2$/g of equivalent black carbon at the operation wavelength of 670 nm, the aerosol absorption ($\alpha$) at that wavelength can be readily calculated as:

$$\alpha = EBC \times \sigma_{BC} \qquad Eq.\ 1$$
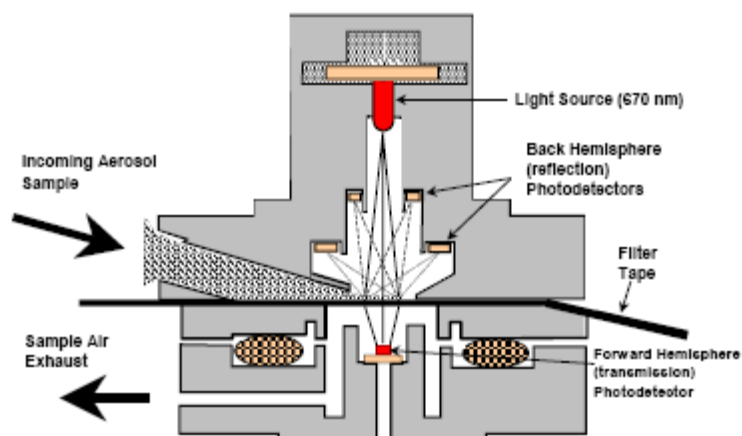


*Fig. 18: MAAP detection chamber (sketch from the manual of the instrument).*

*Range-Resolved Aerosol Light Backscattering and Extinction*

*Raymetrics Aerosol Raman Lidar (S/N 400-1-12, QUANTEL Brilliant B Laser and cooler S/N 120059004 and S/N 120034401, LICEL Transient Recorder & Hi Voltage Supply S/N BS3245 and BS3245b, industrial PC S/N TPL-1571H-D3AE)*

LiDAR measurements are based on the time resolved detection of the backscattered signal of a short laser pulse that is sent into the atmosphere (for an introduction see Weitkamp, 2005). Using the speed of light, time is converted to the altitude where the backscattering takes place. Using the particle-free range of the atmosphere for calibration (where Rayleigh scattering from the air molecules is known), aerosol backscattering and extinction coefficients as well as aerosol optical thickness can be derived using the LIDAR equation. The received power P of the detector is therein given as a function of distance and wavelength by *Eq. 2*:

$$P(R,\lambda) = P_0 \, {}^{c\tau}\!/_2 \, A\eta \, \frac{O(R)}{R^2} \beta(R,\lambda) \exp\left(-2\int_0^R \alpha(r,\lambda)dr\right)$$

*Eq. 2: $P_0$: Power of the laser pulse, c: speed of light, $\tau$: laser pulse length, A: area of the telescope, $\eta$: system efficiency, R: distance, O: overlap function (between laser beam and receiving optics field of view), $\lambda$: wavelength, $\beta$: backscatter coefficient, $\alpha$: absorption coefficient*

The instrument itself was installed on October 8-11th, 2012, and accessories (including radar) on December 11-13, 2012. This lidar emits at 3 wavelengths from IR to UV (1064 nm, polarised-532 nm, 355 nm) and records at 5 wavelengths, namely the emission wavelengths and two vibrational Raman channels at 387 and 607 nm. Measurements at 1064 nm, 532 nm, and 355 nm provide aerosol backscatter profiles, while measurements at 687 nm, and 387 nm provide aerosol extinction profiles during the dark hours of the day. The depolarisation of the 532 nm light beam is also measured. After the re-intallation of the laser in Nov. 2015, the instrument was run in 2016 with a 5 min integration time during time slots covering noon (Mondays) and sunset (Mondays and Thursdays) according to the ACTRIS schedule, and during Calipso overpasses (about once every 8 days at 01:40 or 12:30). Data are inverted using the online Single Calculus Chain developed by EARLINET, after pre-processing to cope with new requirements for submitting data to the ACTRIS-EARLINET data bank.

### 4.2.2.2 Sampling and off-line analyses

Particulate Matter

*Particle sampler: Partisol 2025 S/N 2025B22156220203*
*Micro-balance: MC5 S/N 50208287*
*Ion Chromatographs: ICS 2000 S/N 07101404 and 07101405 and DX-120 (Jan.-Feb.)*
*OC-EC analyser: Sunset Lab OCEC analyser S/N 173.*

$PM_{2.5}$ was continuously sampled at 16.7 L min$^{-1}$ on quartz fibre filters with a Partisol sampler equipped with a carbon honeycomb denuder. The sampled area is 42 mm Ø. Filters were from PALL Life Sciences (type TISSUEQUARTZ 2500QAT-UP). Filter changes occurred daily at 08:00 UTC.

Filters were weighed at 20 % RH before and after sampling with a microbalance Sartorius MC5 placed in a controlled (dried or moisture added and scrubbed) atmosphere glove box. They were stored at 4 °C until analysis.

Main ions ($Cl^-$, $NO_3^-$, $SO_4^{2-}$, $C_2O_4^{2-}$, $Na^+$, $NH_4^+$, $K^+$, $Mg^{2+}$, $Ca^{2+}$) were analysed by ion chromatography with electrochemical eluent suppression (ICS2000) after extraction of the soluble species from an aliquot of 16 mm Ø in 10 ml 18.2 MOhm cm resistivity water (Millipore mQ).

Organic and elemental carbon (OC+EC) were analysed using a Sunset Dual-optical Lab Thermal-Optical Carbon Aerosol Analyser (S/N 173-5). $PM_{2.5}$ samples were analysed using the EUSAAR-2 thermal protocol according to EN 16909. It has been developed to minimize biases inherent to thermo-optical analysis of OC and EC (Cavalli et al., 2010), and is described in the table below.

No measurement of $PM_{10}$ or $PM_{coarse}$ was performed in 2016.

*Table 2: Parameters of the EUSAAR-2 analytical protocol*

| Fraction Name | Plateau Temperature (°C) | Duration (s) | Carrier Gas |
|---|---|---|---|
| OC 1 | 200 | 120 | He 100% |
| OC 2 | 300 | 150 | He 100% |
| OC 3 | 450 | 180 | He 100% |
| OC 4 | 650 | 180 | He 100% |
| cool down | | 30 | He 100% |
| EC1 | 500 | 120 | He:O$_2$ 98:2 |
| EC2 | 550 | 120 | He:O$_2$ 98:2 |
| EC3 | 700 | 70 | He:O$_2$ 98:2 |
| EC4 | 850 | 110 | He:O$_2$ 98:2 |

Wet-only deposition

*Precipitation sampler:* Eigenbrodt *Model NSA 181/KS S/N 3313 and 3312*
*Conductimeter and pH-meter: Sartorius Professional Meter PP-50 S/N 16350322.*
*Ion Chromatographs: ICS 2000 S/N 07101404 and 07101405*
For precipitation collection, two wet-only samplers were used that automatically collect the rainfall in a 1 L polyethylene container. The collection surface is 550 cm$^2$. 24-hr integrated precipitation samples (if any) are collected every day starting at 8:00 UTC. All collected precipitation samples were stored at 4 °C until analyses (ca. every 3 months).Analyses include the determinations of pH and conductivity at 25 °C and principal ion concentrations ($Cl^-$, $NO_3^-$, $SO_4^{2-}$, $C_2O_4^{2-}$, $Na^+$, $NH_4^+$, $K^+$, $Mg^{2+}$, $Ca^{2+}$) by ion chromatography with electrochemical eluent suppression.

KOALA

CO

SO₂

O₃

O₃

NO, NO₂, NOₓ

APS          APS

TEOM        TEOM

Aethalo      Aethalo
meter        meter

EMEPACQ5

Nephelo      MAAP
meter

DMPS         EMEPDMAB

Solar radiation

T, RH, WS, WD

Prec. sampler

RACK002

LIDAR

LIDAR-PC

LAKE.JRC.IT

LAKE2.JRC.IT

Optical Fiber

IES.JRC.IT

RS 485 serial communication

LAN hub

RS 232 serial communication

Field Point, A/D converter

RS 485 to RS 232 serial converter

Multi serial RS 232 port
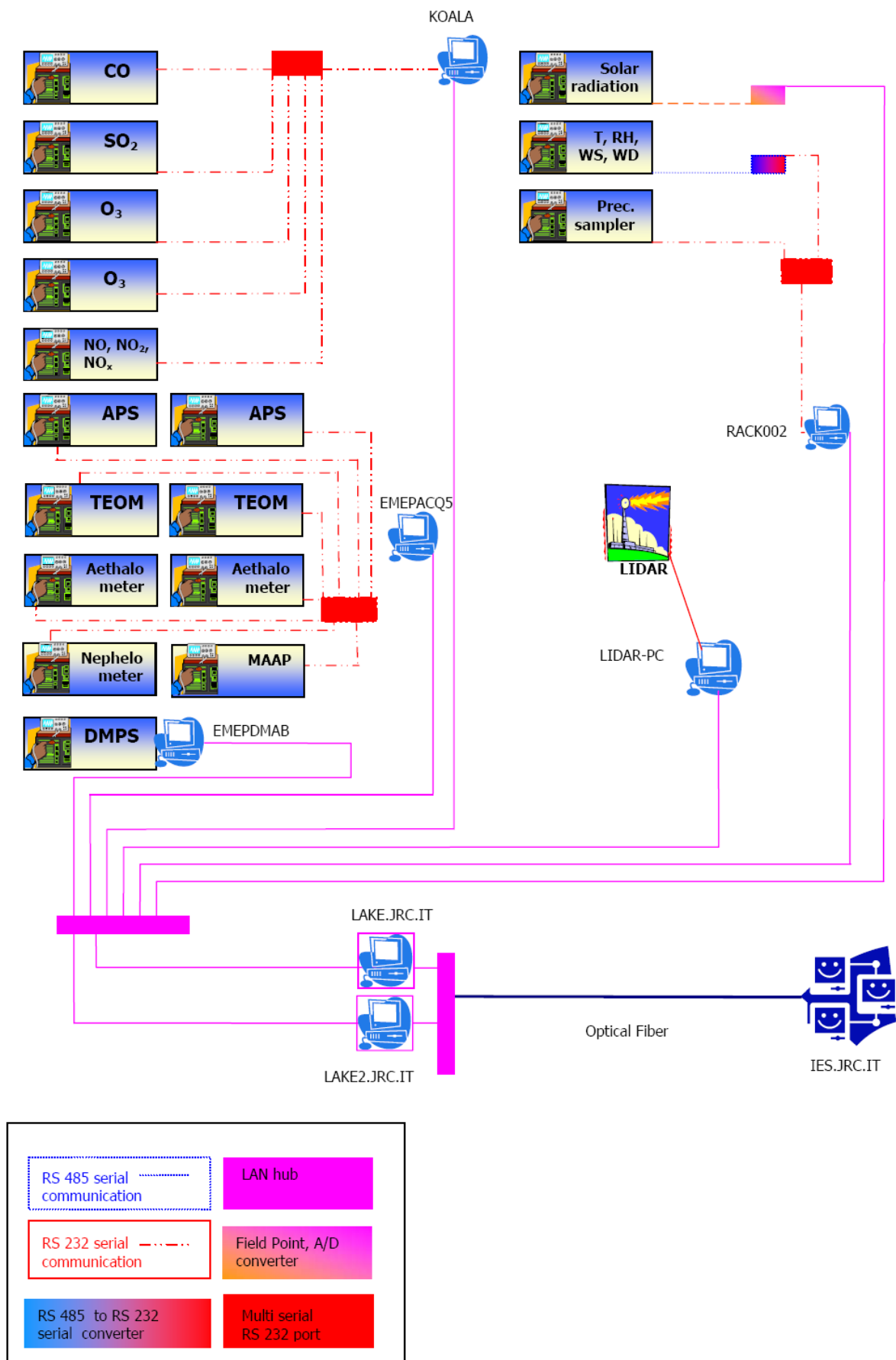
Fig. 19: Set-up of the EMEP- GAW station Data Acquisition System.

### 4.2.3 On-line data acquisition system/data management

The JRC EMEP-GAW station Data Acquisition System (DAS) is a specifically tailored set of hardware and software (developed by the Air and Climate unit, in collaboration with NOS Sistemi s.r.l), designed to operate instruments, acquire both analogue and digital output from instruments and store pre-processed measurement data into a database for further off-line evaluation. The DAS operated and controlled the instrumentation during 2016. No updates were implemented.

The software environment of the DAS is Labview 7.1 from [National Instruments](#) and the database engine for data storage is Microsoft SQL Server 2008.

The DAS is designed to continuously run the following tasks:

- Start of the data acquisition at a defined time (must be full hour);
- Choose the instruments that have to be handled;
- Define the database path where data will be stored (primary in the network, secondary local on the acquisition machine);
- Define the period (10 minutes currently used) for storing averaged data, this is the data acquisition cycle time;
- Obtain data (every 10 seconds currently set) for selected instruments within the data acquisition cycle:
  - o For analogue instruments (currently only the CMP11 Pyranometer), apply the calibration constants to translate the readings (voltages or currents) into analytical values;
  - o Send commands to query instruments for data or keep listening the ports for instruments that have self-defined output timing;
  - o Scan instruments outputs to pick out the necessary data;
- Calculate average values and standard deviations for the cycle period;
- Query instruments for diagnostic data (when available), once every 10 minutes;
- Store all data in a database
  - o With a single timestamp for the gas analysers, FDMS-TEOM and Nephelometer
  - o With the timestamp of their respective measurement for all other instruments.

The following instruments are managed with the DAS (Fig. 19), using three PCs (currently called Emepacq5, Koala and Rack002):

**Emepacq5:**

- Number size distribution for particles diameter >0.500 µm, APS
- On-line FDMS-TEOMs
- Aerosol light absorption, Aethalometer
- Aerosol light absorption, MAAP
- Aerosol light scattering, Nephelometer

**Koala:**

- o Reactive gases: CO, SO2, NO, $NO_2$, $NO_x$, $O_3$

**Rack002:**

- Solar radiation
- Weather transmitter (temperature, pressure, relative humidity, wind speed and direction, precipitation)
- Precipitation data

The data acquired are stored in a Microsoft SQL Server 2008 database on the central database *emep_db* hosted on the pc **Lake2.jrc.it**. If the local network is not available, data are stored in a local database on the acquisition pc itself. Each pc also has software for the synchronisation of **emep_db** with **local db.**

The PC "**Lake.jrc.it**" connects the laboratory to the JRC network (*ies.jrc.it* domain) via optical lines. The schematic setup of the data acquisition system is shown in Fig. 19.

The acquisition time is locally synchronised for all PCs via a network time server running on lake and is kept at UTC, without adjustment for summer/winter time. Data are collected in a data base called *emep_db* that runs on "**Lake2.jrc.it**".

**Lake** is the user gateway for the Station user, to allow granted staff to remotely access the acquisition computers. This PC is also used to share information (life cycle sheets, lidar data) between IES domain and the Station network.

In the web site the projects to which ABC-IS contributes and contact persons can also be retrieved.

The station web site (http://abc-is.jrc.ec.europa.eu/, not optimised under Internet Explorer) runs over two machines. The first is the web server, **ccuprod2**, in the DMZ (demilitarized zone), where the web page code runs and is managed by the Air and Climate Unit IT staff. The development environment was Python and Ajax. The second computer, **emepimag.jrc.it,** in the JRC network, queries the database for data, generate plots and store plots in a folder in ccuprod2, to make them available to the internet. This second machine is managed by ABC-IS data management team and the software has been developed in C-sharp.

## 4.2.4    Data evaluation

The structured data evaluation system (EMEP_Main.m) with a graphic user interface (see **Error! Reference source not found.**) has been used with Matlab Release R2007b (www.mathworks.com) as the programming environment.

The data evaluation is now done with the "EMEP_Data_Handling L0 to L2" vers. 1.9.8.5 - Sep 2016. The not evaluated 10 min data (flagged 3) is now exported to several excel sheets.

After a preliminary data analysis, these data are flagged according to the flags listed below. These files including flags are then imported into the database (level 1 data, 10 min corrected). Finally the hourly and the daily data averages are calculated taking into account the flagging.

| 0 | Good data – used |
|---|---|
| 1 | Good data – not used |
| 2 | Calibration |
| 3 | Not evaluated |
| 5 | questionable |
| 6 | Local contamination |
| 7 | Erroneous data |
| 9 | No data |

Only the evaluation of gas phase data has an automatic removal algorithm for outliers / spikes implemented: $d_i$ = 10 minute average value at time i, $std_i$ = standard deviation for the 10 minute average (both saved in the raw data)

if $std_i > 100 \cdot \overline{std}$ and $|d_i - d_{i\pm1}| > 10 \cdot \overline{std}$

$\Rightarrow d_i = 1/2(d_{i-1} + d_{i+1})$ for $d_{i-1}$ **and** $d_{i+1}$ **no** outliers,

otherwise $d_i = missig\ data$ .
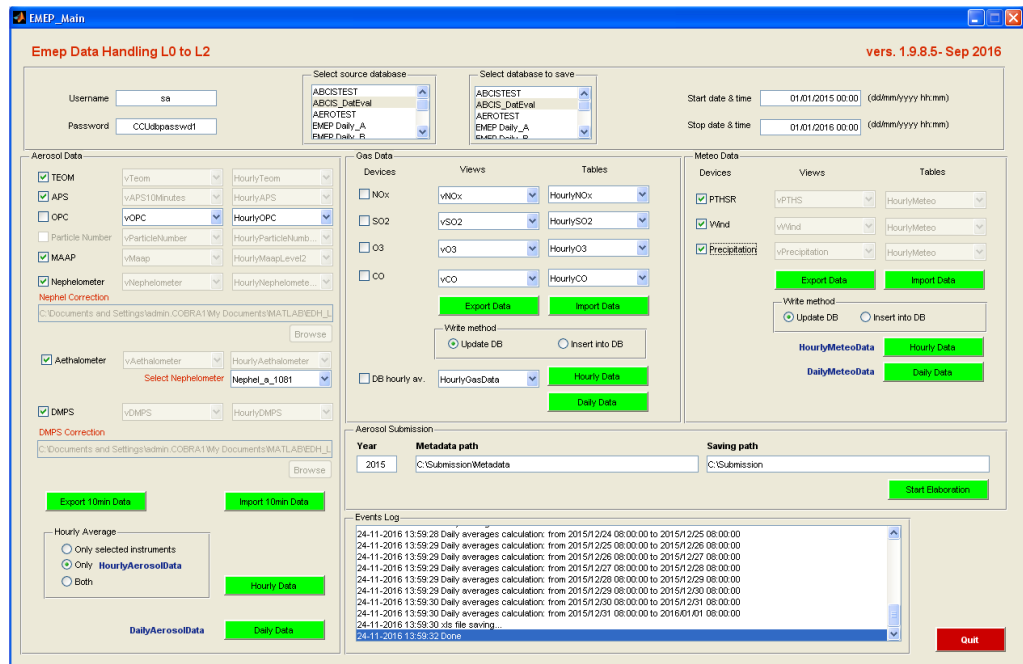


*Fig. 20:* Graphic user interface of the EMEP-GAW station data evaluation.

This algorithm corrects for single point outliers and removes double point outliers. All other situations are considered correct data. To check these data and to exclude outliers for all other measurements, a visual inspection of the 10 min data needs to be performed.

In addition, quick looks of evaluated data for selected time periods can be produced as well as printed timelines in the pdf-format for the evaluated data. All database connections are implemented via ODBC calls (Open DataBase Connectivity) to the corresponding Microsoft SQL server 2008.

Daily averages (8:00 < t ≤ 8:00 +1 day) of all variables and parameters stored in the hourly averages database can be calculated and are subsequently stored in a separate Microsoft SQL Server 2008 database.
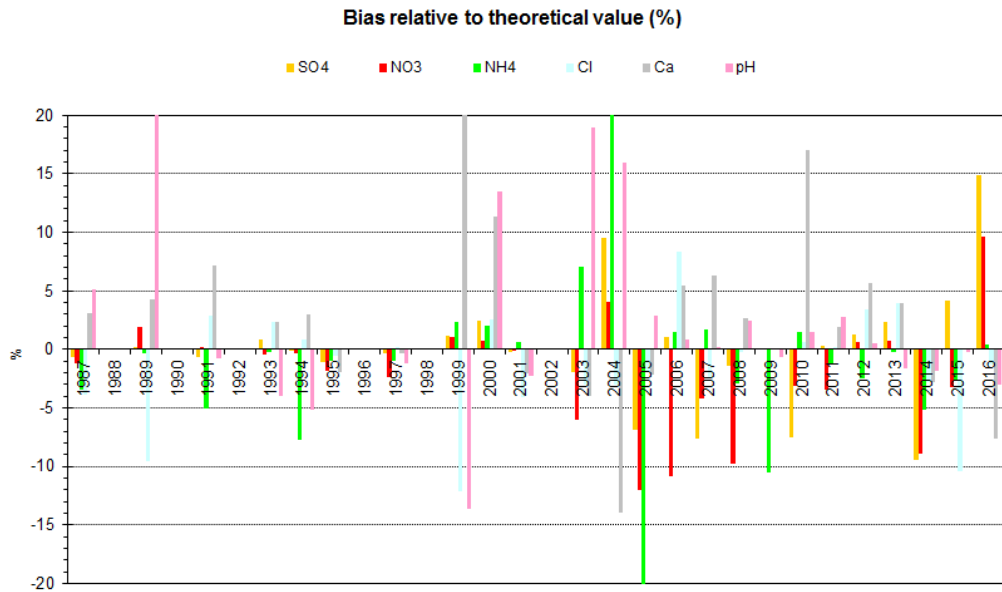
Fig. 21. EMEP inter-laboratory comparisons for rainwater analyses (1987-2016): JRC-Ispra results.
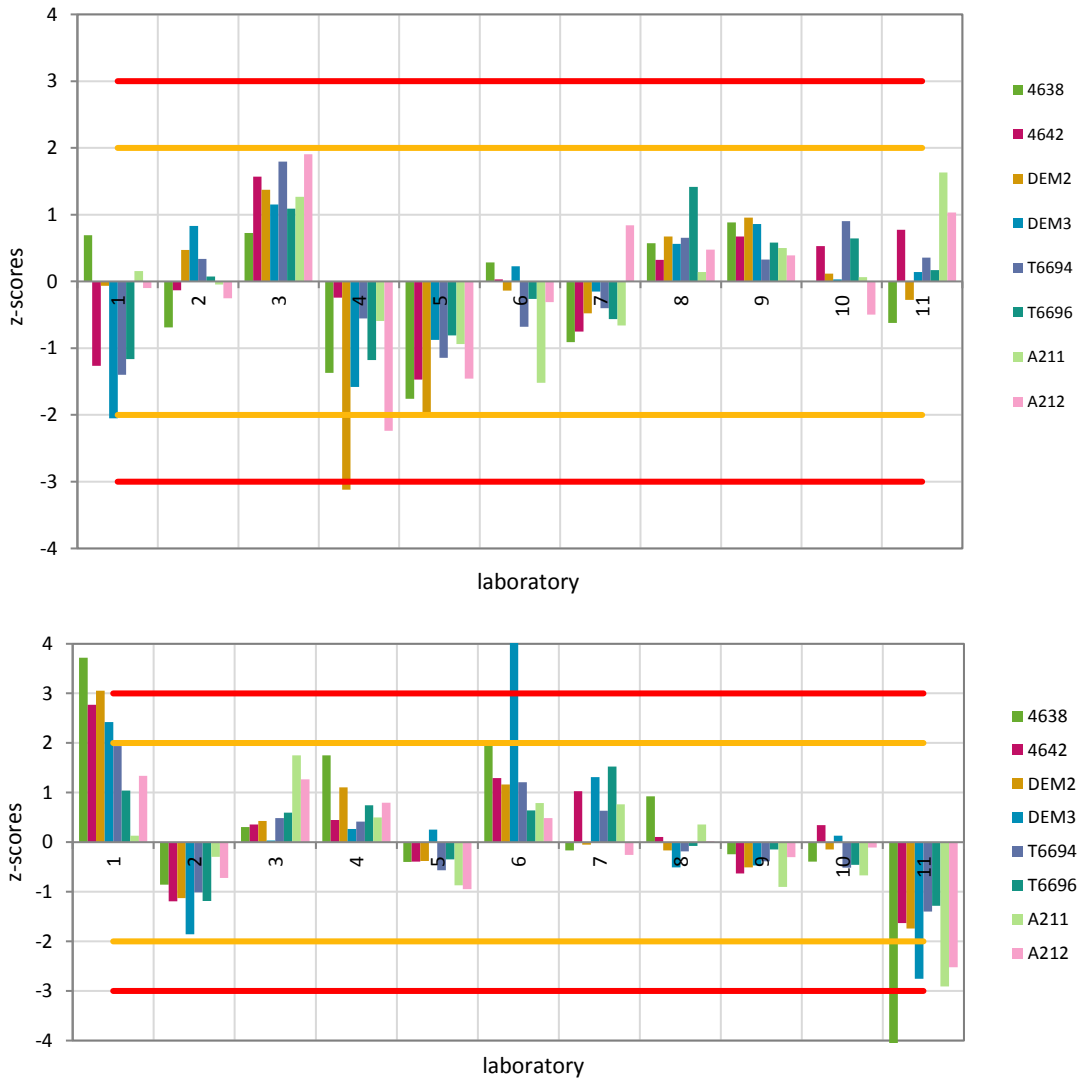


Fig. 22. JRC-Ispra instrument's (#10) performance for the determination of (top) total carbon (TC) and (bottom) elemental carbon (EC/TC ratio) during the ACTRIS inter-laboratory comparison 2016-1.

## 4.3    Quality assurance

At JRC level the quality system is based on the Total Quality Management philosophy, the implementation of which started at the Air and Climate Unit in December 1999. We have been working under ISO 9001 and ISO 14001 since 2010 (more information about our QMS system can also be found in the chapter "Quality management system").

Lacking personnel to specifically follow this business, the JRC-Ispra station for atmospheric research did not renew the accreditation for the monitoring of $SO_2$, $NO$, $NO_2$ and $O_3$ under EN 45001 obtained in 1999. However, measurements and standardised operating procedures are based on recommendations of the EMEP manual (1995, revised 1996; 2001; 2002; 2014), WMO/GAW 227, ISO and CEN standards. Moreover, the JRC-Ispra gas monitors and standards are checked by the European Reference Laboratory for Air Pollution (ERLAP) regularly. This includes annual preventive maintenance, linearity check and Gas Phase Titration (for $NO_x$).

For on-line aerosol measurements, ACTRIS Standard Operating Procedures and QA/QC requirements are followed. Those involve station audits, side by side instrument comparisons at the world calibration centre for aerosol physics (WCCAP) in Leipzig (DE), and specific QC measurements. The station was favourably audited by Dr. T. Tuch (WCCAP) on 22-24 March 2010 under the EUSAAR project (www.eusaar.net), as described in a specific report. The Differential Mobility Particle Sizer took part successfully in the side by side comparison in Leipzig on Jan.25-29th, 2016, see report.

Ion analysis quality was checked through the 34th annual EMEP inter-laboratory comparison (Fig. 21). In this exercise, all ion measurements in the rain water synthetic samples provided by NILU passed the quality test, except $NO_3^-$ (+15%) and $SO_4^{2-}$ (+9%). The mean error for pH measurements was -0.13. The data quality objective within EMEP is 10% accuracy or better for $NO_3^-$ and $SO_4^{2-}$ and 15% accuracy or better for other components for each sample.

The inter-laboratory comparison for organic and elemental carbon analyses organized under the competitive project ACTRIS-2 in 2016 indicates no systematic bias for the determination of total carbon and elemental carbon compared to the robust average among the participants (Fig. 22).

Quality check measurements are reported at least once a year to the ACTRIS Lidar Calibration Centre, which produces a detailed report on the instrument performance.

Data quality for all measurements is also checked whenever possible through comparison among different instruments, mass closure (for PM) and ion balance (for precipitation) exercises.
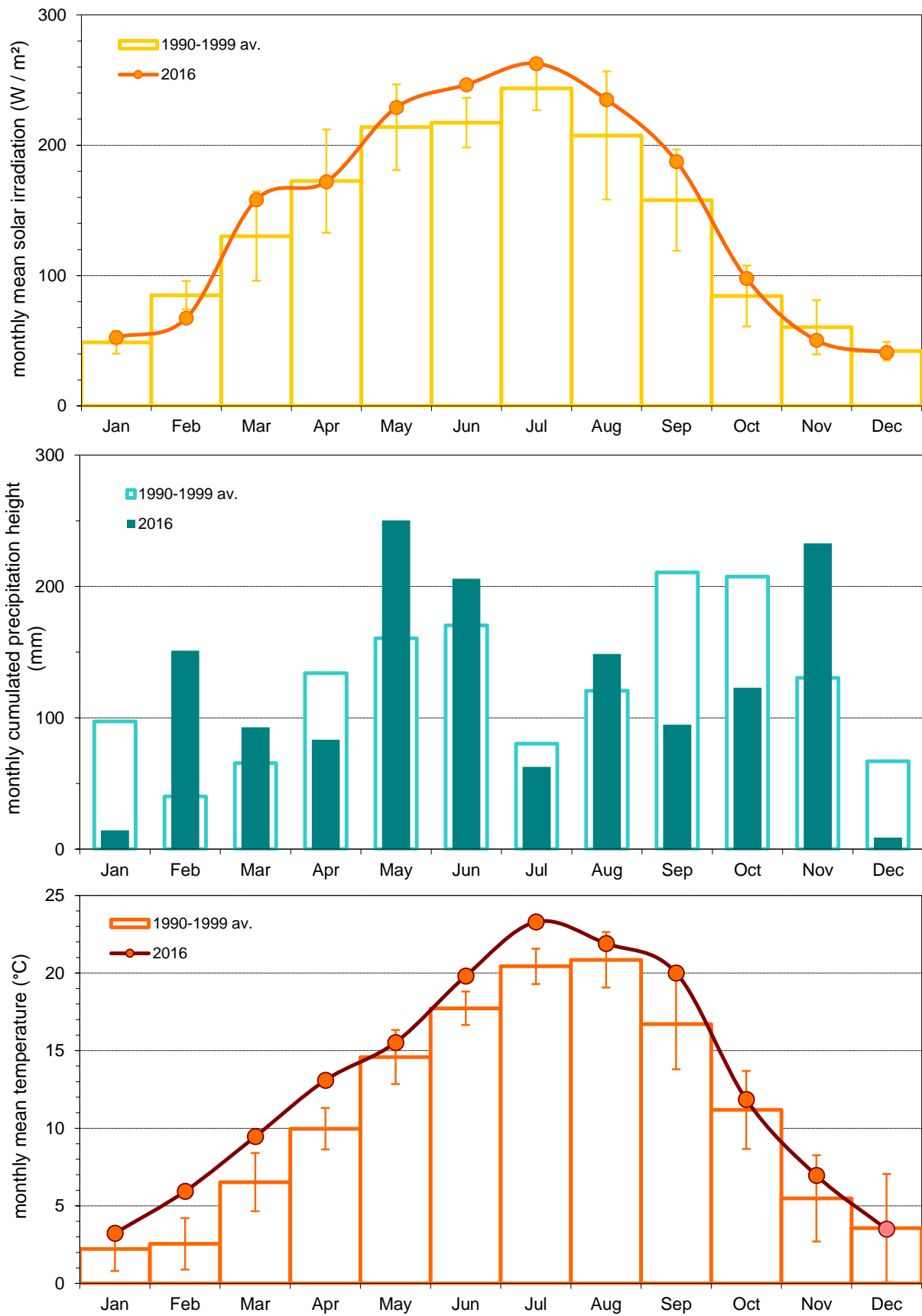
*Fig. 23. Solar global irradiation, precipitation amount, and temperature monthly values observed at the EMEP-GAW station of the JRC-Ispra in 2016, compared to the 1990-1999 period ± standard deviations.*

## 4.4    Results of the year 2016

### 4.4.1    Meteorology

Meteorological data were acquired directly at the EMEP site using a Pyranometer (solar radiation) and a weather transmitter (T, P, RH, precipitation) located at the provisional site at 4 and 5 m above the ground, respectively. Meteorological data are missing for the period 23-30 Dec. 2016. In Fig. 23, monthly values of these meteorological variables for 2016 are compared to the 1990-1999 average used as reference period.

The monthly mean solar radiation was significantly different from average in June only. 2016 was warmer compared to the reference period, especially from Feb. to July.

January and December were particularly dry, while February, May, and November were wetter than usual. The total yearly rainfall was 1470 mm, i.e. very similar to the 1990-1999 average (1484 mm).

### 4.4.2    Gas phase air pollutants

$SO_2$, CO, NOx and $O_3$ were measured almost continuously during the year 2016, except for 12 days in March (logistical constraints and instrument calibrations) and a total of 4 days a few gaps in March, June, and July (annual data coverage 93 -96 %). In addition, $O_3$ data are not available from Dec. 22nd. Expanded uncertainties were calculated to be 8% for $SO_2$, 7% for CO, 12% + 1.0 ppb for NO, 9% +1.4 ppb for $NO_2$ and 7% for $O_3$, which is in line with the *European Directive 2008/50/EC* (less than 15 % at the limit value). To render the time series comparable to the historical data acquired at the EMEP-GAW site at Bd 77p, *10 min $SO_2$, NOx and CO data were flagged for local contamination (1-8% of the data points), and hourly (and daily) averages were computed excluding the data points for which local contamination was identified*.

In 2016, the seasonal variations in $SO_2$, NO, $NO_2$, $NO_x$ and $O_3$ were similar to those observed over the 1990-1999 period (Fig. 24). Concentrations are generally highest during wintertime for primary pollutants ($SO_2$, CO, $NO_x$), and in summertime for $O_3$. Higher concentrations of $SO_2$, CO, $NO_x$ in winter result mainly from a least dispersion of pollutant during cold months (low boundary layer height and stagnant conditions), whereas the high concentration of $O_3$ during summer is due to enhanced photochemical production.

$SO_2$ concentrations (average = 0.7 µg/m³) were not significantly different to 2014 values, and about 6 times less compared to the reference period (1990-1999).

Daily mean CO concentrations ranged from 0.12 to 1.2 µg m$^{-3}$ (0.1 – 1.0 ppmv), which are typical values in a regional background station like the atmospheric observatory in Ispra. The lowest values were observed in very clean air masses during Föhn events and windy summer days, and the highest values during cold winter nights.
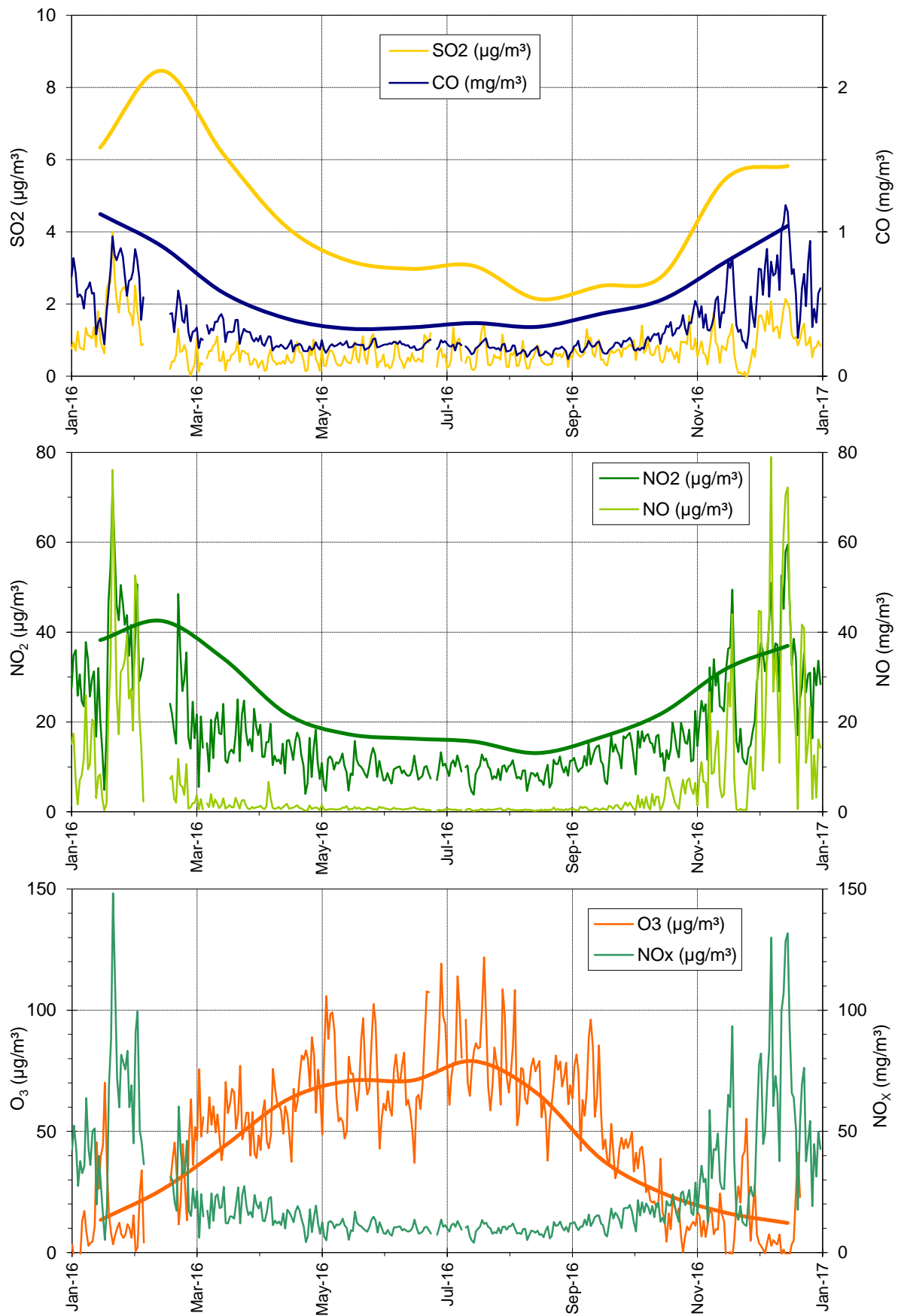
*Fig. 24. Seasonal variations of the 24 hr averaged concentrations of SO₂, CO, NO₂, NO, O₃ and NOₓ in 2016 (thin lines) and 1990-1999 monthly averages (thick lines: yellow=SO₂, blue=CO, green=NO₂, orange=O₃).*

NO$_2$ concentrations (annual average = 18 µg m$^{-3}$) were on average 30% lower than during 1990-1999 and similar to the 2014 values, i.e. 10% less than the 2015 levels. NO concentrations (annual average = 6.5 µg m$^{-3}$) were 35% greater than in 2014 and 2015. Due to the short atmospheric lifetime of NO, NO concentrations are much sensitive to the filtering for local contamination.

The temporal coverage for O$_3$ measurements was 93% in 2016, and measurements are lacking mainly in Feb. and Dec. (Fig. 16), when low levels occur (Fig. 24). O$_3$ indices for 2016 are therefore very robust. The annual average O$_3$ concentration in 2016 (48 µg m$^{-3}$, 24 ppb) was 4% lower than in 2015, and similar to 2014, i.e. in line with the relatively high O$_3$ concentrations observed since the early 2010's.

The vegetation exposure to above the ozone threshold of 40 ppb (AOT 40 = Accumulated dose of ozone Over a Threshold of 40 ppb, normally uses for "crops exposure to ozone") was 23230 ppb h, i.e. 20%less than in 2015, but about 50% more than 2014 (cloudy and wet summer).

For quantification of the health impacts (population exposure), the World Health Organisation uses the SOMO35 indicator (Sum of Ozone Means over 35 ppb, where means stands for maximum 8-hour mean over day), i.e. the accumulated ozone concentrations dose over a threshold of 35 ppb (WHO, 2008). In 2016, SOMO35 was 3360 ppb day (Fig. 25), again less than in 2015 (4030), and more than in 2014 (2950). Extreme O$_3$ concentrations (>180 µg m$^{-3}$ over 1 hour) were observed on 8 days in 2016, to be compared to 8, 18, 2, and 17 extreme events in 2012, 2013, 2014 and 2015, respectively. The value 180 µg m$^{-3}$ over 1 hour corresponds to the threshold above which authorities have to inform the public (European Directive 2008/50/EC on ambient air quality and cleaner air for Europe).
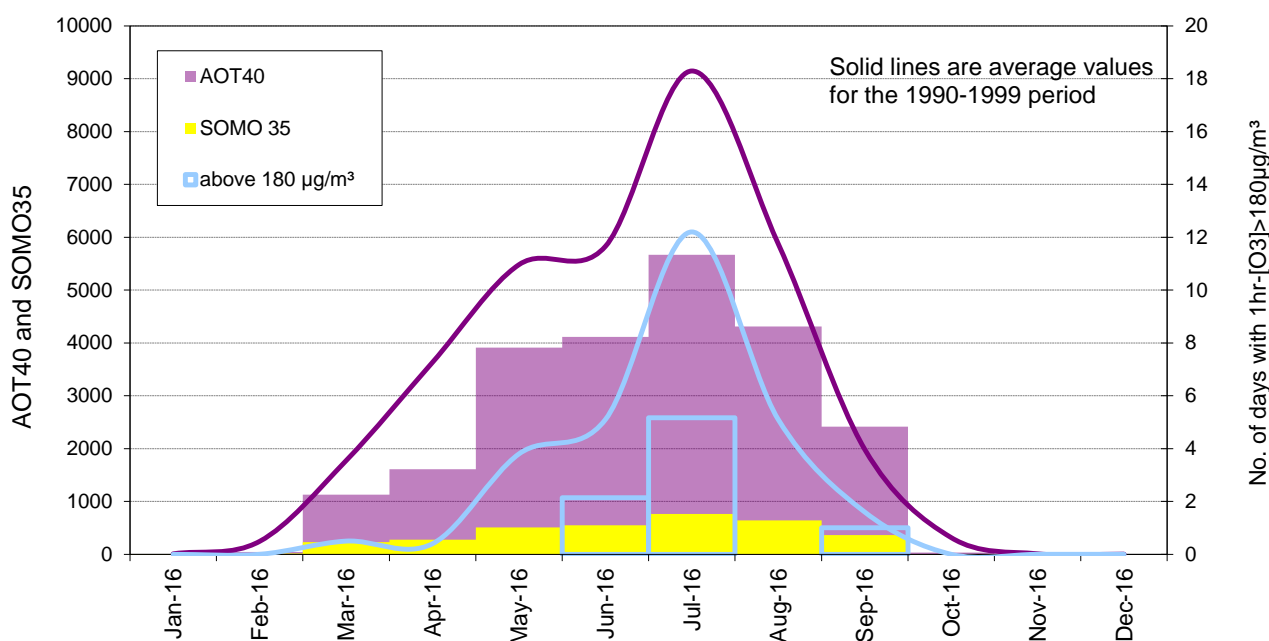


*Fig. 25: AOT 40 (ppb h), SOMO35 (ppb day) and number of exceedances of the 1-hour averaged 180 µg/m³ threshold values in 2016 (bars), and reference period values 1990-1999 (lines).*
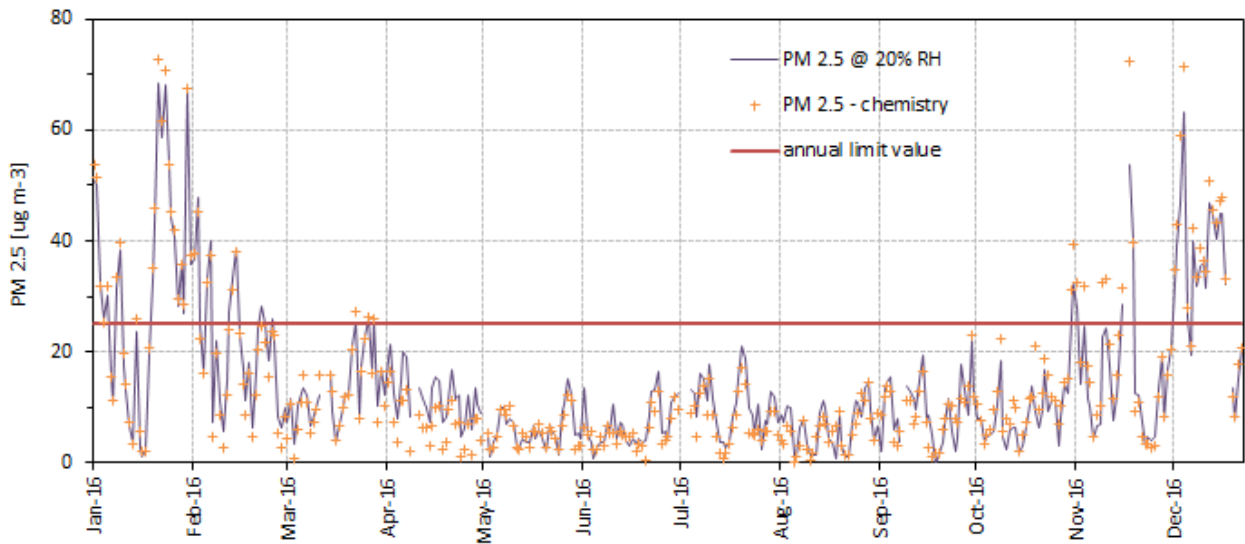
Fig. 26: 24hr-integrated PM$_{2.5}$ mass concentrations from off-line gravimetric measurements at 20 % RH and chemical determination of main constituents in 2016.The red line indicates the annual limit value of 25 µg/m³ to be reached by 2015 (European directive 2008/50/EC).
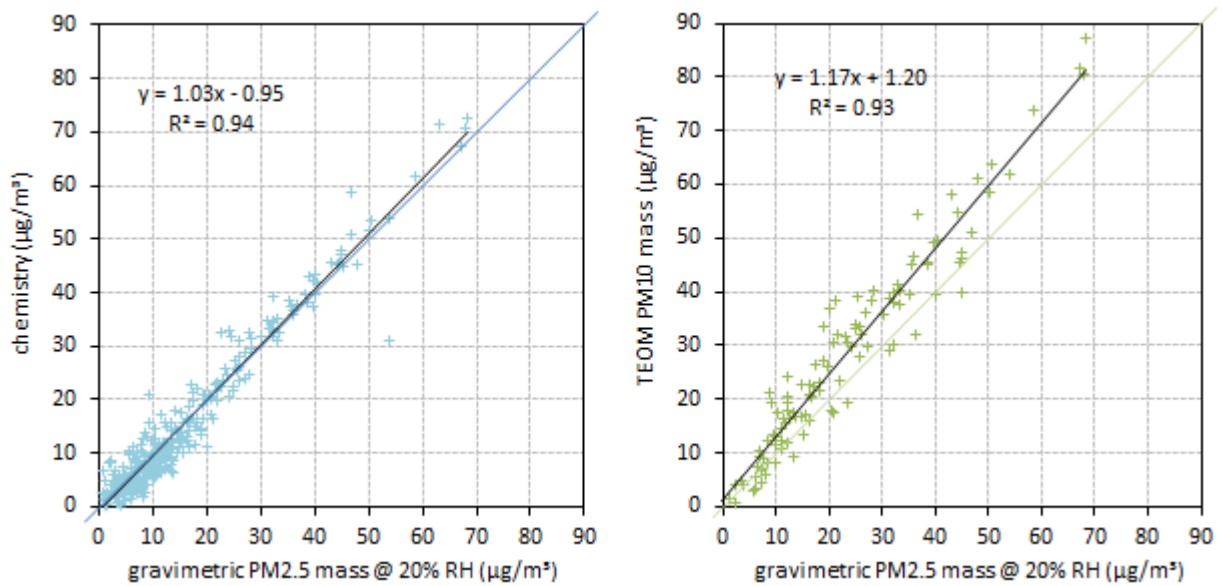


Fig. 27. Regressions between the gravimetric PM$_{2.5}$ measurements at 20 % RH and the sum of the PM$_{2.5}$ chemical constituents (left), and the FDMS-TEOM PM10 measurements (right) in 2016.

During the reference period 1990-1999, the information level of 180 µg m$^{-3}$ had been exceeded 29 times per year on average. The other "protection of human health factor" mentioned by the European Directive 2008/50/EC (120 µg m$^{-3}$ as maximum daily 8-hour average) was exceeded 77 times in 2016, leading to a 3-year average of 55 exceedances per year, well above the Directive threshold (25 exceedances per year).

### 4.4.3    Particulate phase

#### *4.4.3.1 Particulate matter mass concentrations*

PM$_{2.5}$ concentrations (Fig. 26) measured gravimetrically at 20 % relative humidity (RH) averaged 14.6 µg m$^{-3}$ over 2016 (data coverage = 97%). This was the 2$^{nd}$ lowest value observed since this measurement was started in 2002 (lowest value = 13.1 µg m$^{-3}$ in 2014), well below the European annual limit value of 25 µg m$^{-3}$ to be reached by 2015 (European directive 2008/50/EC). Gravimetric measurements of PM$_{2.5}$ mass at 20% RH and the sum of PM$_{2.5}$ mass constituents determined from chemical analyses are well correlated (Fig. 27), but relative differences increase with decreasing mass concentrations.

Due to severe technical problems, the annual data coverage for the FDMS-TEOM measurements of PM$_{10}$ was only 31%. The number of exceedances of the 24-hr limit value (50 µg m$^{-3}$) observed in 2016 (12) can therefore not be compared to the 21, 16, and 38 exceedances observed in 2015, 2014, and 2013, respectively. Likewise, the annual PM$_{10}$ average (28.4 µg m$^{-3}$) cannot be considered as representative of the year 2016.

The correlation between gravimetric PM$_{2.5}$ and PM$_{10}$ concentrations measured with a TEOM-FDMS (Fig. 27, right hand) was acceptable (R²=0.93) in 2016.The regression suggests an offset of about 1 µg m$^{-3}$ from the TEOM, and a ratio between PM$_{10}$ and PM$_{2.5}$ of 1.2 on average.
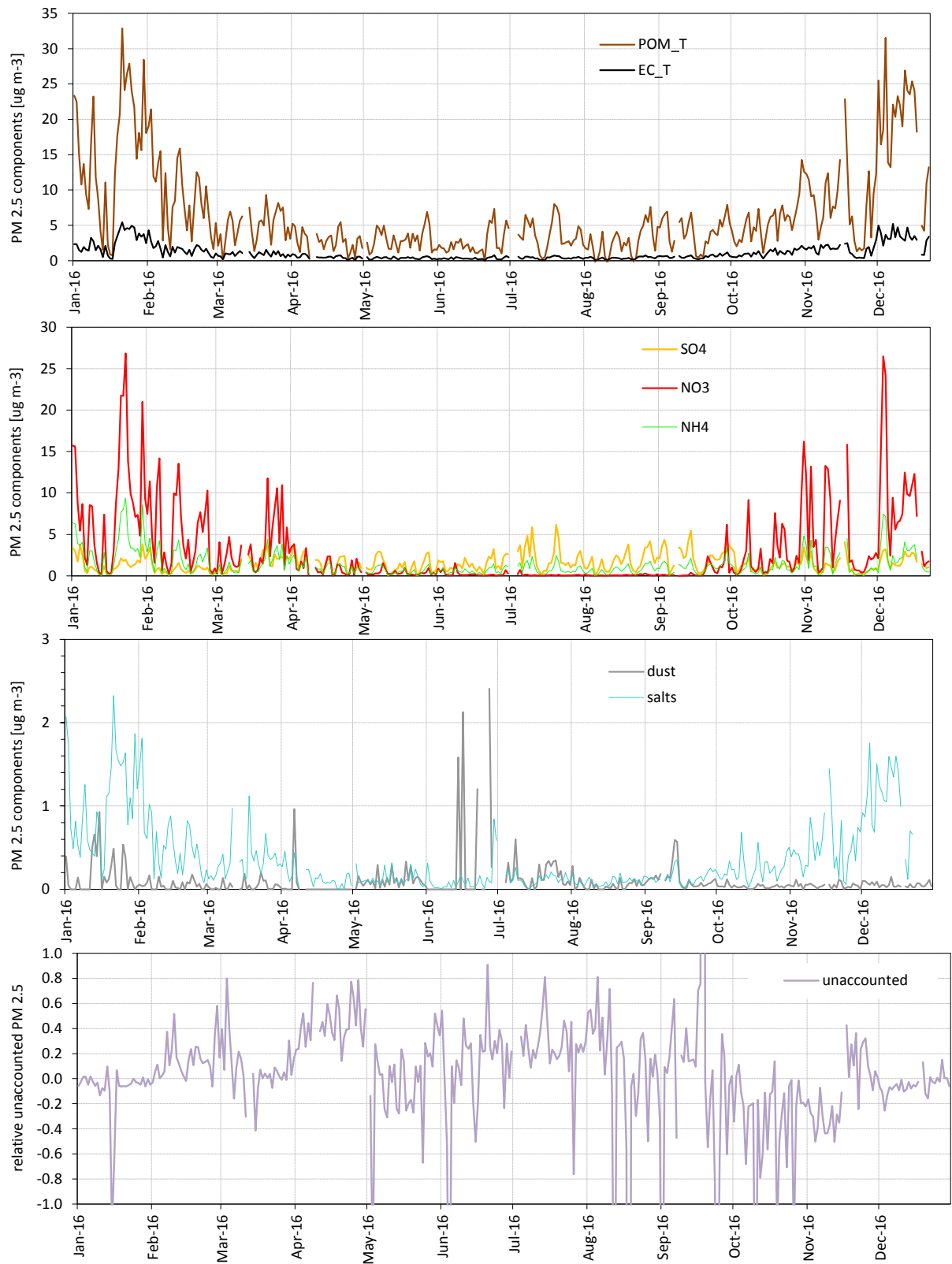
*Fig. 28. 24-hr integrated concentrations of the main PM₂.₅ constituents in 2016, and the relative unaccounted mass.*

### 4.4.3.2 PM$_{2.5}$ chemical composition

Main ions (Cl$^-$, NO$_3^-$, SO$_4^{2-}$, C$_2$O$_4^{2-}$, Na$^+$, NH$_4^+$, K$^+$, Mg$^{2+}$, and Ca$^{2+}$), OC and EC were determined from the quartz fibre filters collected for PM mass concentration measurements for the whole of 2016 (data coverage = 97%).

Fig. 28 shows the temporal variations in the PM$_{2.5}$ main components derived from these measurements. Particulate organic matter (POM) is calculated by multiplying OC (organic carbon) values by the 1.4 conversion factor to account for non-C atoms contained in POM (Russell et al., 2003). "Salts" include Na$^+$, K$^+$, Mg$^{2+}$, and Ca$^{2+}$. Dust is calculated from Ca$^{2+}$ concentrations and the regression (slope = 4.5) found between ash and Ca$^{2+}$ in the analyses of ash-less cellulose filters (Whatman 40) in previous years. Most components show seasonal variations with higher concentrations in autumn and winter, and lower concentrations in summer, like PM$_{2.5}$ mass concentration. This is mainly due to changes in pollutant horizontal and vertical dispersion, related to seasonal variations in meteorology (e.g. lower boundary layer in winter). The amplitude of the POM, NH$_4^+$ and NO$_3^-$ seasonal cycles may be enhanced due to equilibrium shifts towards the gas phase, and/or to enhanced losses (negative artefact) from quartz fibre filters during warmer months. Indeed, historical data (May – Sept. 2013) show that the concentration of NH$_4$NO$_3$ in PM$_{2.5}$ determined from filters can be 1/5 of the concentration measured in the submicron aerosol with an ACSM (see 2013 annual report).

NH$_4^+$ follows NO$_3^-$ + SO$_4^{2-}$ very well as indicated by the regression shown in Fig. 29. This correlation results from the atmospheric reaction between NH$_3$ and the secondary pollutants H$_2$SO$_4$ and HNO$_3$ produced from the oxidation of SO$_2$ and NO$_x$, respectively. The slope of this regression is very close to 1, which means that sufficient NH$_3$ was available in the atmosphere to neutralise both H$_2$SO$_4$ and HNO$_3$. This furthermore indicates that PM$_{2.5}$ aerosol was generally not very acidic in 2016.
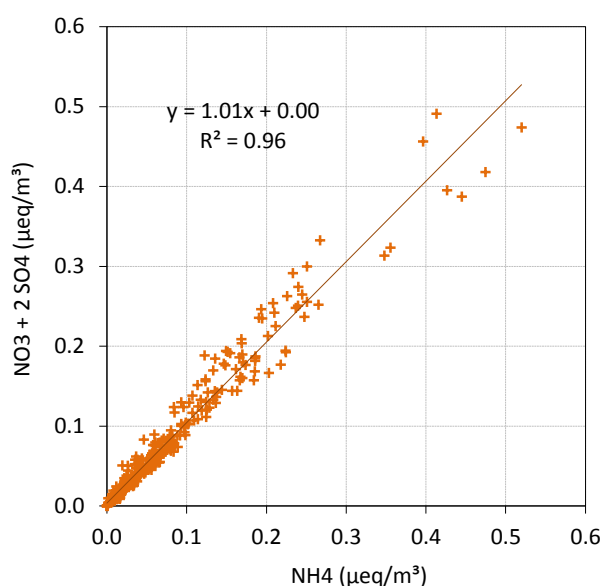


*Fig. 29. SO$_4^{2-}$ + NO$_3^-$ vs. NH$_4^+$ (µeq/m³) in PM$_{2.5}$ for 2016*
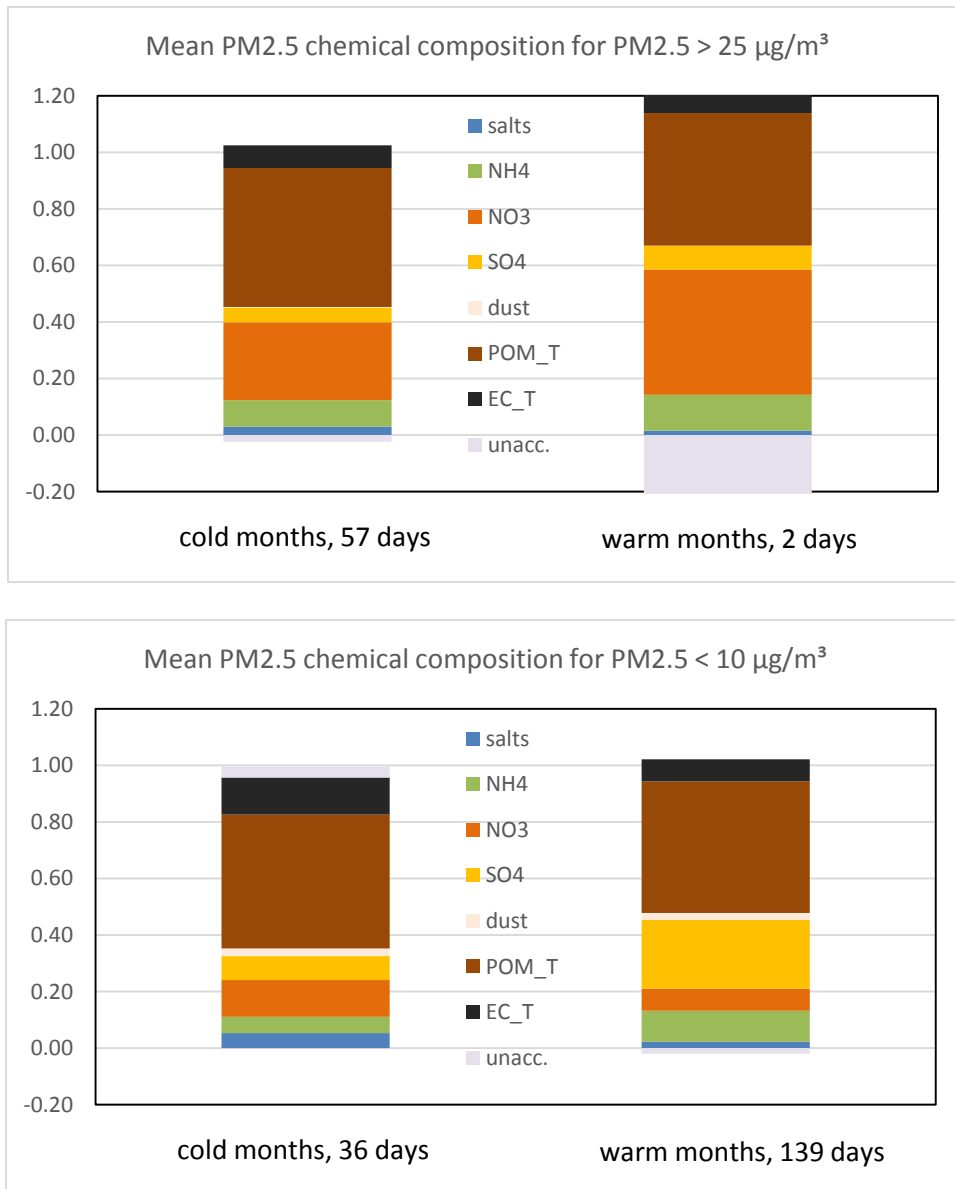
*Fig. 30: Average composition of $PM_{2.5}$ in 2016 for days on which $PM_{2.5}$ > 25 µg/m³ (top) and $PM_{2.5}$ < 10 µg/m³ (bottom), over cold (Jan., Feb., Mar., Nov., Dec.) and warm (Apr. – Oct.) months.*

### 4.4.3.3 Contribution of the main aerosol constituents to PM$_{2.5}$

The contributions of the main aerosol components to PM$_{2.5}$ are presented in Table 3 (annual averages) and in Fig. 30 (a) for days on which the "24-hr limit value for PM$_{2.5}$ of >25 µg/m³ was exceeded" during the cold months (Jan., Feb., March, Nov. and Dec., 57 cases) and the warm months (Apr. to Oct, 2 cases) and (b) for days on which 24-hr integrated PM$_{2.5}$ concentration was below 10 µg / m³ during cold (36 cases) and warm months (139 cases).

These PM$_{2.5}$ compositions may not always represent accurately the actual composition of particulate matter in the atmosphere (mainly due to possible negative sampling artefacts), but are useful to assess which components contributed to the PM$_{2.5}$ mass collected by a quartz fibre filter downstream of a 20 cm-long carbon monolith denuder.

Over the whole year 2016, carbonaceous species accounted for 54% of PM$_{2.5}$ (EC: 8%, POM: 46%), and secondary inorganics for 39% (NH$_4$: 9%, NO$_3$: 14%, and SO$_4$: 16%). In both the cold and the warm seasons, particulate air pollution days are characterised by a strong increase in NO$_3^-$ contribution. Considering low PM$_{2.5}$ concentration days, summertime is characterised by higher SO$_4^{2-}$ concentrations (faster SO$_2$ photochemical conversion) and lower NO$_3^-$ concentrations (equilibrium shifted towards the gas phase as temperatures increase). Dust and salts do not contribute significantly to the PM$_{2.5}$ mass, their contribution is larger on cleanest days compared to most polluted days.

*Table 3*: Annual mean concentrations and contributions of major PM$_{2.5}$ constituents in 2016

| constituent | salts<br>Cl$^-$, Na$^+$, K$^+$, Mg$^{2+}$, and Ca$^{2+}$ | NH$_4^+$ | NO$_3^-$ | SO$_4^{2-}$ | POM | EC | dust | unaccounted |
|---|---|---|---|---|---|---|---|---|
| Mean concentration (µg m$^{-3}$) | 0.38 | 1.34 | 2.93 | 1.51 | 6.76 | 1.14 | 0.10 | |
| Mean contribution (%) | 2.6 | 9.4 | 13.9 | 15.6 | 45.7 | 8.0 | 1.5 | 3.1 |
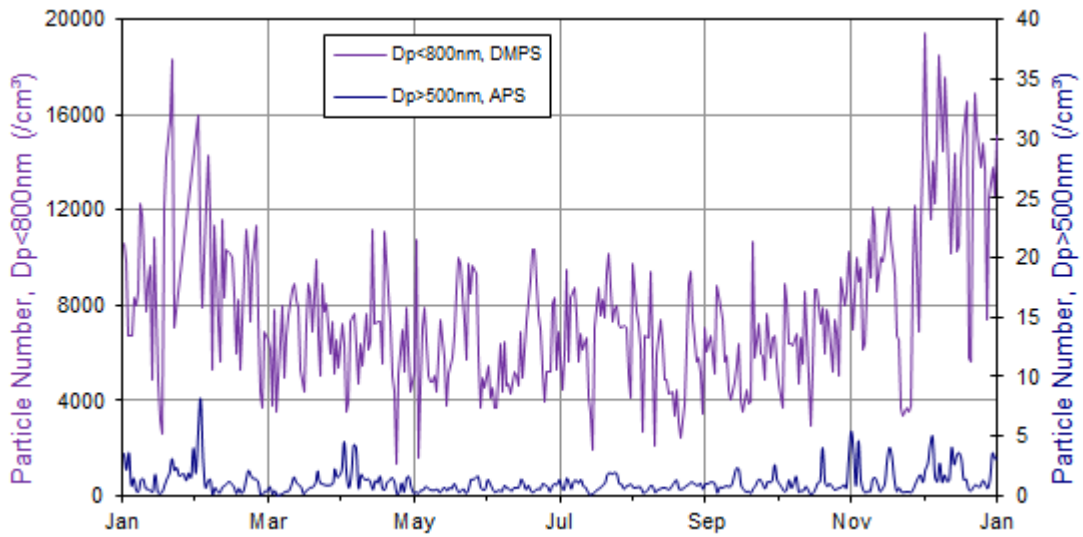
*Fig. 31. 24 hr – mean particle number concentrations for Dp < 600 nm and Dp >500 nm.*
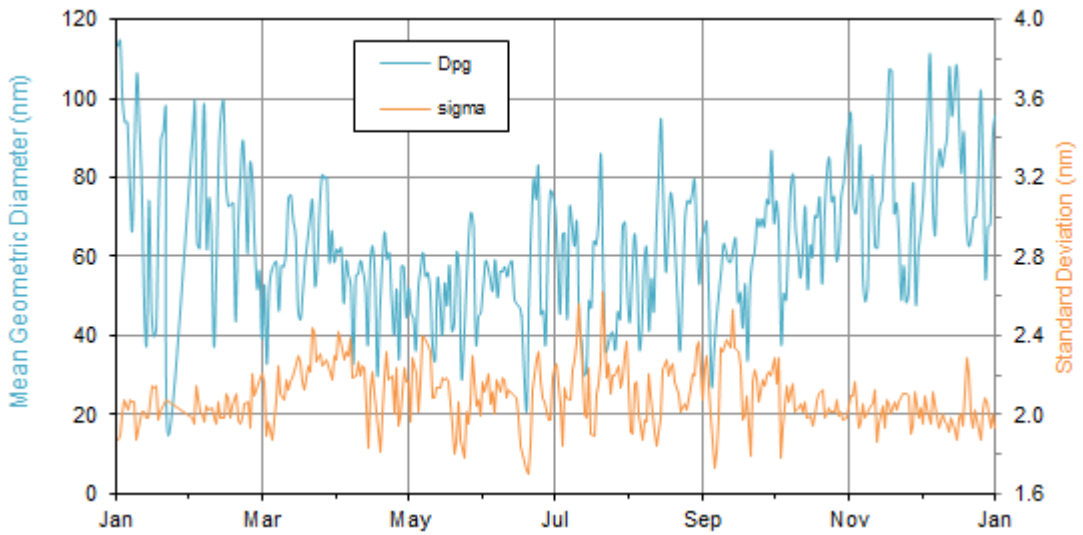


*Fig. 32. 24 hr - averaged particle geometric mean mobility diameter (from the DMPS) and standard deviation*
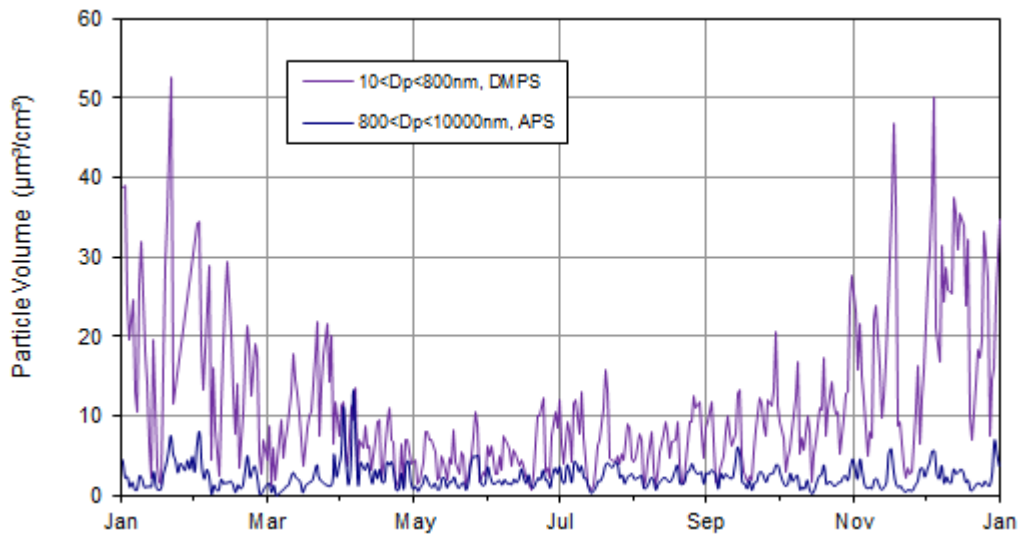


*Fig. 33. 24 hr - averaged particle volume concentrations for Dp< 800 nm and Dp > 800 nm.*

### 4.4.3.4 Aerosol micro-physical properties

Measurements of the particle number size distributions smaller than 800 nm diameter were carried out using a Differential Mobility Particle Sizer almost continuously in 2016, except for an 8-day gap for inter-comparison at the WCCAP in Leipzig (24 -31 Jan.) and a few short breakdowns, resulting in a data coverage of 96%. The DMPS data presented here have been corrected for inlet diffusion losses and CPC efficiency.

Particle number concentrations averaged over 24 hr (from 08:00 to 08:00 UTC) ranged from 1360 to 19400 cm$^{-3}$ (average: 7600 cm$^{-3}$) and followed a seasonal cycle similar to that of PM mass concentrations, with maxima in winter and minima in summer (Fig. 31). The vicinity of internal and external roads led to numerous episodes of local contamination, which were flagged during the data analysis process. Excluding the data points affected by local contamination (10% of the data), the annual mean particle number drops by 8%.

The mean mode diameter at RH < 30 % ranged between 15 and 1115 nm (average = 63 nm) in 2016. The variations in particle size distribution characteristics (Fig. 32) show seasonal patterns as well: the mean geometric diameter is generally larger in winter (about 60-100 nm) than in summer (about 40- 60 nm, with peaks at 80 nm), whereas the standard deviation of the distribution follows an opposite trend (with a variability larger in summer than in winter).

The size distribution of particles larger than 500 nm was measured using an Aerodynamic Particle Sizer almost continuously over 2016 (data coverage: 99%). Aerodynamic diameters were converted to geometric diameter assuming a particle density of 1.50. As previously observed, particles larger than 500 nm generally (90th percentile) accounted for <0.03% of the total particle number only (Fig. 31), but for more than 30 % of the total particle volume on average (Fig. 33). The seasonal variations in particle volume concentration reflect the changes in particle number and mean geometric diameter, with larger volumes in winter than in summer.
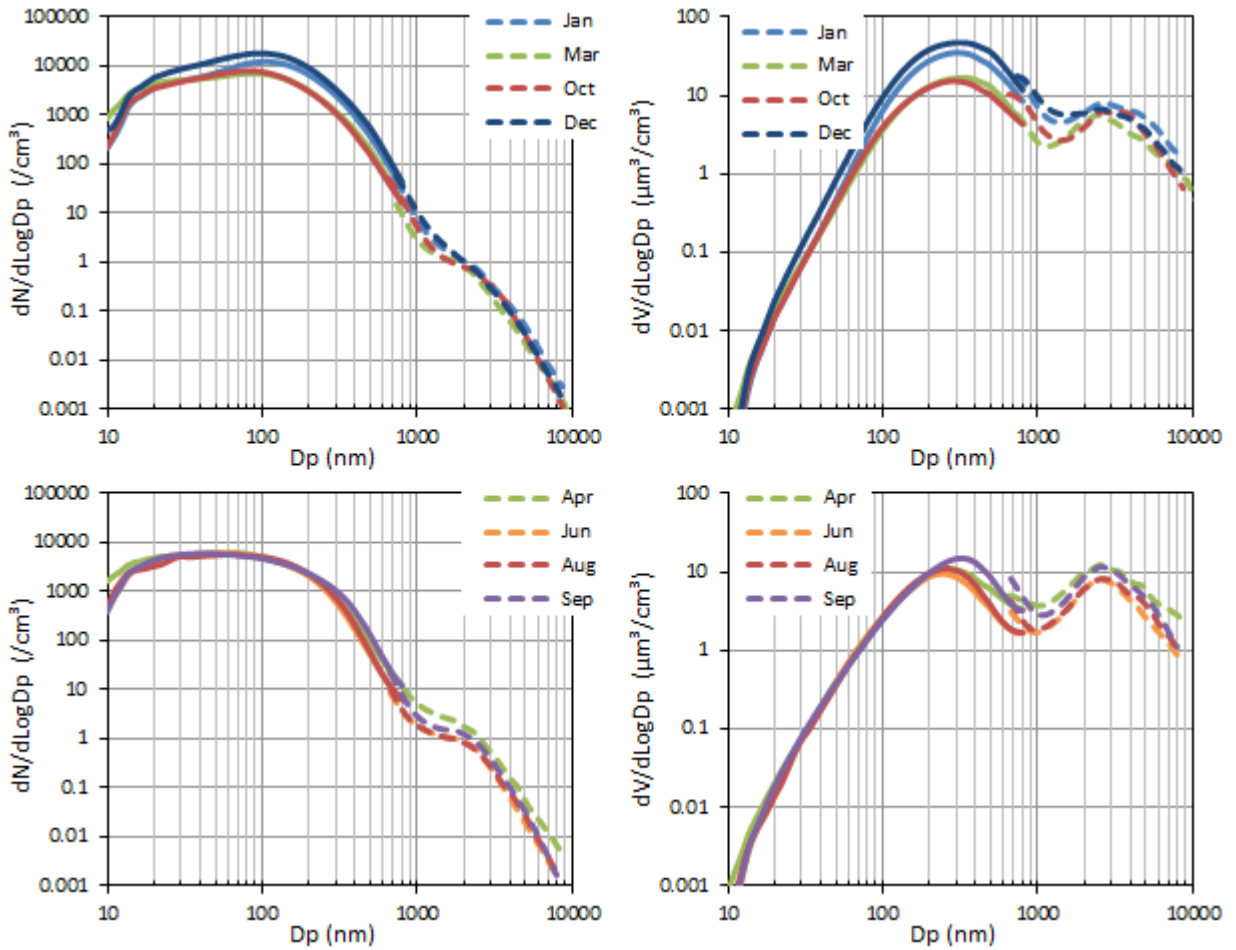
Fig. 34. Monthly mean particle number (left) and volume (right) size distributions measured in 2016 with a DMPS (10-800 nm, solid lines) and an APS (0.85-10 μm, dashed lines). A density of **1.25 g cm$^{-3}$** was used to convert aerodynamic to geometric diameters, except for June – Sept (1.5).
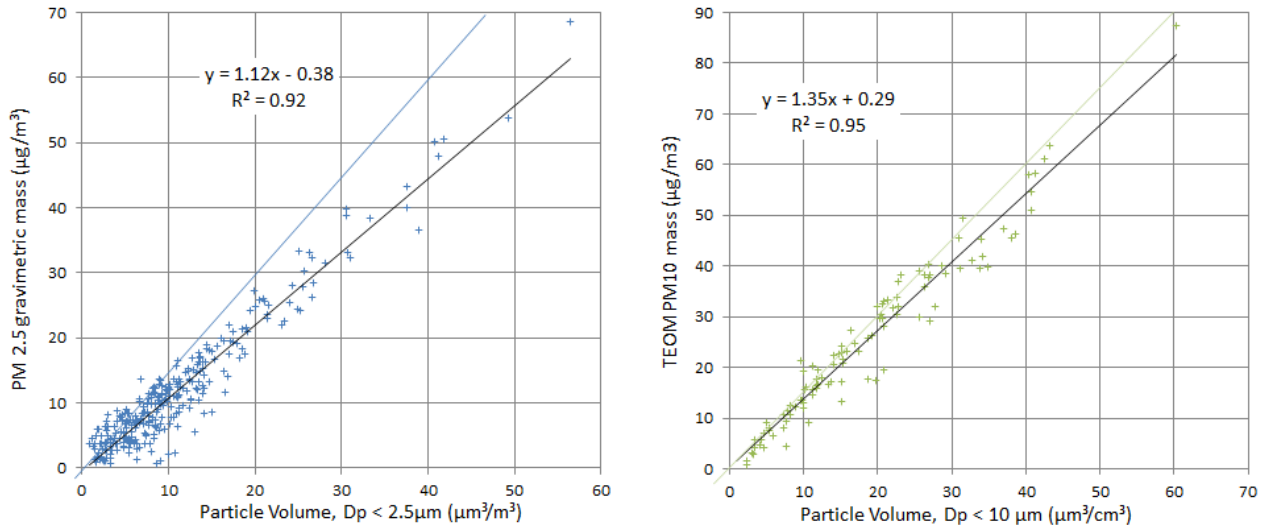


Fig. 35. 2016 regressions between (left) PM$_{2.5}$ mass concentrations determined from gravimetric measurements at 20 % RH and particle volume (Dp < 2.5 μm) calculated from DMPS and APS measurements (<40% RH), and (right) between PM$_{10}$ mass concentrations measured with the TEOM-FDMS at 30 % RH and particle volume (Dp < 10 μm) at <40% RH.

Fig. 34 illustrates the large domination of sub-μm particles in the particle number size distribution. Even particle volume (and therefore PM mass) is dominated by sub-μm particles (almost half of the particle volume actually sits in particles < 300 nm). The apparent good agreement between particle number size distributions (Fig. 34) measured with the DMPS and the APS was obtained by using an aerosol density of 1.25 g cm$^{-3}$) to convert aerodynamic diameters (measured by the APS) to mobility diameters (measured by the DMPS) for all months, except June-Sept. when 1.5 fits better, to be compared with the range (1.6 ± 0.1 g cm$^{-3}$) expected for atmospheric particles (McMurry et al., 2002).This could be explained by a DMPS over-counting for particles larger than 300 nm, as also suggested by the 2013 DMPS inter-comparison at the WCCAP in Leipzig.

Both comparisons between PM mass and aerosol particle volume concentrations show a good correlation (Fig. 35). The slope of the regression between PM$_{2.5}$ at 20 % RH and particle volume suggests an aerosol density of 1.12 (to be compared to 1.16, 1.24, 1.20, 1.31, 1.38 and 1.37 in 2015, 2014, 2013, 2012, 2011 and 2010, respectively), while the regression between PM$_{10}$ mass and aerosol volume concentration (for Dp < 10 μm) suggests a density of 1.35, a bit less than the nominal value of 1.5 g cm$^{-3}$ assumed to convert aerodynamic diameters to mobility diameters for particle volume calculation. This might indicate that PM$_{2.5}$ gravimetric measurements were underestimated.
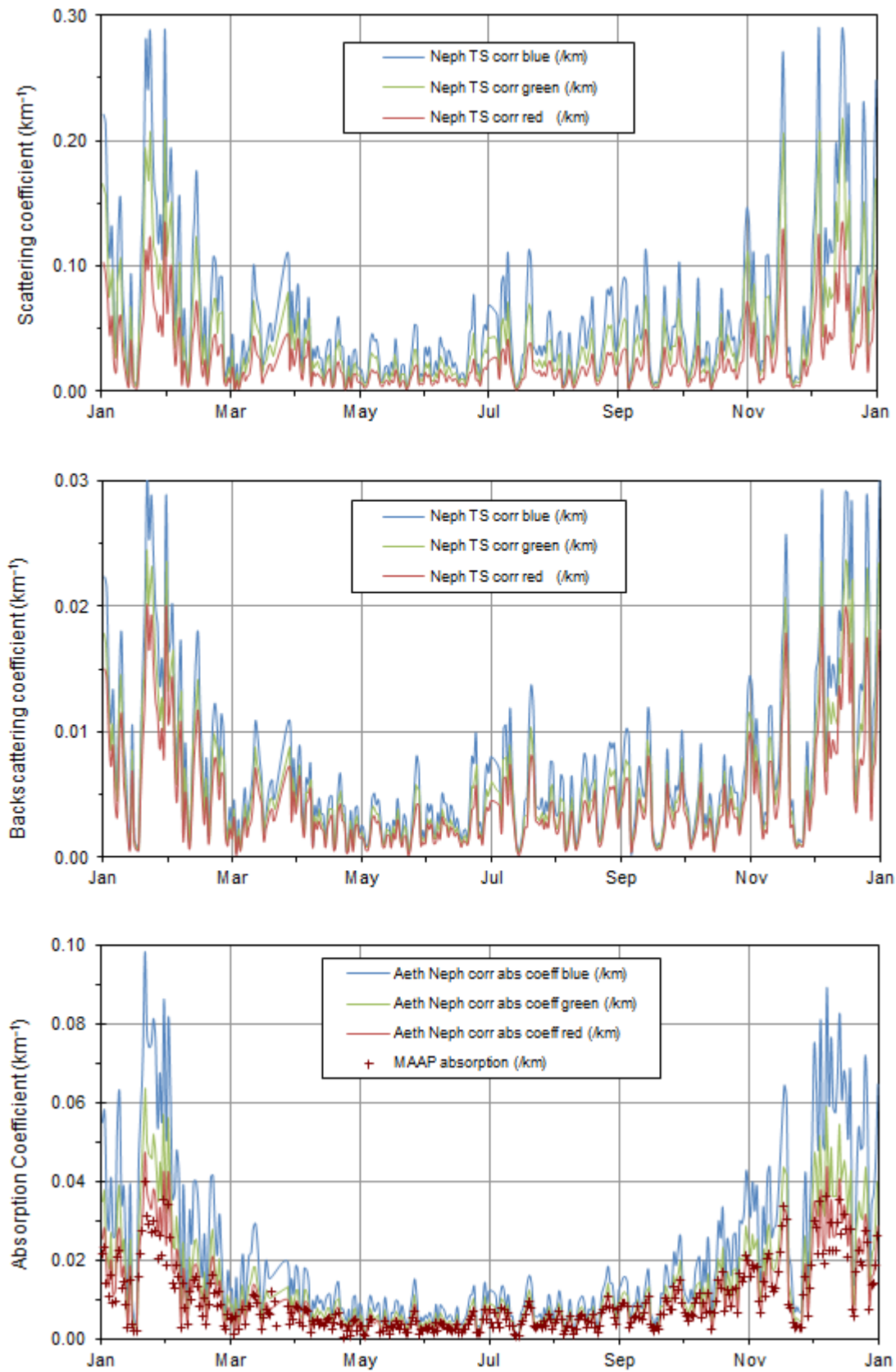
*Fig. 36. Daily mean atmospheric particle light scattering (top), backscattering (middle), and absorption (bottom) coefficients at three wavelengths, derived from Nephelometer, Aethalometer and MAAP measurements (not corrected for RH) performed in 2016.*

### 4.4.3.5 Aerosol optical properties

Aerosol optical properties have been monitored continuously during 2016 (data coverage = 98% for both light scattering and light absorption measurements). Data from the Nephelometer (Fig. 36 (a and b) have been corrected for angular non idealities (truncation to 7 – 170°, slightly not cosine-weighted distribution of illumination) according to Anderson and Ogren (1998), but not for RH effects. Thanks to the implementation of a Nafion dryer and the reduction of the sampling flow rate to 6-12 L min$^{-1}$, the Nephelometer internal RH was maintained below 40% for 90% of the time, with exception occurring mainly in July - Sept. At 40% RH, aerosol scattering is on average increased by about 20 % compared to 0% RH in Ispra (Adam et al., 2012).

Atmospheric particle absorption coefficients at 7 wavelengths were derived from the Aethalometer AE-31 data corrected for the shadowing and multiple scattering effects when Nephelometer data were available, according to Weingartner et al. (2003), making use of coefficients derived from Schmid et al. (2006), i.e. 3.60, 3.65 and 3.95 at 470, 520, and 660 nm, respectively (Fig. 36 c).

Both scattering and absorption coefficients follow seasonal variations (Fig. 36) in line with PM mass variations, mainly controlled by pollutant dispersion rates.

The uncertainty in the multiple scattering correction factor may introduce a quite large uncertainty in the aerosol absorption coefficient values, since correction factors ranging from 2 to 4 have been proposed (Weingartner et al., 2003; Arnott et al., 2005). The use of the correction factors listed above leads to an aerosol absorption coefficient at 660 nm somewhat larger than the absorption coefficient obtained from the Multi Angle Absorption Photometer (MAAP) for 670 nm, above all with the instruments settings set at the calibration workshop in Sept. 2015 (Fig. 37). NB: in December 2015, it was recommended by ACTRIS that the coefficient 3.5 should be used for all wavelengths without any correction for the filter loading.
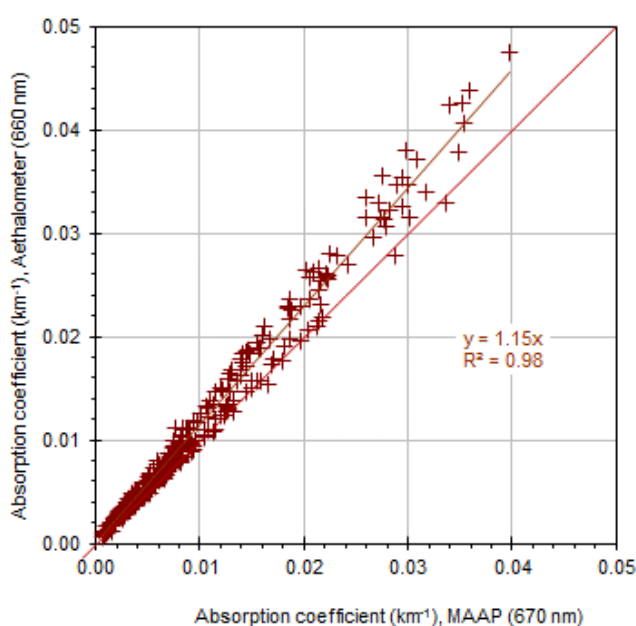


*Fig. 37. Comparison between the Aethalometer and MAAP derived light absorption coefficients at 660 and 670 nm, respectively. Data points are daily averages (2016).*
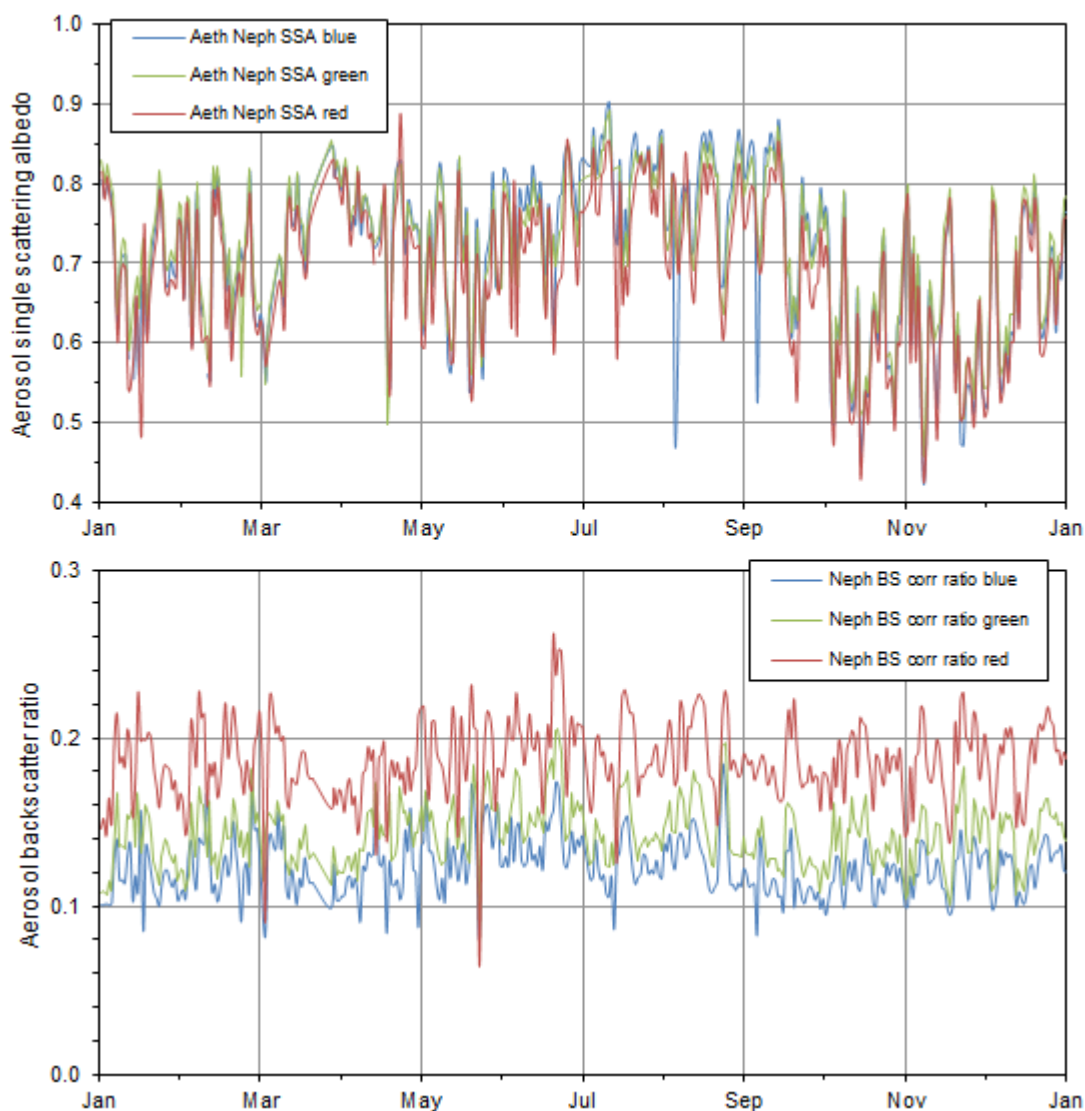
*Fig. 38. Aerosol 24-hr averaged single scattering albedo and backscatter to total scatter ratio at three wavelengths corresponding to blue, green and red, as calculated for 2016 (RH < 40%).*
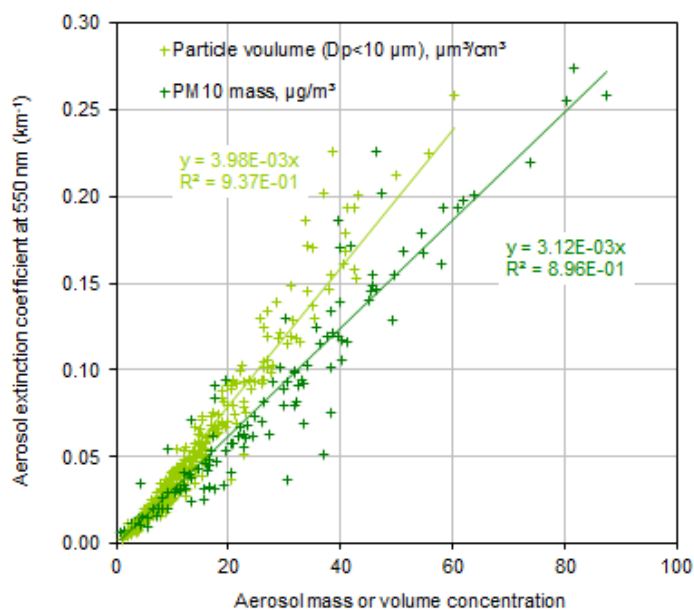


*Fig. 39. Regression between the aerosol extinction coefficient and $PM_{10}$ mass (FDMS-TEOM) and volume (DMPS + APS) concentrations in 2016.*

The 24 hr-averaged aerosol single scattering albedo (SSA) at $\lambda$ = 550 nm (at RH generally < 40 %) ranged from 0.46 to 0.89 (annual average 0.72), with generally higher values in spring and summer compared to autumn and winter (Fig. 38, top). In 2016, the lowest aerosol single scattering albedo values were affected by the proximity of the provisional measurement site to the internal and external roads of the JRC. As a consequence, the mean SSA was lower than in 2010-2013 (0.75-0.79), when measurements were performed at the historical site (Fig. 1). Excluding the values clearly affected by local influences, the mean single scattering albedo was 2% greater. The absorption coefficients were flagged for local contamination before submission to the WDCA data bank (EBAS).

The backscatter / total scatter ratio at 550 nm (Fig. 38, bottom) ranged from 0.08 to 0.20 (average 0.14), with no significant change compared to previous year.

The aerosol extinction coefficient and particle mass or volume concentrations are rather well correlated (Fig. 39). The slope of the regression between extinction and mass (based on data from 4 months only) shows that the mass extinction cross section was on average 3.1 m$^2$ g$^{-1}$ in 2016 (vs 2.5 in 2015, 2.8 in 2014, and 3.4 in 2012 and 2013), i.e. still low compared with 4.7 m$^2$ g$^{-1}$, the value calculated based on the aerosol mean chemical composition during 2016, and mass cross section coefficients for the various constituents found in the literature (see Table 4). Based on the particle volume determination, and assuming a mean aerosol density of 1.5 g cm$^{-3}$, the mass extinction cross section would be even lower (2.7 m$^2$ g$^{-1}$). The agreement between these two estimates of the aerosol extinction cross section deteriorated since 2010 – 2012, which underlines the necessity of implementing urgently new independent measurements of the light extinction.

*Table 4:* Mean aerosol chemical composition (PM$_{2.5}$) in 2016 and extinction cross section.

| | 2016 PM$_{2.5}$ comp. (%) | $\sigma_{ext}$ (m²/g) | Reference (for $\sigma_{ext}$) |
|---|---|---|---|
| "sea salt" | 3 | 1.3 | Hess et al., 1998 |
| NH$_4^+$, NO$_3^-$ and SO$_4^{2-}$ | 40 | 5.0 | Kiehl et al., 2000 |
| organic matter | 47 | 3.6 | Cooke et al., 1999 |
| elemental carbon | 8 | 11 | Cooke et al., 1999 |
| Dust | 2 | 0.6 | Hess et al., 1998 |
| **Total** | **100** | **4.7** | |

hours of valid measurements (2016)
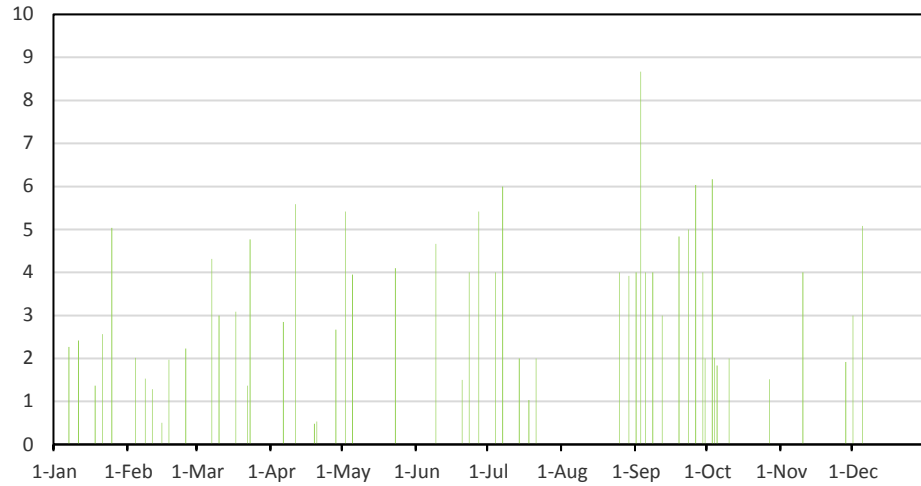
Fig. 40. Aerosol vertical profile measurements performed daily with the Raman Lidar in 2016.
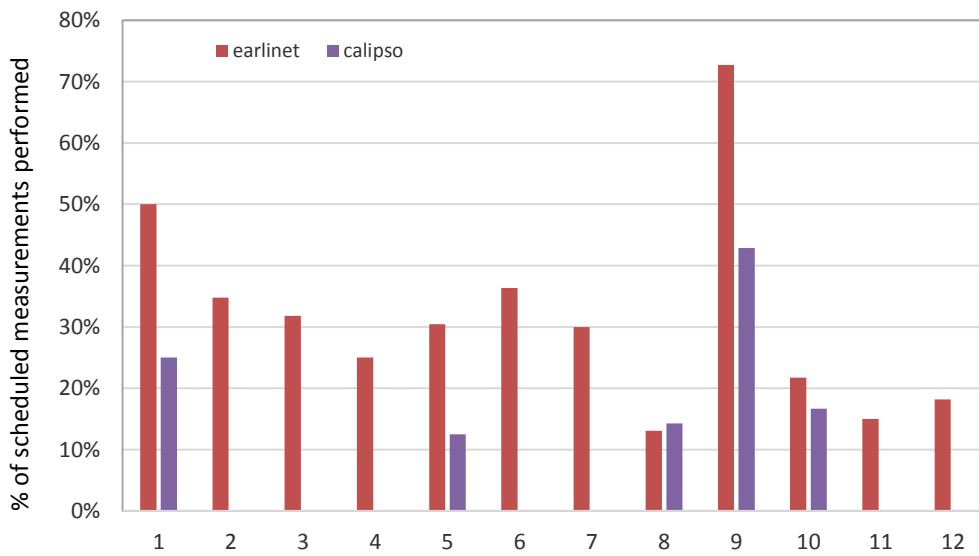


Fig. 41. Scheduled aerosol vertical profiling measurements performed monthly during the EARLINET climatology and Calipso overpass time slots in 2016. Calipso was not taking measurements in Feb. March 2016.

### 4.4.3.6 Aerosol vertical profiles

The Raman LiDAR from Raymetrics was operated for measuring aerosol vertical profiles from the historical EMEP Ispra site (Bd 77R) for the whole of 2016, weather and staff availability permitting.

In 2016, the LiDAR was operated for 177 hours (Fig. 40) according to the ACTRIS requirements: at noon (2hr) and sunset (4-5 hr) on Mondays, and sunset (4-5 hr) on Thursdays (EARLINET climatology), plus during Calipso overpasses (every ~9 days at 01:40 and 12:35 UTC). The scheduled measurements were covered at 32% and 11% (Fig. 41), respectively, while ACTRIS' target is 50%. This is due to electrical power instability until a proper UPS was installed (Sept. 2016), and to the fact that the LiDAR could not be run automatically, while only 1 operator is qualified to operate it.

LiDAR data from Ispra were for the first time in 2016 successfully submitted to the ACTRIS-EARLINET Single Calculus Chain (SCC) for data inversion. Fig. 42 shows an example of aerosol light extinction and backscatter profiles signal at 532 nm measured in Ispra and retrieved using the SCC for December 5th, 2016, from 16:30 to 18:30 UTC. The data show a pollution accumulation close to the Earth's surface in the evening, and another pollution layer at about 2000 m above the ground.
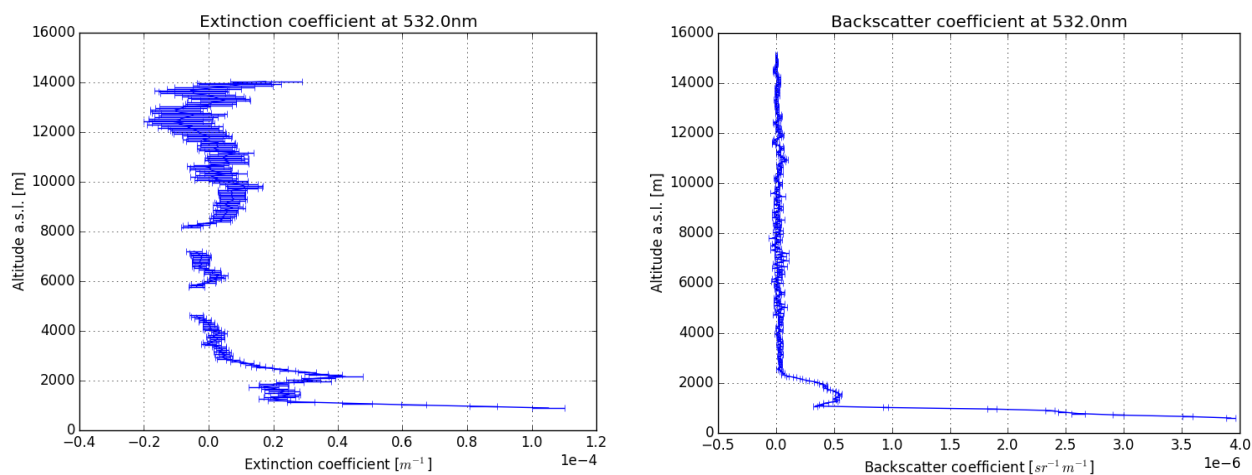


*Fig. 42: Examples of aerosol light extinction and backscatter profiles obtained at ABC-IS with the Raman LiDAR using the ACTRIS Single Calculus Chain, for December 5th[th], 2016, between 16:30 and 18:30.*
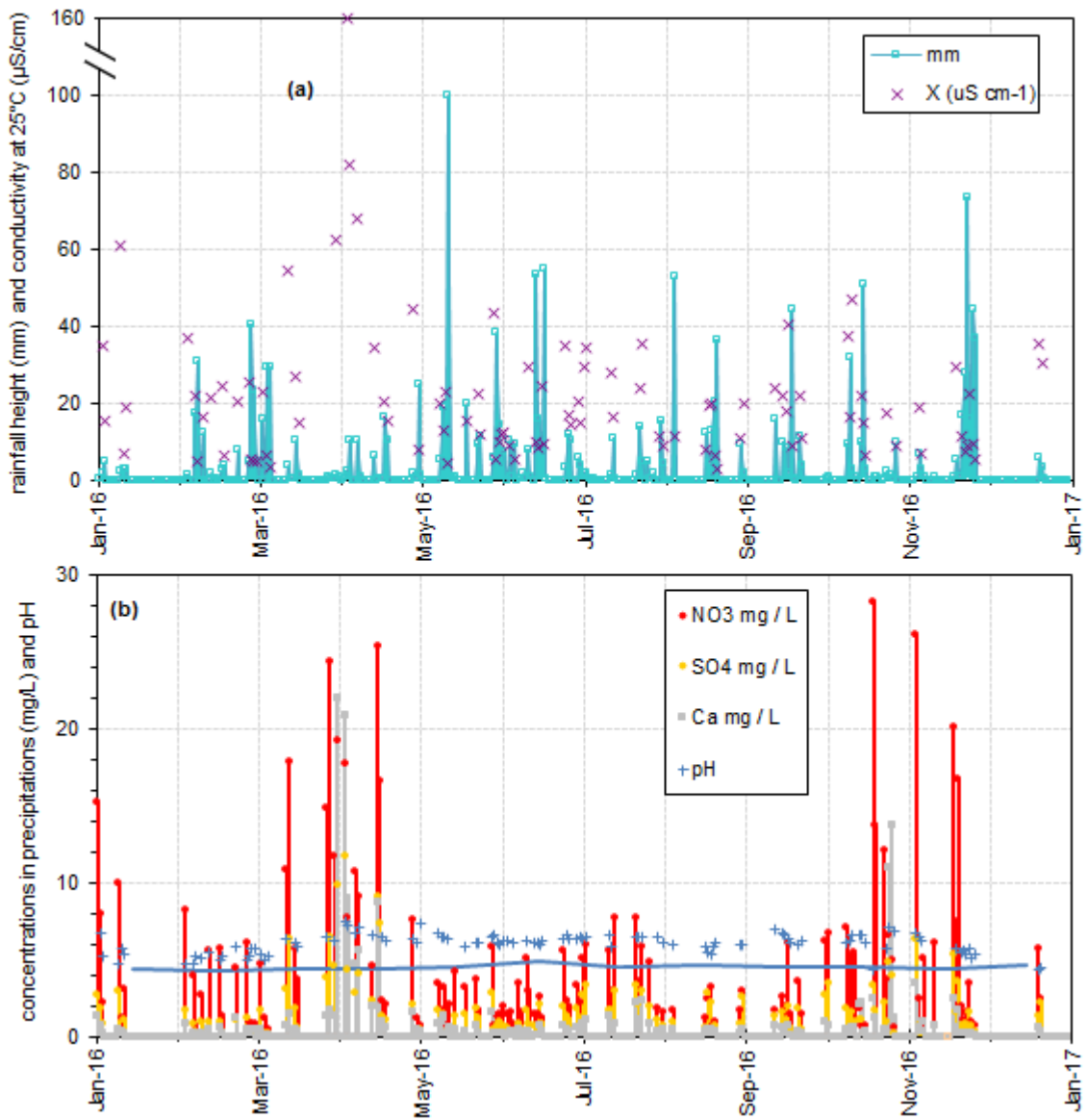
*Fig. 43* (a) *Precipitation amount, conductivity and* (b) *concentrations of 3 major ions in precipitation (bars) and pH (crosses) in 2016, and during the 1990-99 period (line).*
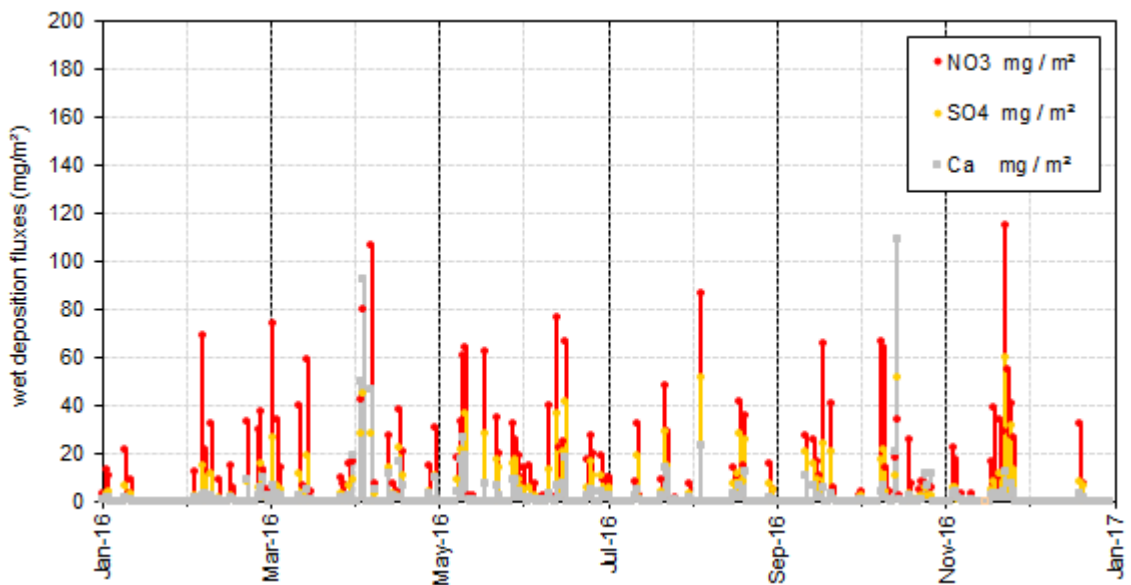


*Fig. 44. Wet deposition fluxes of 3 main ions measured in rain water in* 2016.

## 4.4.4    Wet deposition chemistry

In 2016, 143 precipitation samples were collected. The ionic content, acidity (pH) and conductivity were measured in 129, 105 and 98 of these samples (those where the water volume was sufficient minus 4 major events). The precipitation height measured during the collected events ranged from 0.05 to 100 mm (Fig. 43a) for a total of 1468 mm.

The ranges of concentrations measured in these samples are indicated in Table 5. Volume weighted mean concentrations of the anthropogenic species $NO_3^-$ and $SO_4^{2-}$ and $NH_4^+$ were in 2016 less than the 1990-1999 averages, while concentrations of all the marine or crustal components were similar. All precipitation samples collected in 2016 but 5 were acidic (pH < 7.0), and 25 had a pH<5.6 (equilibrium with atmospheric $CO_2$), compared to 43 in 2015, and 58 in 2014. Only 3 samples had a pH < 4.6 (compared to 18 in 2015, and 9 in 2014 and 2013).

Wet deposition was evenly distributed over February - November, while almost no wet deposition occurred in January and December (Fig. 44). In 2016, the annual wet deposition flux of the main acidifying and eutrophying species was 1.4, 3.0, and 1.5 g m$^{-2}$ for $SO_4^{2-}$, $NO_3^-$, and $NH_4^+$, respectively, i.e. very similar ($NO_3^-$ & $NH_4^+$) or lower ($SO_4^{2-}$) than in 2015, and with no big difference compared to the previous years (see also section 4.6 next page).

*Table 5: Statistics relative to the precipitation samples collected in 2016 (averages are volume weighted)*

|  | pH | cond. | Cl- | NO3- | SO42- | Na+ | NH4+ | K+ | Mg2+ | Ca2+ |
|---|---|---|---|---|---|---|---|---|---|---|
|  |  | µS / cm | mg / l | mg / l | mg / l | mg / l | mg / l | mg / l | mg / l | mg / l |
| Average | 5.21 | 16.79 | 0.41 | 2.60 | 1.09 | 0.28 | 1.15 | 0.07 | 0.07 | 0.67 |
| Min | 4.30 | 2.99 | 0.06 | 0.47 | 0.15 | 0.04 | 0.13 | 0.01 | 0.01 | 0.08 |
| Max | 7.45 | 160.0 | 12.4 | 28.2 | 11.7 | 7.7 | 13.2 | 1.2 | 1.3 | 21.9 |
| 1990-1999 | 4.40 | 24.86 | 0.44 | 3.94 | 3.07 | 0.23 | 1.25 | 0.09 | 0.06 | 0.45 |
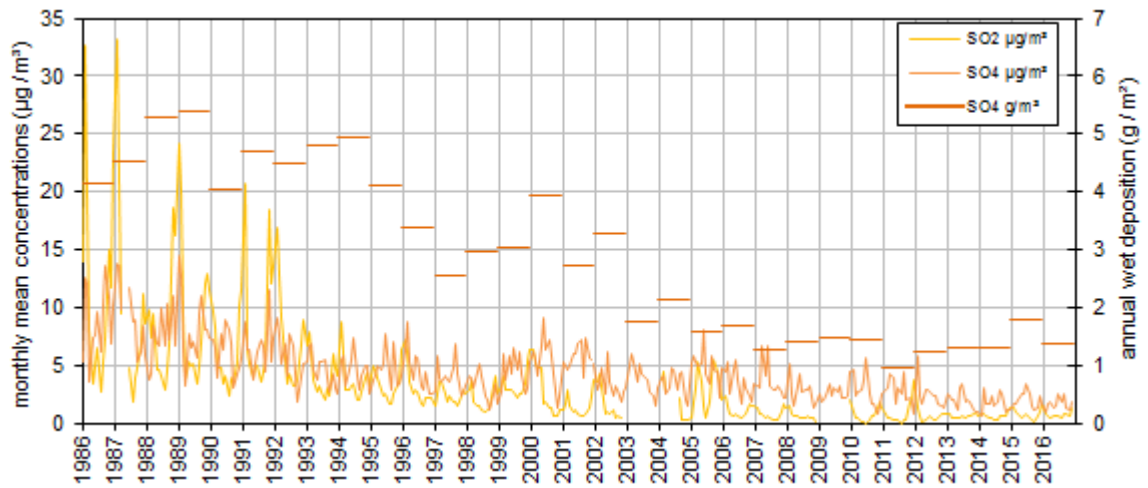
Fig. 45. Oxidized sulphur species monthly mean concentrations and yearly wet deposition.
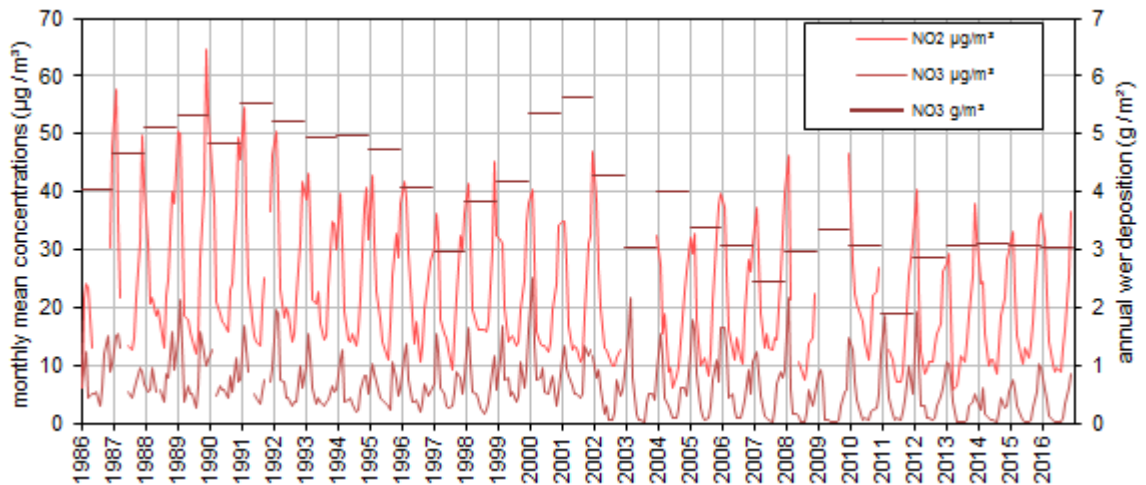


Fig. 46. Oxidized nitrogen species monthly mean concentrations and yearly wet deposition.
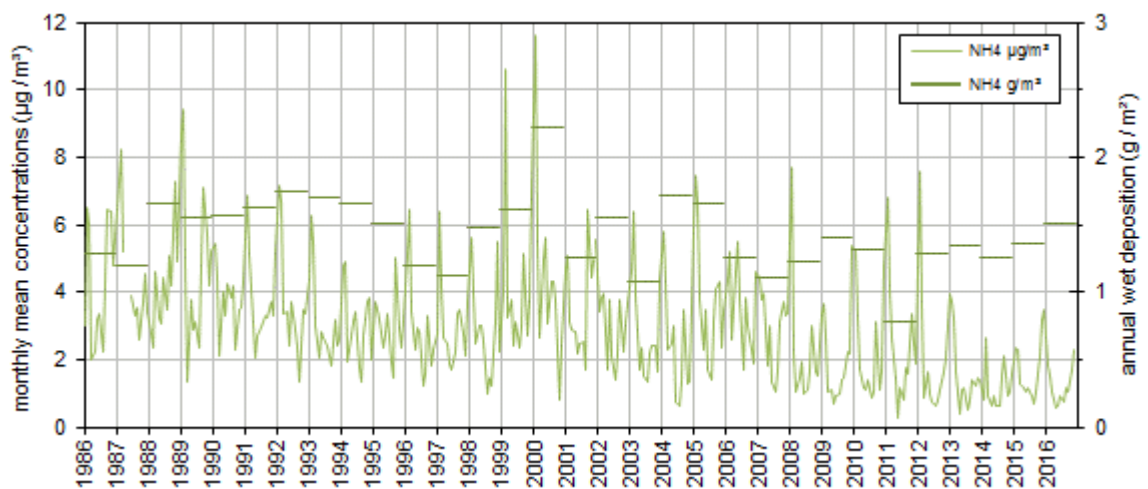


Fig. 47. Reduced nitrogen species monthly mean concentration and yearly wet deposition.

## 4.5 Results of year 2016 in relation to 30 years of measurements

### 4.5.1 Sulphur and nitrogen compounds

The annual mean $SO_2$ concentration in 2016 was slightly greater than in 2015, but in line with the range of values (0.6 – 0.8 µg/m³) observed at our station in the 2010's. $SO_2$ concentrations are nowadays ~10 times smaller than in the 90's, and less than half compared to the 2000's. Annual mean particulate $SO_4^{2-}$ concentration reached its historical minimum, 15% less than in 2015, and a few % less compared to the previous record of 2014 (when summer was exceptionally wet). In 2016, $SO_4^{2-}$ concentrations were on average less than half compared to the 2000's, and 1/3 compared to the 90's. It should be kept in mind that $SO_4^{2-}$ concentrations were measured in $PM_{10}$ or in $PM_{2.5}$ from 2002 onwards, whereas it was measured in TSP (Total Suspended Particulate) from 1986 to 2001. However, simultaneous sampling of $PM_{10}$ and TSP over 14 months showed that $SO_4^{2-}$ in $PM_{10}$ is generally less than 5 % lower than in TSP. $SO_4^{2-}$ is mainly present in the $PM_{2.5}$ fraction at our site (see Fig. 24 of the ABC-IS annual report 2010). From 2005 onwards the calculations were as follows:

$$SO_4^{2-}(PM_{10}) = SO_4^{2-}(PM_{2.5}) \times <SO_4^{2-}(PM_{10})/ SO_4^{2-}(PM_{2.5})>$$

the average $<SO_4^{2-}(PM_{10})/ SO_4^{2-}(PM_{2.5})>$ being calculated based on the simultaneous $PM_{10}$ and $PM_{2.5}$ samples collected in 2010-2012.

Particulate $SO_4^{2-}$ concentrations decreased much less than $SO_2$ concentrations, which suggests that locally produced $SO_2$ decreased much more than possibly long-range transported $SO_4^{2-}$ over the past 25-30 years. $SO_4^{2-}$ wet deposition in 2016 was 25% less than in 2015, and similar to the values of 2013 and 2014.

In 2016, the annual mean $NO_2$ concentration was close to the lowest values observed over the past decade, and 30% less compared to the 90's. Monthly mean concentrations of nitrogen dioxide ($NO_2$) do not show such a pronounced decreasing trend as seen for $SO_2$ over the past 30 years (

Fig. 46). Over the last decade, $NO_2$ maxima are not significantly lower than during the previous one, which does not reflect the 30 % abatement in $NO_x$ emissions reported in the emission inventories for this period. The particulate $NO_3^-$ annual mean concentration observed in 2016 was the 2nd lowest record observed at our station, similar to the 2015 value, and beaten only by the 2014 lowest record (associated with exceptional precipitations), and half of the average over 1990 – 2010. It should be noted that since October 2000, $NH_4^+$ and $NO_3^-$ have been measured mostly from quartz fibre filters, which are known to lose $NH_4NO_3$ at temperatures > 20 °C, as demonstrated e.g. by the comparison with the ACSM measurements we performed in Ispra in 2013. This might contribute significantly to the fact that $NO_3^-$ summertime minima are particularly low since 2002. Furthermore, $NO_3^-$ was measured from $PM_{10}$ or in $PM_{2.5}$ from 2002, and no more from TSP, as over the 1986 to 2001 period. However, simultaneous sampling of $PM_{10}$ and TSP over 14 months showed that $NO_3^-$ in $PM_{10}$ is generally less than 5 % lower than in TSP, like $SO_4^{2-}$. From 2005 and onwards the calculations were as follows

$$NO_3^-(PM_{10}) = NO_3^-(PM_{2.5}) \times <NO_3^-(PM_{10})/ NO_3^- (PM_{2.5})>$$

the average $< NO_3^-(PM_{10})/ NO_3^-(PM_{2.5})>$ being calculated based on the simultaneous $PM_{10}$ and $PM_{2.5}$ samples collected in 2010-2012. $NO_3^-$ wet deposition annual flux observed in 2016 was among the 5 lowest ever recorded since 1986 in Ispra, less than the 2013 - 2015 values, and similar to the average value over the last decade.
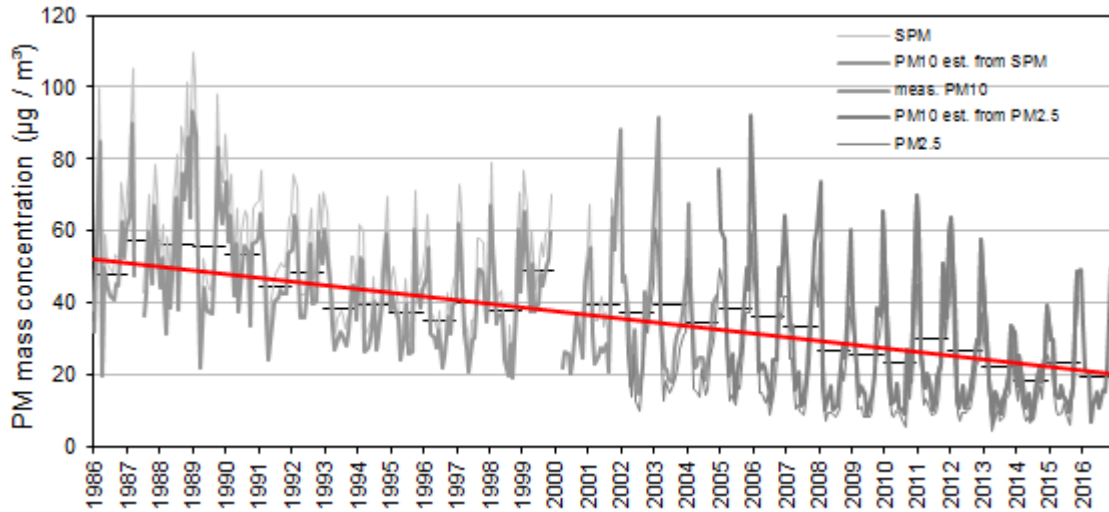
*Fig. 48.* *Particulate matter mass concentration monthly (grey) and annual (black) averages. The red line is the long term trend over annual averages. All values are gravimetric measurements or estimates from gravimetric measurements.*
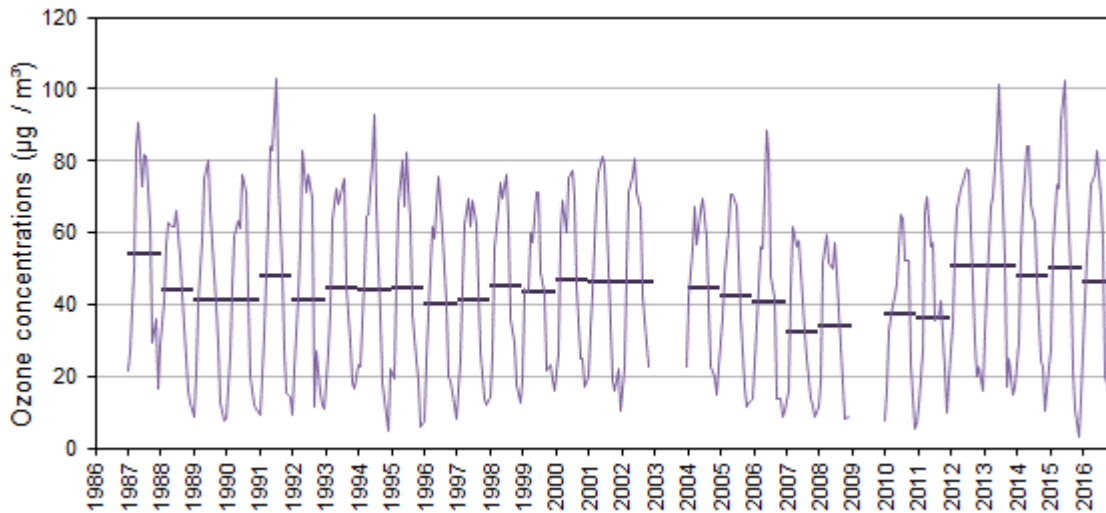


*Fig. 49. Ozone yearly and monthly mean concentrations at JRC-Ispra.*
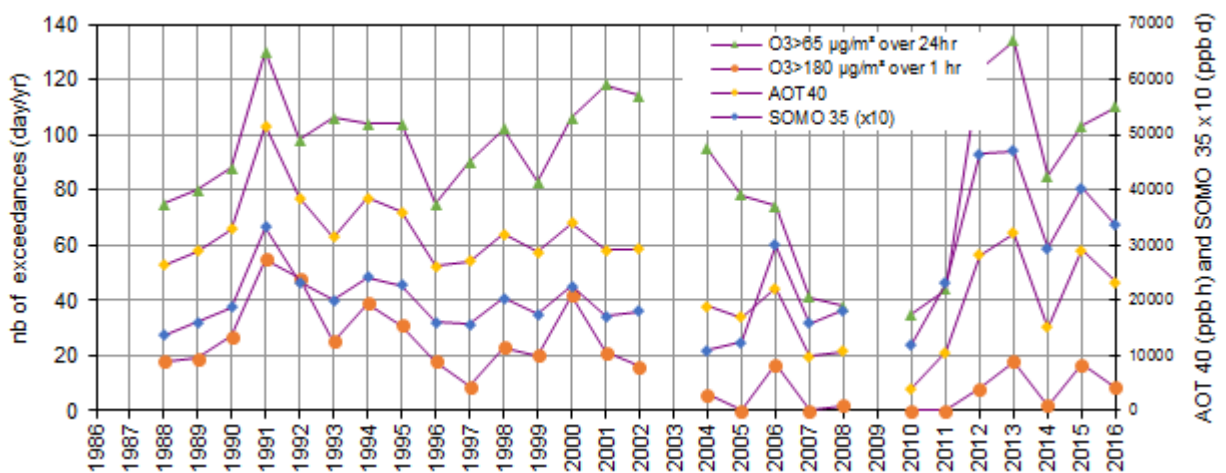


*Fig. 50. AOT40, SOMO35 values, and number of O₃ limit value exceedances.*

Despite relatively high concentrations in January, the annual mean concentration of $NH_4^+$ in particulate matter has also reached its 2nd historical minimum in 2016 (Fig. 47), beaten by the 2014 value. It was half the 1990 – 2010 average.

It should be noted that from the year 2002, $NH_4^+$ was measured in the $PM_{10}$ or in the $PM_{2.5}$ fraction. From 2005 and onwards, $NH_4^+$ concentrations in $PM_{10}$ were calculated as follows:

$$NH_4^+(PM_{10}) = NH_4^+(PM_{2.5}) \times <NH_4^+(PM_{10})/ NH_4^+(PM_{2.5})>$$

where the average $<NH_4^+(PM_{10})/ NH_4^+(PM_{2.5})>$ is calculated based on simultaneous $PM_{10}$ and $PM_{2.5}$ measurements performed in 2010-2012. On average, $NH_4^+$ can neutralize nearly 100% of the acidity associated with $NO_3^-$ and $SO_4^{2-}$ in the particulate phase (see Fig. 29). $NH_4^+$ is also quite well correlated with $NO_3^- + SO_4^{2-}$ in rainwater. $NH_4^+$ annual wet deposition in 2016 was quite big, and close to 25% greater than the average recorded in Ispra over the last decade.

## 4.5.2    Particulate matter mass

The 2016 annual mean $PM_{2.5}$ concentration measured at 20% RH (14.6 µg/m³) was 15% less than in 2015, reaching the 2nd lowest value obtained since 2002. The annual value for $PM_{10}$ at 50% RH estimated from $PM_{2.5}$ measurements is therefore in line with the general decreasing trend of - 1.0 µg m$^{-3}$ yr$^{-1}$ over the 3 last decades (Fig. 48). It should however be kept in mind that $PM_{10}$ concentrations were estimated from TSP mass concentration measurements (carried out by weighing at 60 % RH and 20 °C cellulose acetate filters sampled without any particle size cut-off and "dried" at 60 °C before and after sampling) over 1986-2000, based on a comparison between TSP and $PM_{10}$ over the Oct. 2000 - Dec. 2001 period ($R^2$ = 0.93, slope = 0.85), and derived from measured $PM_{2.5}$ values for years 2005-2016. After the historical low winter concentrations observed in winter 2013 – 2014, winter concentrations were high again in winter 2015 and 2016, at least partly due to the exceptionally dry Dec. 2015, and Jan. and Dec 2016. Summertime PM minima showed a robust decreasing trend over 1986 – 2010, and a more modest decreasing trend since the slight increase in 2011.

## 4.5.3    Ozone

Fig. 49 shows monthly and yearly mean $O_3$ concentrations observed since 1987. Ozone was not measured in 2009 and there was a major data acquisition breakdown in 2003. Annual average $O_3$ concentrations have been consistently high over 2012 – 2015. In 2016, the annual mean $O_3$ concentration went back down to the values observed in the early 2000's, remaining higher than between 2007 and 2011. While summertime peaks' remained high since 2012, winter minima decreased regularly over this period. Ozone indicators (Fig. 50) for 2016 all (except 1) show a slight improvement compared to 2015, without reaching the relative minimum observed in 2014 due to the unusual summertime weather conditions.
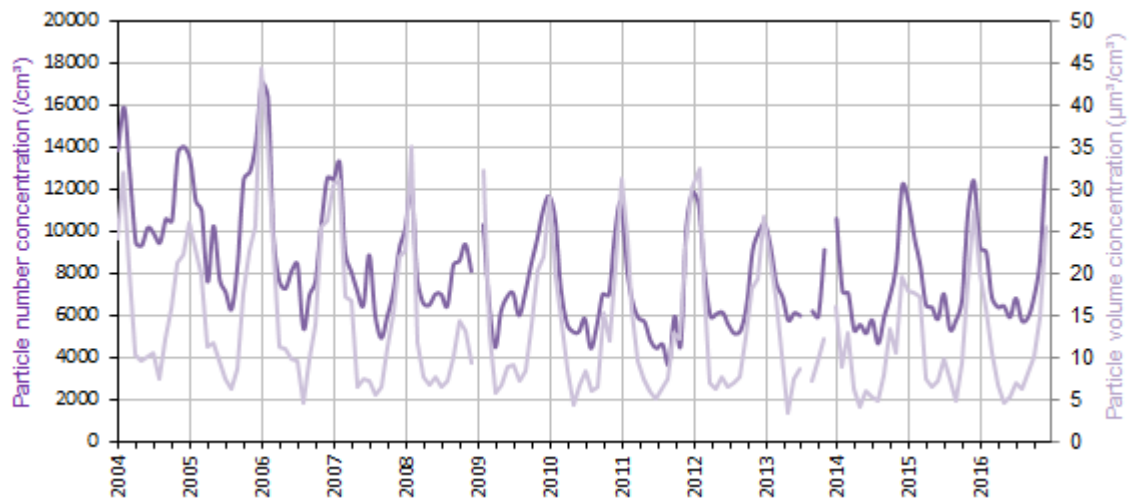
Fig. 51. Particle number (left) and volume (right) monthly mean concentrations.
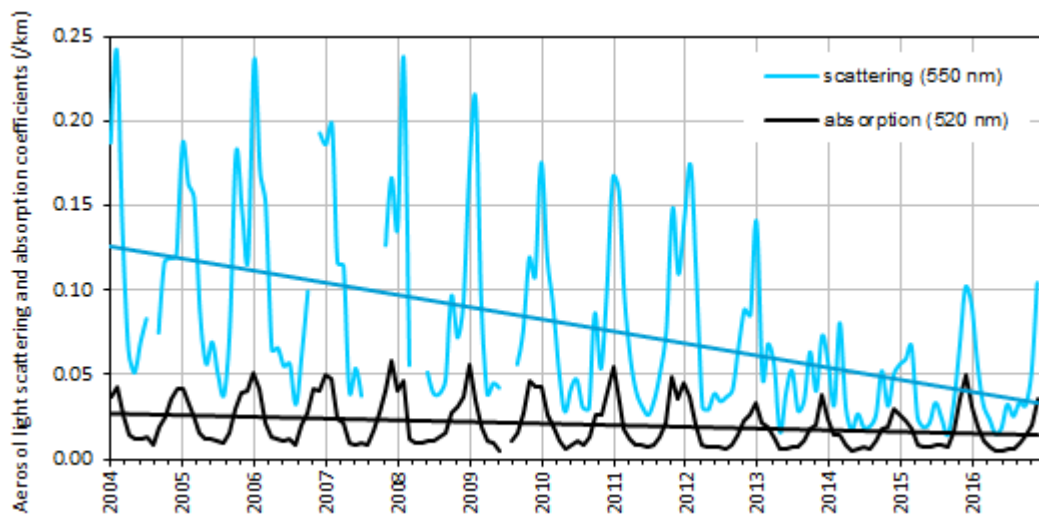


Fig. 52. Aerosol green light scattering and absorption monthly mean coefficients
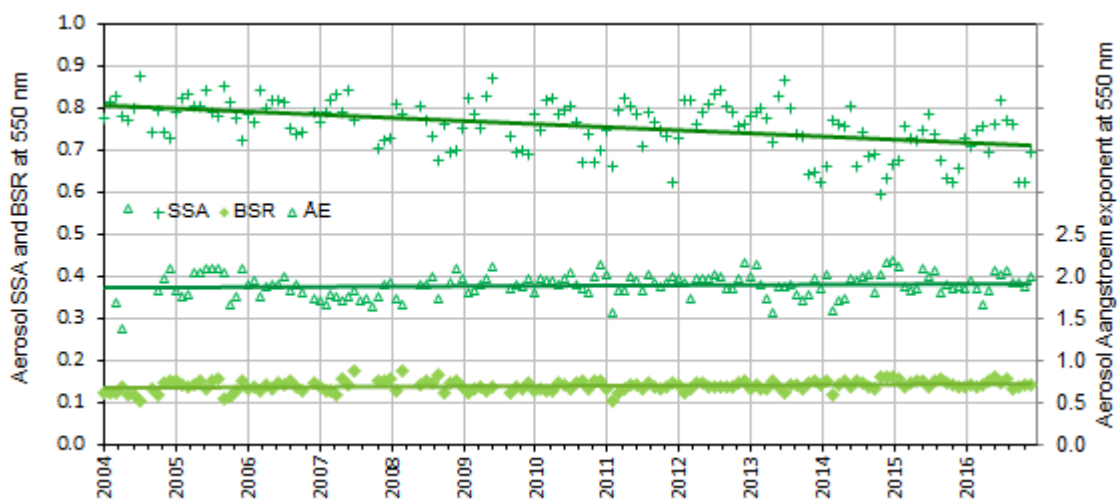


Fig. 53. Aerosol optical characteristics at 550 nm (monthly means): single scattering albedo and backscatter ration (left hand axis) and scattering Ångström exponent (right hand axis).

Both indicators for the vegetation protection (number of days with a 24-hour mean $O_3$ concentration > 65 µg/m³, vegetation protection limit, and the AOT40, Accumulated Ozone exposure over a Threshold of 40 ppb), remain in the late 2010's similar to values observed in the 1990's. The population exposure indicator SOMO 35 (Sum of Ozone Means Over 35 ppb, where means stands for maximum 8-hour mean over day) is higher than ever. Only the number of days with extreme maximum $O_3$ concentrations (limit of 180 µg/m³ over 1hr exceeded), although higher in the recent years than for several years in the 2000's, remain low compared to the 1990's.

### 4.5.4    Aerosol micro-physical and optical properties

Measurements of the aerosol microphysical properties started at the atmospheric research station of the JRC-Ispra site in 2004, which represents one of the longest time series for this kind of measurements.

Sub-µm aerosol particle volume concentrations have clearly decreased until 2015 (Fig. 51), in line with the decrease in $PM_{10}$ and $PM_{2.5}$ mass concentrations (Fig. 48). The peaks in aerosol volume monthly mean concentrations in Dec.2015 – Jan. 2016 and Dec. 2016 are consistent with the peaks in PM mass concentrations observed for the same months. Until 2013 – 2014, the particle number concentrations also decreased both during summer and winter months. However, summertime monthly means are rather constant, and wintertime maximum concentrations constantly increase since 2014.

The aerosol light scattering coefficient has also clearly decreased over the past 13 years (Fig. 52), consistent with the decrease in PM mass and particle volume (or surface) concentrations, despite the wintertime peaks in Dec.2015 – Jan. 2016 and Dec. 2016 already observed for other particulate pollution metrics. Simultaneously, the aerosol absorption coefficient has also decreased slightly, but much less rapidly than the scattering coefficient. As a consequence, the aerosol single scattering albedo (SSA = scattering/(scattering + absorption)) significantly decreased over the past 13 years, while the aerosol backscatter ratio only slightly increased (Fig. 53). The latter could be explained by a decrease in the mean particle diameter, also suggested by the increase in the scattering Ångström exponent. The impact of these changes is a decrease of the direct cooling effect by atmospheric particles at the top of the atmosphere (Putaud et al., 2014).

## 4.6    Conclusions

The data coverage in 2016 ranged from 87 to 99% for the various instruments measuring near surface (3 to 4.5 m agl) concentrations, except for the FDMS-TEOM (31%) which was operated only for Jan. to March, and in Dec. 2016. The remote aerosol vertical profiler was operated for the whole year, weather and staff availability permitting, and covered more than 30% of the scheduled measurement slots.

2016 as a whole was warmer (especially from February to September) compared to the reference period (1990 – 1999), and June was significantly sunnier than usual. Precipitation was

similar to the climatological average, but January and December were particularly dry, which can probably explain at least partly the relatively high particulate pollution levels observed during these months compared to the recent years.

The impact of the weather conditions on $O_3$ concentrations is difficult to quantify, but it is probably not sufficient to explain the relatively high $O_3$ concentrations and indicators observed in 2016, in line with the high values observed since 2012 and similar to the values experienced in the 1990's. However, the frequency of extreme $O_3$ pollution events remains relatively low compared to the early 1990's. In contrast, the annual mean concentrations of $SO_2$, $NO_2$ and CO were close to their observed minima and confirm the general trend of improvement in these air quality indicators over the last 3 decades.

Daily $PM_{2.5}$ aerosol sampling on quartz fibre filter, using a Partisol sampler equipped with a carbon monolith denuder, and subsequent gravimetric and chemical analyses, showed that the concentration of $PM_{2.5}$ mass and of most of its components ($SO_4^{2-}$, $NO_3^-$, $NH_4^+$, POM and EC) decreased in 2016 compared to 2015, without reaching the lowest records observed in 2014, which was an exceptionally wet year. However, the data from 2016 still confirm the mitigation of particulate air pollution observed since 1986. $PM_{2.5}$ average chemical composition was dominated by carbonaceous species (POM: 46%, EC: 8%), followed by secondary inorganics ($NH_4^+$: 9%, $NO_3^-$: 14%, $SO_4^{2-}$: 16%). It is worth mentioning that in 2016 the unaccounted mass averaged only 3%, with generally higher percentages observed at low concentrations. As previously observed, there was a clear increase of $NO_3^-$ contribution to $PM_{2.5}$ when shifting from cleaner ($PM_{2.5} < 10$ µg/m³) to more polluted periods ($PM_{2.5} > 25$ µg/m³) during both cold and warmer months. $PM_{2.5}$ (from gravimetric analyses at 20% RH) annual mean mass concentrations (15 µg/m³) was below the EU annual limit value (25 µg/m³). The low data coverage for $PM_{10}$ measurements does not allow us to calculate the annual average and the number of exceedances of the $PM_{10}$ limit value for 2016. The long-term time series of PM concentrations still suggests a decreasing trend of - 1.0 µg m⁻³ yr⁻¹ over the last 3 decades.

The annual mean particle number concentration (average: 7600 cm⁻³) was lower than in (dry) 2015, but greater than in (wet) 2014. The 13-yr time series shows that the particle number concentration has decrease till 2012, but no longer since then, especially in December and January where particle number increased in 2015 and 2016. Particle number size distributions were in 2016, as usual, generally broadly bimodal, with a submicron mode at ca. 100 nm (dry) and a less pronounced coarse mode around 2 µm. Nevertheless, both the aerosol light backscatter ratio and the Ångström exponent suggest that the mean particle diameter tends to decrease slowly. The atmospheric aerosol scattering and absorption coefficients derived from Nephelometer and Aethalometer measurements in dried atmosphere (generally lower than 40%) also show a decreasing trend over the past 12 years. However, the absorption coefficient does not decrease as fast as the scattering coefficient, and as a consequence, the aerosol single scattering albedo (0.72) was in 2016 greater than in 2015 (0.70), but significantly less compared to recent years also (0.76 in 2013, 0.79 in 2012 and 0.77 in 2011), with a possible impact on

the climate cooling effect of the aerosol. The measurements of the light absorption and scattering by aerosols remain difficult and prone to uncertainties. To better constrain these measurements, we urgently need to begin making measurements of light extinction based on the cavity attenuated phase shift (CAPS) technique.

All the aerosol extensive variables measured at JRC-Ispra (at ground level) have similar seasonal variations with summer minima. These variables are generally well correlated and lead to variable degrees of chemical, physical, and optical closure. In 2016, a reasonable overlap between the particle size distributions as measured with the DMPS and the APS was obtained for a particle density of 1.25 g/cm³, except for the summer months (1.5 g/cm³). This value is reasonably consistent with the average sub-2.5 µm aerosol density of 1.1 $g/cm^3$ determined from the regression between the gravimetric $PM_{2.5}$ mass and the DMPS + APS volume. However, such a density is low compared to literature values (1.6 ±0.1), and is also low compared to 2010 - 2012 values (1.3 – 1.4 $g/cm^3$). In contrast, the ratio between the $PM_{10}$ mass concentration measured with the FDMS-TEOM and the aerosol volume DMPS + APS volume leads to a density of 1.35 $g/cm^3$. It is unlikely that the density of $PM_{10}$ and $PM_{2.5}$ are so different from each other. This difference might indicate a systematic bias in one of these measurements in 2016. Similarly, the mean mass extinction cross section (i.e., the extinction-to-mass ratio) of 2.7 to 3.1 $m^2\ g^{-1}$ (depending on the measurements used to calculate this variable) obtained in 2016, as well as the values of 2.5 for 2015, 2.8 for 2014, 3.4 for 2012-2013 and 3.9 for 2011, are low compared to the value that can be calculated from the mean $PM_{2.5}$ chemical composition, which averages to 4.7 $m^2\ g^{-1}$ in 2016 for the previous years, which suggests that either the aerosol volume and $PM_{10}$ concentrations were overestimated, or the extinction coefficient calculated as scattering + absorption was underestimated. Again, a direct measurement of the aerosol light extinction would be very useful to address this issue.

Aerosol vertical profiles were obtained with the Raymetrics Raman LiDAR for the whole of 2016. Mainly due to unsuitable meteorological conditions and staff unavailability, only 30% of the profiles scheduled by ACTRIS could be measured. Data have been successfully processed using the ACTRIS Single Calculus Chain and submitted to the ACTRIS/EARLINET data base for the first time in 2016.

The concentrations of the ions measured in rainwater were in 2016 generally ($Cl^-$, $NO_3^-$, $SO_4^{2-}$, $Na^+$,) lower than in 2015, except for $NH_4^+$ and $Ca^{2+}$. The annual wet deposition fluxes of the main acidifying and eutrophying species (1.4, 3.0, and 1.5 g $m^{-2}$ for $SO_4^{2-}$, $NO_3^-$, and $NH_4^+$, respectively) were similar to the fluxes observed during the previous years. In contrast, only 3 rain samples with pH<4.6 (i.e. 10 times more acidic than due to the equilibrium with atmospheric $CO_2$) were observed in 2016, compared to 18 in 2015 and 9 in 2014 and 2013.

Ground-level 2016' data listed by EMEP and ACTRIS as core variables have all been reported to EBAS by mid-2017, as requested by these programs. They can be freely downloaded from these data centres.

*Fig. 54: the* flux tower of 24 m at the Pinus pinea site in San Rossore

# 5. Atmosphere – Biosphere flux monitoring at the forest station of San Rossore

## 5.1 Location and site description

The measurement site 'San Rossore' (43°43.9205'N, 10°17.45817E, 4 m a.s.l.), operated by the Air and Climate Unit, is located in the Parco San Rossore (www.parcosanrossore.org), approximately 9 km west of Pisa and 1200 m east of the seashore in a Mediterranean forest ecosystem (see Fig. 54). The Climate Change and Air Quality Unit began to operate the predecessor site in the Parco San Rossore site in 1999; the present location is running since 2013.

The measurement site is situated in an almost flat area with a morphology characterized by the presence of sandy dunes. The vegetation in the direct vicinity is a pinewood established in 1921 following artificial seeding and it is dominated by the evergreen tree Pinus pinea with very sparse Quercus ilex. The average canopy height is approximately 19 m whereas the needles start at about 16.5 m. The understory vegetation is confined to the forest edges and canopy gaps and very sparse.

The area has a Mediterranean – type climate within the sub-humid zone, with a mean annual rainfall of 876 mm $yr^{-1}$ and a range of 534 – 1270 mm for the period 1980 – 2005. The long-term data were obtained from a meteorological station located at a distance of approximately 10 km and managed by the Regional Hydrological Service of Tuscany. Rain falls mainly during autumn and winter with about 50% occurring between September and November, while the driest months are July and August. The average annual temperature is approximately 14.2 °C with the average temperature of the coldest month (January) being 7 °C and that one of the warmest month (August) being 25 °C. The wind regime is characterised by a sea – land breeze circulation, i.e. the air flows quite predictable from the west (sea) during day and from east (land) during night.

The scientific activities were at that moment primarily embedded into the ICOS initiative. ICOS (Integrated Carbon Observation System, www.icos-ri.eu) is one of the pan-European research infrastructure projects identified by the European Strategy Forum on Research Infrastructures (ESFRI) for implementation. After its preparatory phase planned for 2008 until 2013 with an extension towards 2015, during which monitoring infrastructure and technical procedures are developed, its operational phase will run for 20 years from 2016 onwards.

*Table 6: ICOS class 2 Ecosystem Station core parameters.*

| Core variables continuous | Core variables daily to monthly | Core variables yearly |
|---|---|---|
| $CO_2$, $H_2O$ and energy fluxes | leaf area index | biomass (above ground) |
| wind speed and direction | | soil carbon |
| $CO_2$ concentration vertical profile, normal precision | | stem diameter |
| net radiation:<br>• incoming/reflected global radiation<br>• incoming/outgoing longwave radiation<br>• Albedo | | above-ground Net Primary Production (NPP) |
| diffuse global radiation | | litter fall |
| incoming / reflected under canopy Photosynthetic Active Radiation (PAR) | | land-use history |
| temperature and relative humidity vertical profile | | managements and natural disturbances |
| air pressure | | C and N import and export on managed sites |
| precipitation, through-fall, snow depth | | |
| soil heat flux | | |
| ground water level | | |
| soil temperature profile | | |
| water content profile | | |

*Table 7: ICOS variables measured continuously during 2016 in San Rossore*

| | |
|---|---|
| FLUXES | $CO_2$, latent heat, sensible heat |
| METEOROLOGY | 3D wind speed, temperature, relative humidity, pressure, precipitation |
| RADIATION | short & long wave incoming & outgoing, direct & diffuse photosynthetic active radiation |
| SOIL | temperature profile, water content profile, heat flux, water table height |

Once in operational mode, greenhouse gas concentrations and fluxes will be monitored on a routine basis following a very strict quality controlled protocol, both in terms of measurement instrumentations required to be used and procedures to be followed. The JRC plans to contribute with a class 2 Atmospheric Station (AS) for the high precision monitoring of greenhouse gas concentrations and a class 2 Ecosystem Stations (ES), the San Rossore forest flux tower, for the monitoring of ecosystem fluxes. Class 2 stations provide data for less parameter compared to class 1 stations and thus require less investment for instrumentation and have lower running costs in terms of instruments and staff. The mandatory variables to be monitored at the class 2 Ecosystem Station are shown in Table 6.

With regards to data reporting as in the previous years, quality checked data for 2016 have been submitted for the measurement site under the station name IT-SR2 to the Fluxnet database at the European Fluxes Database Cluster at [www.europe-fluxdata.eu](www.europe-fluxdata.eu).

## 5.2   Measurements in 2016

Despite being still in the upgrading phase of the measurement site to comply with ICOS class 2 requirements, the monitoring program at the new Pinus pinea site continued well. The main parameters measured are summarised in Table 7.

Fluxes of $CO_2$, $H_2O$ and sensible heat were measured with eddy covariance technique using EddyMeas (Olaf Kolle, www.bgc-jena.mpg.de) for data acquisition and evaluated with the EdiRe software package from the University of Edinburgh (www.geos.ed.ac.uk/abs/research/micromet). The ancillary parameters (meteorology, radiation and soil) were obtained with respective sensors and the data quality checked for instrument malfunctioning, obvious outliers and consistency. In the following chapters, first the instruments used are described and then daily averages of the different variables measured during the course of 2016 are presented.

## 5.3  Description of the instruments

### 5.3.1  Infrastructural

#### 5.3.1.1 Sensor location

The instruments for eddy covariance flux system, i.e. sonic anemometer and fast gas analyser, solar radiation and meteorological parameters are mounted on the top of the guided wire tower at a height of 24 m above ground, 5 m above the canopy top at 19 m.

Soil parameters are measured at an undisturbed soil plot approximately 20 m west of the tower.

A wooden hut complements the installation hosting IT and communication equipment, a UPS system and is also used for storage.

#### 5.3.1.2 Data acquisition

Eddy covariance flux data are stored with high frequency, i.e. 10 Hz, as chunks of 30 minutes on a local laptop connected to the sonic anemometer. Data from the sensors located on the tower top are read every 10 s and averaged and stored every 30 minutes by a CR3000 data logger from Campbell (www.campbellsci.co.uk) also installed on the tower top. Soil measurements are handled the very same way by a CR3000 installed on the ground.

For eddy covariance flux data, the start time of every 30 minutes measurement period is saved as the reference time, whereas for all other data, the end of the 30 minutes measuring period is used. The time reference used for all San Rossore measurements is has been changed in October 2015 to local solar time (UTC+1) to comply with ICOS requirements.

#### 5.3.1.3 Power supply, IT & communication infrastructure

The fixed line power supply of approx. 4 kW is locally backed up by an UPS system MSM 10 from Riello (www.riello-ups.de) to protect the system for transient power outages and provide an autonomous running time of approx. 19 hours for the installation. Computers and data loggers are connected via a local TCP/IP network. In addition, a cellular router TK704U from Welotec (www.welotec.com) provides internet access via the mobile 3G network. For safety reason at the remote site, a 3G repeater provides mobile phone coverage also on the forest ground in the vicinity of the site.

Measurement data is automatically transferred from San Rossore via ftp to a server (sanrosso@ftp-ccu.jrc.it) in Ispra at 6:00 local solar time. Remote connection to a computer at the site can be established as well.

### 5.3.2 Ecosystem fluxes

#### 5.3.2.1 Sonic Anemometer for 3D wind direction Gill HS-50

Sonic anemometers determine the three dimensional wind vectors at high frequency using the speed of sound. The Gill HS-50 (www.gill.co.uk) emits ultrasonic pulses between its pairs of transducers, measures the flight time of the pulses to the paired transducer and calculates the wind speed in the direction of the transducer pair (see Fig. 55). Combining the results from the three transducer pairs, the 3-dimensional wind speed is calculated at a frequency of 10 Hertz. After a rotation of the coordinate system during the data processing to align it with the north direction, horizontal and vertical wind speeds and the wind direction are calculated besides their use for flux calculations. As the speed of sound measured with the anemometer depends on the temperature, the so-called sonic temperature is reported by the instrument as well.

Due to the absence of moving parts and the fact that no calibration is required, the instrument is very robust and reliable. Instrument servicing is done at the manufacturer.
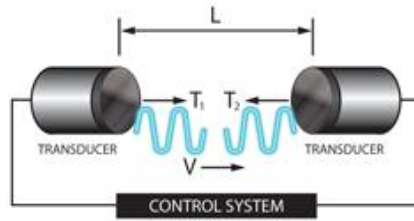
$$T_2 = \frac{L}{C - V} \qquad \text{and} \qquad T_1 = \frac{L}{C + V}$$

therefore

$$V = \frac{L}{2}\left\{\frac{1}{T_1} - \frac{1}{T_2}\right\} \qquad C = \frac{L}{2}\left\{\frac{1}{T_1} + \frac{1}{T_2}\right\}$$

*Fig. 55: Measurement principle of sonic anemometers, sketch from www.gill.co.uk*
*(T: travelling time of sound pulses, L: distance between transducers, C: speed of sound, V: wind speed in direction of transducers)*

### 5.3.2.2 Fast infrared gas analyser (IRGA) for CO$_2$ & H$_2$O concentration LI-7200 FM from Licor

For the determination of CO$_2$ and H$_2$O fluxes with the eddy covariance technique, fast analysers (10 to 20 Hertz) for concentration measurements of the gases of interest are obligatory. At the San Rossore forest flux tower, a LI-7200 FM system from LI-COR (www.licor.com) has been installed, consisting of the LI-7200 enclosed CO$_2$/ H$_2$O analyser, the LI-7550 analyser interface unit and the LI-7200-101 flow module.

The LI-7200 is a high performance, non-dispersive, enclosed open path infrared CO$_2$/H$_2$O analyser based on the infrared absorption of CO$_2$ and H$_2$O at ambient conditions that provides concentration measurements at a frequency of up to 20 Hertz. With the flow module, ambient air is drawn into to analyser through the sample inlet at a set flow rate of 15 l/min. In the sample volume of 16.09 cm$^3$ (see Fig. 56), light from the infrared source is absorbed at characteristic wavelengths for CO$_2$ and H$_2$O. This specific absorption is a function of the gas concentration in the sample volume. Using the absorption measurements at the CO$_2$ & H$_2$O wavelengths, at a non-absorbing wavelength plus calibration factors and measured temperature and pressure, the LI-7200 reports molar densities, mass densities or mole fraction of the two gases.

Zero and span checks and calibrations are done regularly using zero gas from a cylinder plus a dew point generator (RH CAL from EdgeTech) and a CO$_2$ standard from a cylinder.
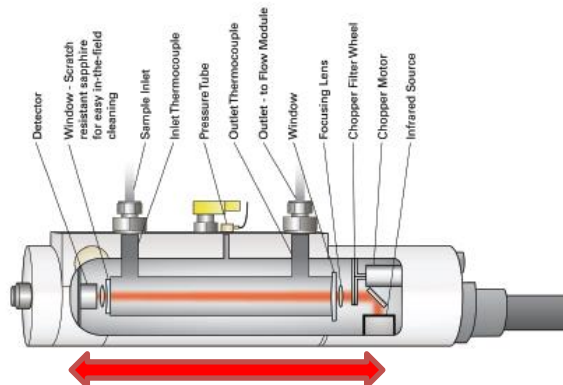


*Fig. 56: LI-7200 analyser head (from www.licor.com), arrow indicates sampling volume*

### 5.3.3 Radiation instruments

#### 5.3.3.1 Net radiometer Kipp & Zonen CNR4

The net radiometers CNR 4 from Kipp & Zonen ([www.kippzonen.com](www.kippzonen.com)) measures the energy balance between incoming and reflected radiation in the short (305 – 2800 nm) and long (5-50 µm) wavelength range to obtain the net radiation at the earth's surface. The short wavelength range is measured with two CM3 pyranometers, one facing upwards and one downwards. For the long range, two CG3 pyrgeometers facing opposite directions are used. The design of the instrument ensures a field of view of 180° upwards and downwards for the respective sensors. The CNR 4 features a blower and heating system to minimize the influence of dew and frost on the radiation measurements.

The energy $E_{short}$ of the short wave or so-called global (solar) radiation is calculated from the voltages provided by the CM3's using their sensitivity $C_{CM3}$: $E_{short} = V/C_{CM3}$. To calculate the energy $E_{long}$ of the long wave radiation from the reported voltages, besides the sensitivities of the CG3's $C_{CG3}$, also the sensor temperature $T$ measured with a PT-100 is needed: $E_{long} = V/C_{CG3} + 5.67 \cdot 10^{-8} \cdot T^4$. The net radiation over all wavelengths is then easily calculated by adding the respective energies: $E_{net} = E_{short}^{up} + E_{long}^{up} - E_{short}^{down} - E_{long}^{down}$. In addition, the Albedo of the earth's surface defined as the ratio of outgoing to incoming solar radiation can be obtained with the instrument as well: $Albedo = E_{short}^{downt}/E_{short}^{up}$.

Calibration and instrument checks at the factory are recommended every two years according to the manufacturer.

#### 5.3.3.2 Photosynthetic active radiation Delta-T BF5

With the Sunshine Sensor BF3 from Delta-T ([www.delta-t.co.uk](www.delta-t.co.uk)), total (in the sense of direct plus diffuse) solar radiation, diffuse radiation and the sunshine state is measured as photosynthetic active radiation (PAR) of the solar spectrum, i.e. from 400-700 nm. To distinguish between direct and diffuse radiation, a set of seven photodiodes (PD) is arranged under a patterned hemispherical dome with 50% black bands such that at any position of the sun in the sky at least one photodiode is completely in the shade and at least one is fully exposed to direct sunlight. This design eliminates the necessity of frequent alignment of the shading parts to the position of the sun. The diffuse radiation is then given by $PAR_{diffuse} = 2 \cdot PD_{min}$ and the direct radiation by $PAR_{direct} = PD_{max} - PD_{min}$

The instrument reports $PAR_{diffuse}$, $PAR_{total} = PAR_{diffuse} + PAR_{direct}$ and sunshine state. The latter one indicates sunshine if

$$PAR_{total}/PAR_{diffuse} > 1.25 \text{ and } PAR_{total} > 50 \, \mu mol \cdot m^{-2} \cdot s^{-1}.$$

### 5.3.4 Meteorological sensors

#### 5.3.4.1 Temperature & relative humidity UMS KPK1/5-ME

To measure ambient temperature and relative humidity, a combined sensor KPK1/5-ME from UMS ([www.ums-muc.de)](www.ums-muc.de) is installed into a passive radiation shield.

#### 5.3.4.2 Ambient air pressure Keller Druckmesstechnik PAA-41

Ambient air pressure is measured with a PAA-41 capacitive pressure sensor from Keller Druckmesstechnik (www.keller-druck.com) using a ceramic measurement cell for enhanced reliability.

#### 5.3.4.3 Rain sensor UMS ARG 100/std

The ARG 100/std from UMS ([www.ums-muc.de)](www.ums-muc.de) is a tipping bucket type of rain gauge. It features a collecting funnel with a surface area of 500 cm$^2$ and a resulting resolution of 0.2 mm of rain fall per tip.

### 5.3.5 Soil instruments

#### 5.3.5.1 Soil heat flux sensors HFP01 from Hukseflux

Three thermal sensors HFP01 from Hukseflux ([www.hukseflux.com](www.hukseflux.com)) have been buried ten centimetres underground in the undisturbed soil around the tower to obtain a good spatial averaging of the soil heat flux. The determination of the heat flux is based on measuring the temperature difference of two

sides of a plate that is exposed to a heat flow using a number of thermocouples connected in series (see Fig. 57) with the convention that positive values indicate a heat flux into the soil, a negative one heat flux out of the soil. Ignoring possible errors, the temperature difference between the hot and cold side of the sensor is proportional to the heat flow. As the thermocouples provide a voltage proportional to the temperature, the voltage output of the sensor is proportional to the heat flow across the sensor.
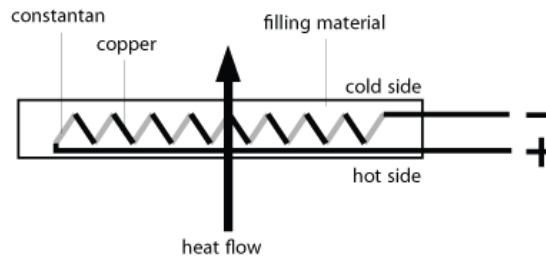


*Fig. 57: Sketch of a soil heat flux sensor (drawing from www.wikipedia.org)*

### 5.3.5.2 Soil water content vertical profile with TRIME-TDR from IMKO

Profile measurements of soil water content are performed using the TRIME-TDR (Time domain Reflectometry with Intelligent MicroElements with) from IMKO (www.imko.de). Based on Time-Domain-Reflectometry, the sensor generates high frequency electromagnetic pulses that propagate along a wave guide and reflected back into the sensor. Depending on the dielectric constant of the material surrounding the waveguide, the round trip time of the hf-pulses varies between some tens and thousand picoseconds. As the dielectric constant of soil and thus the round trip time strongly depends on the soil moisture content, measuring this time gives the water content of the soil surrounding the sensor. Burying several sensors at depths of 5, 30, 50, 100 cm below ground provides the soil humidity profile.

### 5.3.5.3 Soil temperature profile with Th3-v probe from UMS

For the measurement of soil temperatures at different depths, a Th3-v probe from UMS (www.ums-muc.de) is used. This probe features a convenient set of 6 temperature probes in a profile system buried at 5, 10, 20, 30, 50 and 100 cm below ground.

### 5.3.5.4 Ground water level CS456-SA from Campbell Scientific

The ground water level is monitored with a Diver from Campbell Scientific (www.campbellsci.co.uk). The device is placed in a water filled hole, 1.9 m below ground, and logs autonomously the pressure. Combining the measurement with the barometric pressure at the site gives the height of the water column above the sensor. Together with the known sensor depth below ground, the water table height can be easily calculated (see also Fig. 58):

$$WL = TOC - CL - WC \text{ with } WC = 9806.65 \cdot \frac{(p_{Diver} - p_{baro})}{\rho \cdot g};$$

$g = 9.81$ m/s$^2$, $\rho = 1.00$ kg/m$^3$
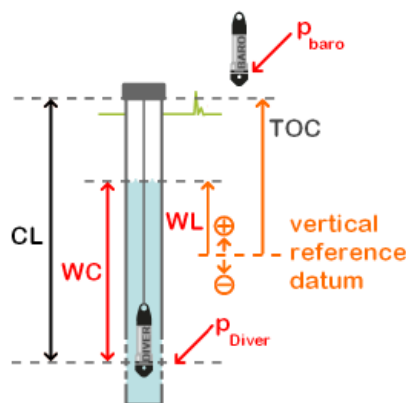


*Fig. 58: Principle of water level calculation using the Diver (sketch from www.swstechnology.com).*
*CL: cable length, TOC: top of container, WC: water column, WL: water level relative to a reference, p: pressure.*

*Table 8: Processing steps for flux calculations using the EdiRe Software package.*

| EdiRe Process | brief description |
|---|---|
| Preprocessed Files | data from input file, gas concentrations as molar densities |
| Extract | all high speed data |
| Despike | all high speed data |
| Linear | conversion of raw data from voltages into physical variables |
| 1 chn statistics | averages of 3D wind, sonic temperature and gas concentration |
| Gas conversion | conversion of molar densities to molar fraction |
| Filter – detrend | linear detrending of gas concentrations |
| Wind direction | align with geographic direction |
| Rotation coefficients | perform 3D coordinate rotation |
| Cross Correlate | gas concentrations with vertical wind speed |
| Remove Lag | remove time lag between anemometer and gas analyser |
| Friction Velocity | calculate u* |
| Sensible heat flux coefficient | |
| Latent heat of evaporation | |
| 2 chn statistics | calculate covariances, i.e. uncorrected fluxes |
| Sonic T - heat flux correction | |
| Stability – Monin Obhukov | calculate z/L stability parameter |
| Frequency response | calculate high frequency correction for all fluxes |
| Webb correction | calculate water density fluctuation correction for all fluxes |
| Stationarity | perform stationarity test |
| Integral Turbulence | calculate integral turbulence |
| Cospectra | calculate co-spectra for all fluxes |
| Storage | calculate storage term |
| User defined | determine quality flag (0,1,2) for all flux data according to Carboeurope methodology |

### 5.3.6    Flux data processing

Data evaluation for flux data is done using the free EdiRe software package developed at the micrometeorology group from the University of Edinburgh (www.geos.ed.ac.uk/abs/research/micromet/EdiRe/). As input data, EdiRe uses the 30 min raw flux data files in the binary *.slt format plus 30 minute averaged pressure, temperature and relative humidity data in ASCII format. As time convention, the start of the measurement period has to be assigned to the input data, the middle of the measurement period is assigned to the output data.

The main processing steps used within EdiRe to arrive at final, 30 minute averaged flux data that are corrected for various effects are listed in Table 8.

In order to obtain budgets from e.g. annual datasets that unavoidably contain gaps in the data, a gap filling procedure must be established to calculate the missing values based on drivers for the respective parameter. In addition, partitioning of the measured $CO_2$ flux (that is the Net Ecosystem Exchange, NEE), into Gross Primary Production (GPP, the gross carbon uptake) and respiration of the Ecosystem (Reco) enables a better understanding of the underlying ecosystem exchange processes. Gap-filling and partitioning of the data is done with the online tool at:

www.bgc-jena.mpg.de/bgi/index.php/Services/REddyProcWeb.
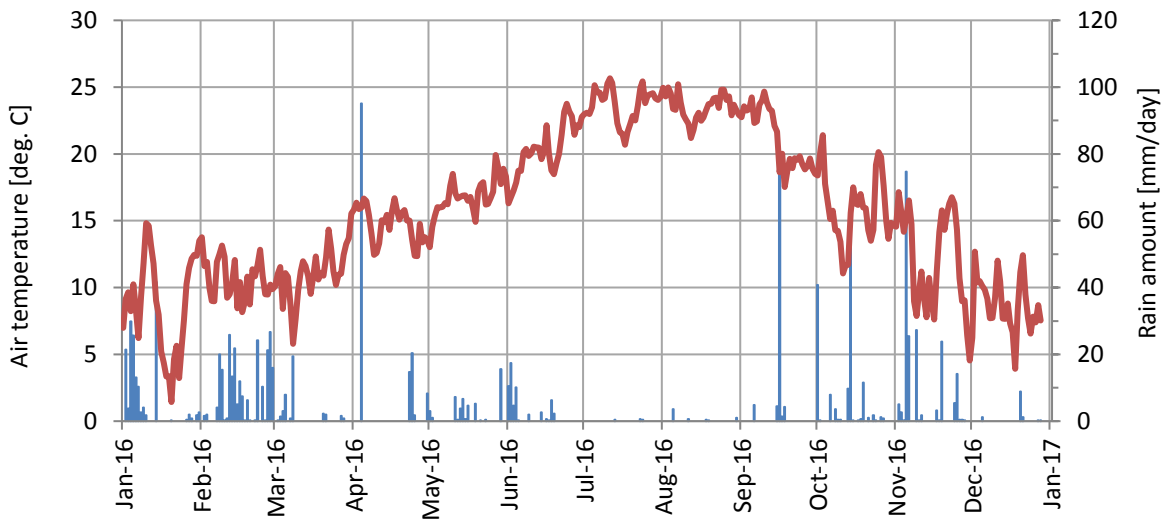
*Fig. 59: Daily averages of air temperature (left) and daily sum of precipitation (right) as measured in the Parco San Rossore.*
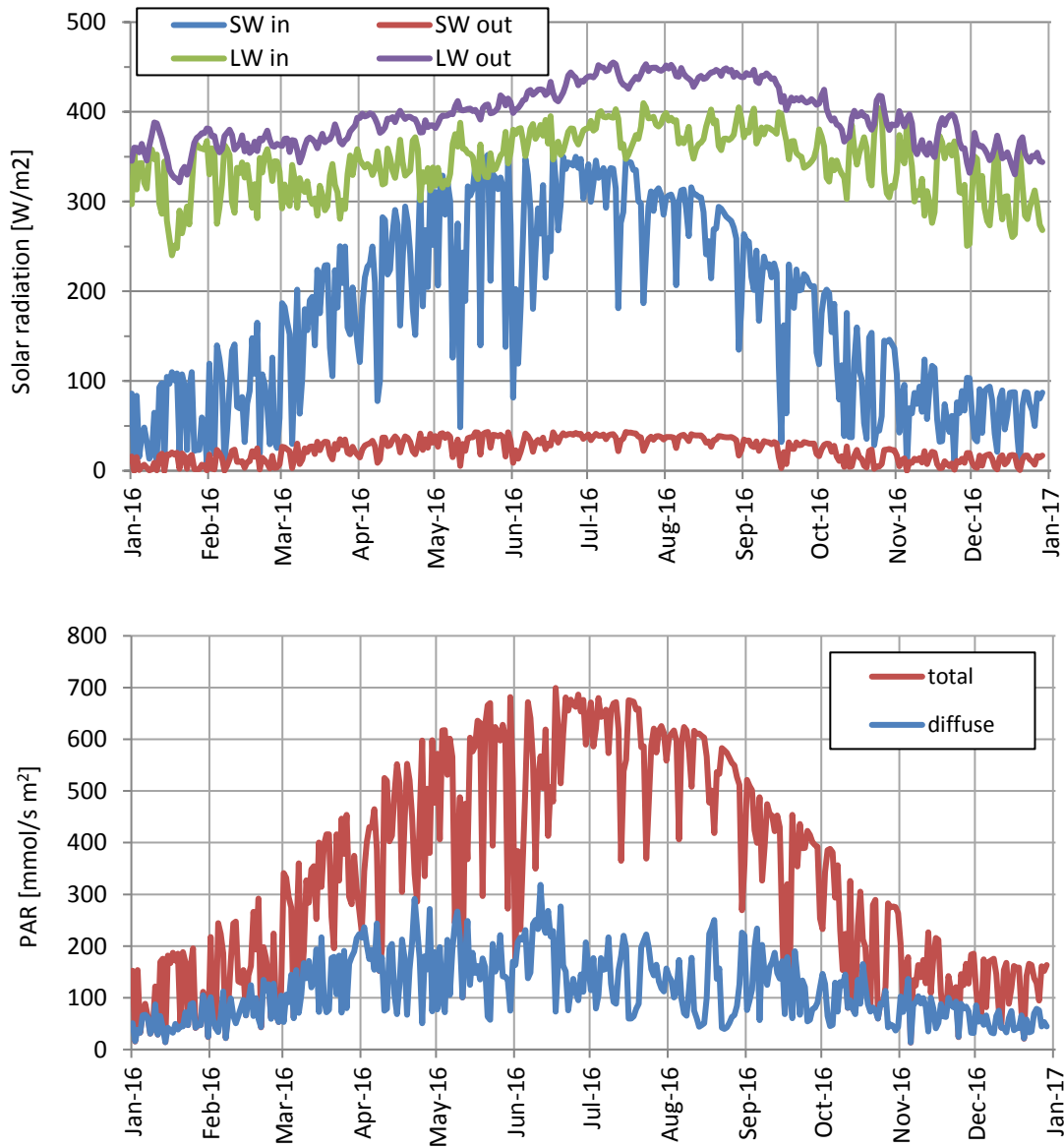




*Fig. 60: Daily averages of short wave incoming radiation (top) and incoming photosynthetic active radiation (bottom).*

## 5.4 Results of the year 2016

### 5.4.1 Meteorology

Daily averages for the annual cycle of air temperature and precipitation are shown in Fig. 59. The annual mean temperature for 2016 was 15.6° C (15.9° C for 2015), 1.4° C above the long term average of 14.2° C. With a total measured rainfall of 1123 mm (924 mm in 2015), 2016 was a slightly wetter year for San Rossore with a mean annual rainfall of 876 mm yr$^{-1}$. Also regarding rainfall pattern, 2016 was an average year with most precipitation in spring / autumn and a rather long, dry period during summer.

The predominant sea – land breeze wind circulation can be seen from the statistical evaluation of the 3D wind direction measurements and is shown in Fig. 61. The red plot shows the frequency distribution of the wind for winds speed > 0.5 m/s in terms of its origins; the blue line indicates the average wind speed per directional bin. The average annual wind speed was 1.6 m/s.
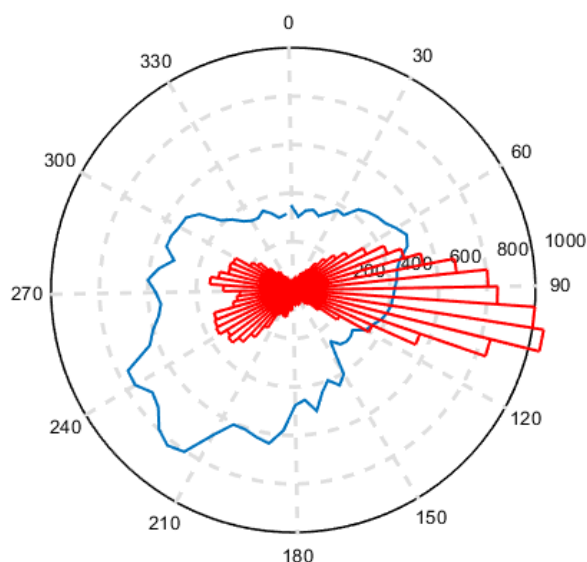


*Fig. 61: Wind rose for 30 min. averages of wind measurements with wind speed >0.5 m/s. Red: directions of the wind origin, blue: average wind speeds per direction interval in a.u.*

### 5.4.2 Radiation

In Fig. 60 , the annual cycle of short & long wavelength incoming & outgoing radiation are plotted as measured with the CNR 4 net radiometer above the forest canopy at 24 m.

The surface albedo, i.e. the ratio between SWout and SWin (305 – 2800 nm) averages to approximately 0.12 for the summer period and 0.14 for the winter period of the measurement. On the bottom part of Fig. 60, the photosynthetic active radiation (PAR) part of the solar spectrum (approx. 400 – 700 nm) is shown as total and diffuse incoming radiation.
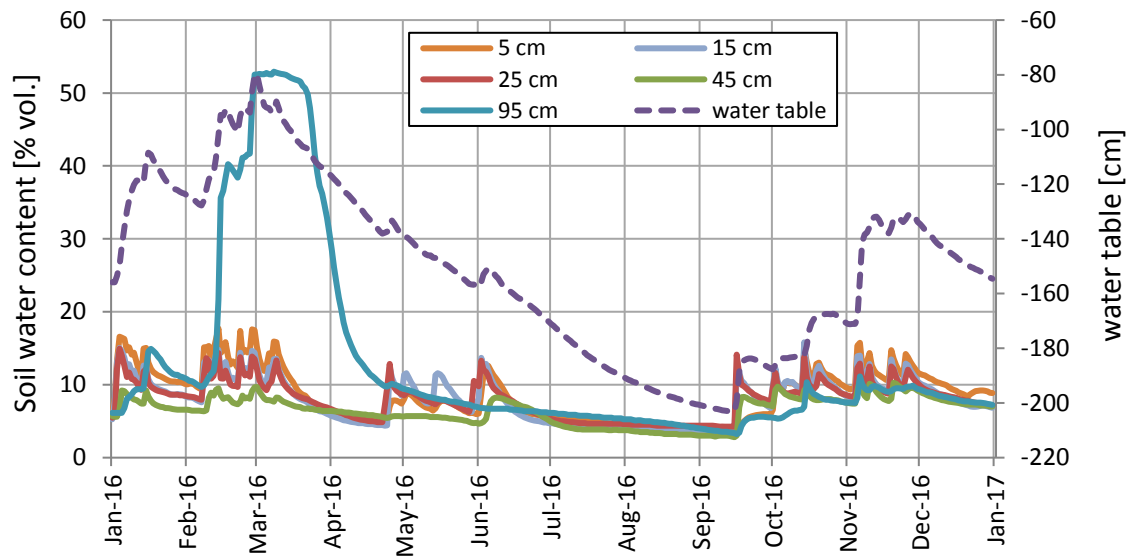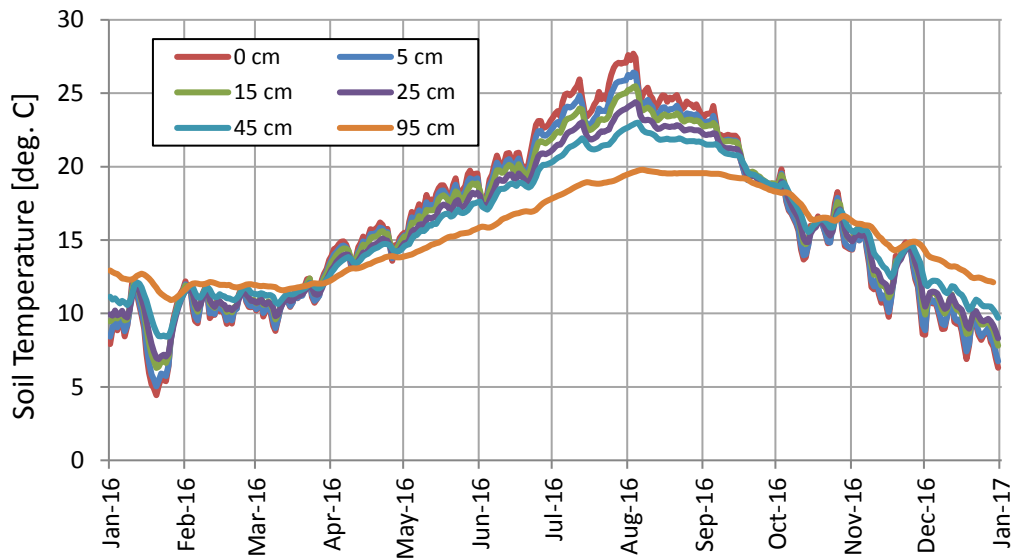
*Fig. 62: Profiles of soil temperature (top) and soil water content plus water table (bottom) measured as daily averages.*
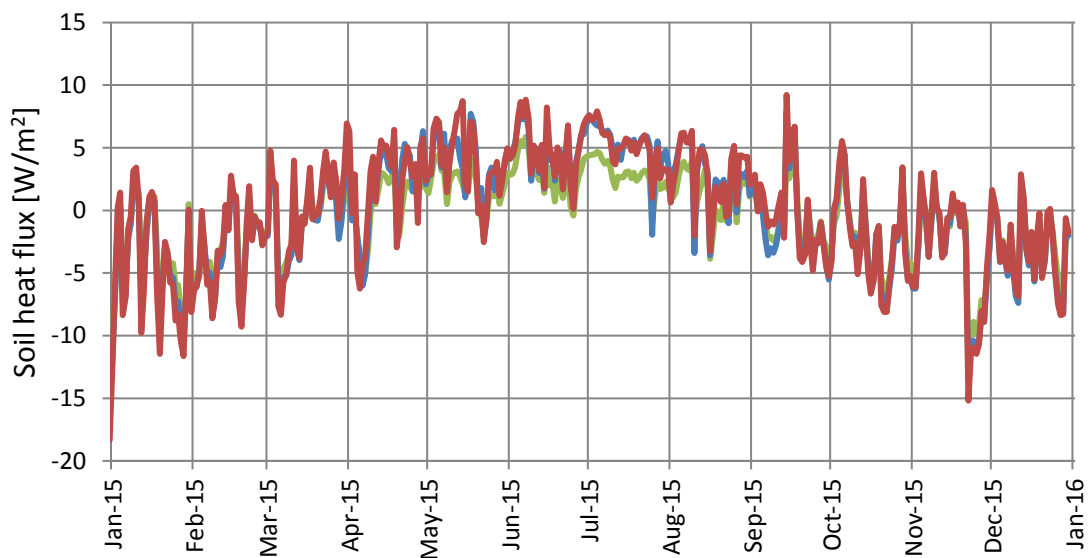


*Fig. 63: Soil heat fluxes measured with three identical sensors located some meters apart.*

### 5.4.3    Soil variables

The soil variables monitored in 2016 were the temperature at six different depths (0, 5, 15, 25, 45 and 95 cm) relative to the transition of the top organic layer and mineral soil at approx. 5 cm below surface, soil water content profile (5 cm, 15, 25, 45 and 95 cm), soil heat flux at 5 cm (using the convention that positive values indicate a heat flux into the soil, negative values out of the soil) plus water table depths measured with a well requiring a minimum water level of 260 cm below ground. The daily averages of these measurements are illustrated in Fig. 62 and Fig. 63.

### 5.4.4    Eddy covariance flux measurements

The daily averages of $CO_2$ and heat fluxes measured during 2016 are shown in Fig. 64 and Fig. 66, respectively. To obtain the eddy covariance flux data for the 30 minute measurement periods, the high frequency data from the LiCor 7200 infrared gas analyser for $CO_2$ and $H_2O$ have been evaluated together with the anemometer data using the EdiRe software package from the University of Edinburgh.

The Carboeurope quality classification for the flux data points for 2016 is used also for San Rossore. A value of 0 indicates strong turbulence and good stationarity, giving reliable EC flux values. A QF = 1 indicates acceptable quality and flux data with QF = 2 are unreliable and thus should not be used in further calculations. For the measurements at San Rossore, the distribution of quality flags for all flux data are given in Table 9, which shows that 62 – 78 % of the data depending on the flux type are usable for further data evaluation and interpretation.

*Table 9: Total number of flux data points and percentage of data points with quality flags according to the Carboeurope methodology (H: sensible heat, LE latent heat, FC $CO_2$ flux).*

|  | H [%] | LE [%] | FC [%] |
|---|---|---|---|
| **data points** | 17489 | 17489 | 17489 |
| **QF = 0** | 17 | 6 | 13 |
| **QF = 1** | 61 | 56 | 59 |
| **QF = 2** | 22 | 38 | 28 |
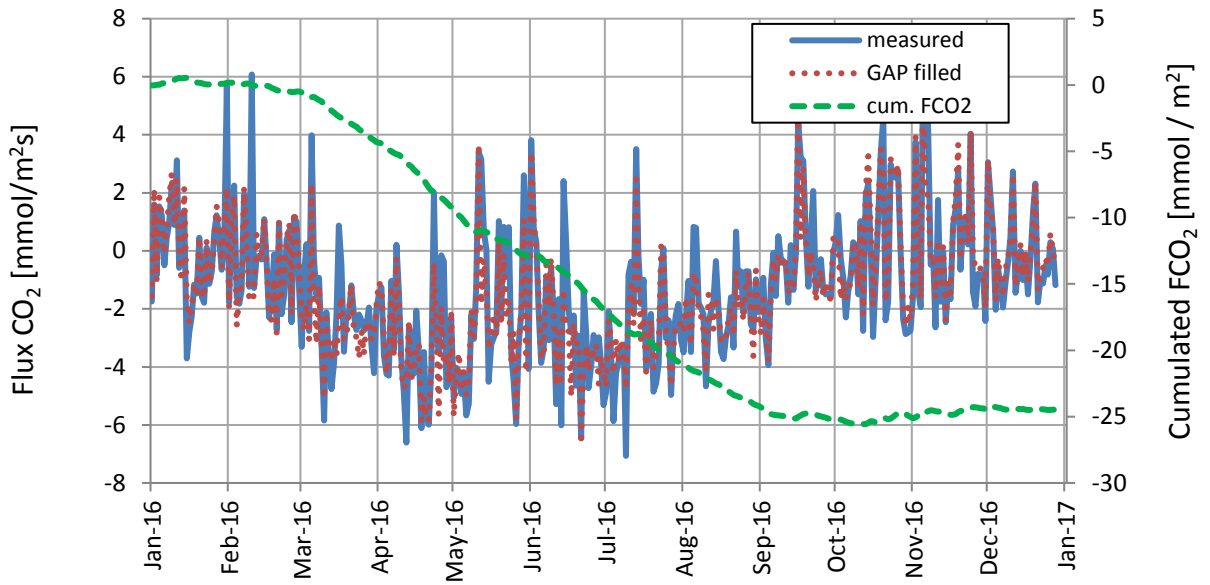
*Fig. 64: Daily averages of measured (blue), gap filled (red) and cumulated (green) $CO_2$ fluxes.*
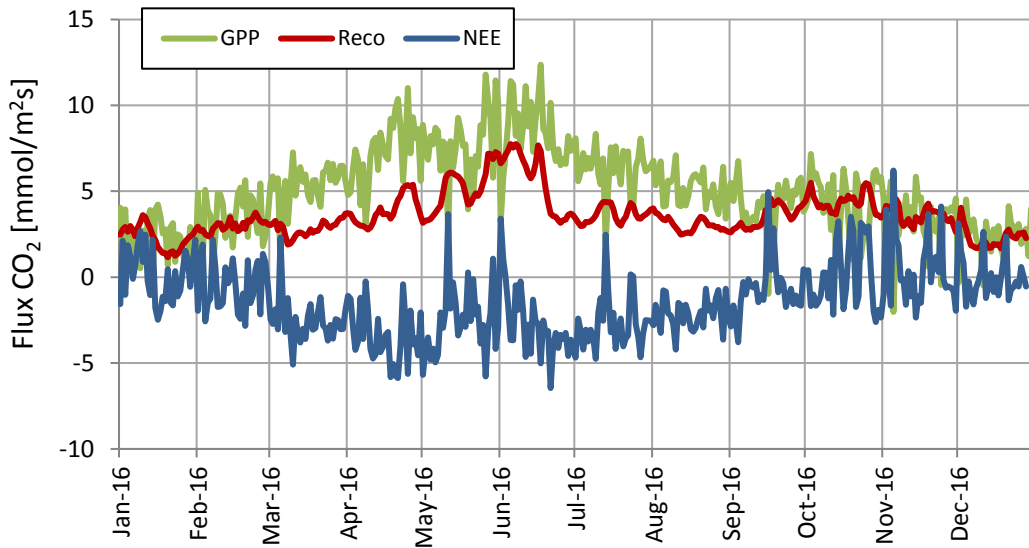


*Fig. 65*: Daily averages of NEE, GPP and Reco.
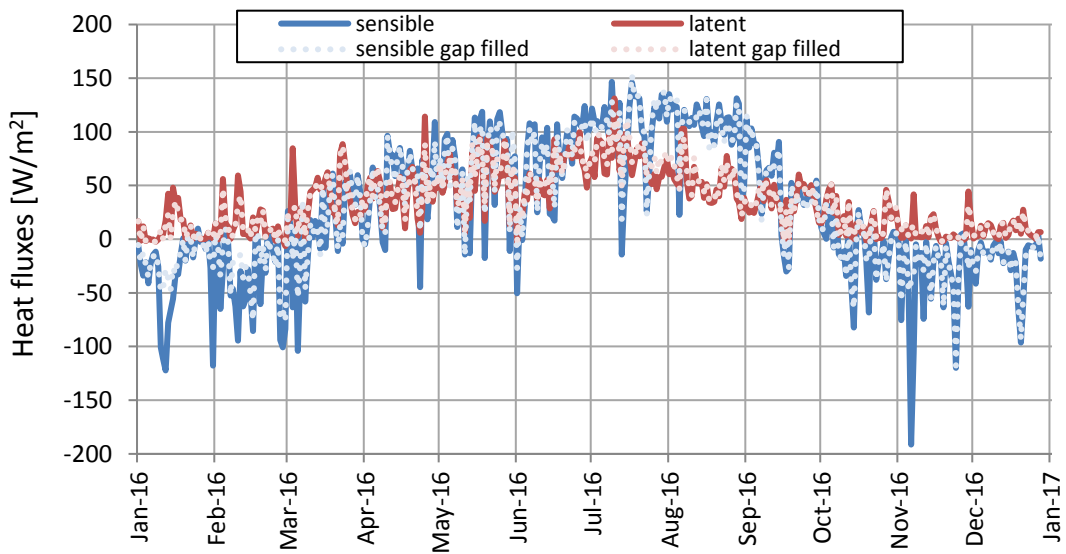


*Fig. 66: Daily averages of latent (red) and sensible (blue) heat fluxes.*

Gap filling of the dataset has been performed without filtering for friction velocities (u*) below a threshold (that would indicate how turbulent the wind is) using the 'Eddy covariance gap-filling & flux-partitioning tool' online available at: www.bgc-jena.mpg.de/~MDIwork/eddyproc/ for missing and quality class 2 data. The cumulated sum of the gap filled 30 min $CO_2$ fluxes is shown in Fig. 64. The plot shows that in 2016 the Pinus pinea stand is a clear sink for $CO_2$ from February until middle of September. Then ecosystem respiration and $CO_2$ uptake balance for the rest of the year. Using the flux partitioning module of the above mentioned online tool, the Net Ecosystem Exchange (NEE), i.e. the $CO_2$ flux measured, has been partitioned into Gross Primary Production (GPP) and Ecosystem Respiration (Reco) according to the equation: *NEE = Reco - GPP* and plotted as daily averages in Fig. 65. Calculating the budgets for 2016 (2015 in parenthesis), NEE sums up to -532 (-557) g C $m^{-2}$ $yr^{-1}$, GPP to -1898 (-1751) g C $m^{-2}$ $yr^{-1}$ and Reco to 1366 (1194) g C $m^{-2}$ $yr^{-1}$.

Comparing 2016 to 2015 it is noteworthy that NEE is very similar despite higher GPP which is then compensated by a higher Reco.

Fig. 66 shows the latent (red) and sensible (blue) heat fluxes for 2016 as daily averages. As it is typical for dryer ecosystems, the sensible heat flux especially in summer is higher than the latent heat flux.

# References

Adam, M., J. P. Putaud, S. Martins dos Santos, A. Dell'Acqua, and C. Gruening, Aerosol hygroscopicity at a regional background site (Ispra) in Northern Italy, Atmos. Chem. Phys., 12, 5703–5717, 2012

Anderson, T.L., and Ogren, J.A., Determining aerosol radiative properties using the TSI3563 integrating nephelometer, *Aerosol Sci. Technol.*, **29**, 57-69, 1998.

Arnott, W.P., Hamasha, K., Moosmüller, H., Sheridan, P.J., and Ogren, J.A., Towards aerosol light-absorption measurements with a 7-wavelength Aethalometer: Evaluation with a photoacoustic instrument and a 3 wavelength nephelometer, *Aerosol Sci. Technol.*, **39**, 17-29, 2005.

Bergamaschi P. and D. Brunner, Analysis of the sensitivity of atmospheric measurements at the JRC Ispra Atmosphere - Biosphere - Climate Integrated monitoring Station, Footprint analysis based on FLEXPART-COSMO model, JRC technical report, EUR 27131 EN, 2015.

Cavalli, F., Putaud, J.P., Toward a standardised thermal-optical protocol for measuring atmospheric organic and elemental carbon: the EUSAAR protocol, *Atmos. Meas. Tech.*, **3**, 79-89, 2010.

Cooke, W.F., Liousse, C., Cachier, H., and Feichter, J., Construction of a 1x1°fossil fuel emission data set for carbonaceous aerosol and implementation and radiative impact in the ECHAM4 model, *J Geophys. Res.*, **104**; 22,137-22, 1999.

Dlugokencky, E.J., P.M. Lang, J.W. Mund, A.M. Crotwell, M.J. Crotwell, and K.W. Thoning (2017), Atmospheric Carbon Dioxide Dry Air Mole Fractions from the NOAA ESRL Carbon Cycle Cooperative Global Air Sampling Network, 1968-2016, Version: 2017-07-28, Path: ftp://aftp.cmdl.noaa.gov/data/trace_gases/co2/flask/surface/

EMEP manual for sampling and chemical analysis (1995). *EMEP/CCC-Report 1/95. (Revised 1996; 2001; 2002).* 1995*.

European Directive 2008/50/EC. On ambient air quality and cleaner air for Europe. 2008.

Gruening C., et al., JRC Ispra EMEP-GAW regional station for atmospheric research: 2008 report, EUR 24088 EN, (2009), JRC55382.

Hess, M., Koepke, P. Schult, I., Optical Properties of Aerosols and Clouds: The Software Package OPAC, *Bull. of Am. Meteorol. Soc.*, **79**; 831-844, 1998.

Jensen, N. R., Gruening, C., Adams, M., Cavalli, F., Cavalli, P., Grassi, F., Dell'Acqua, A., Martins Dos Santos, S., Roux, D., Putaud, J.-P. JRC Ispra EMEP – GAW regional station for atmospheric research, 2009 report, *EUR 24678 EN*, (2010), *JRC62602*.

Kiehl, J. T., Schneider, T. L., Rasch, P. J., Barth, M. C., Wong, J., Radiative forcing due to sulfate aerosols from simulations with the National Center for Atmospheric Research Community Climate Model, Version 3 (Paper 1999JD900495), *J. Geophys. Res.,* **105**; 1441-1458, 2000.

McMurry, P., Wang, X., Park, K., and Ehara, K. The relationship between mass and mobility for atmospheric particles: A new technique for measuring particle density, *Aerosol Sci. Tech*., **36**, 227–238, 2002.

Mira-Salama, D., Van Dingenen, R., Gruening, C., Putaud, J.-P, Cavalli, F., Cavalli, P., Erdmann, N., Dell'Acqua, A., Dos Santos, S., Hjorth, J., Raes, F., Jensen, N.R. Using Föhn conditions to characterize urban and regional sources of particles, *Atmospheric Research* **90**, 159–16, 2008.

Mueller, T., *Development of correction factors for Aethalometers AE31 and AE33, ACTRIS-2 workshop*, Athens, 2015, http://wmo-gaw-wcc-aerosol-physics.org.

Pépin L., Schmidt M., Ramonet M., Worthy D.E.J. and Ciais, P. Notes des Activités Instrumentales, A new gas chromatographic experiment to analyze greenhouse gases in flask samples and in ambient air in the region of Saclay, Institut Pierre-Simon Laplace (2001), http://www.ipsl.jussieu.fr.

Petzold, A., H., Schönlinner, M., Multi-angle absorption photometry - A new method for the measurement of aerosol light absorption and atmospheric black carbon, *Journal of Aerosol Science*, **35** (4), 421-441, 2004.

Putaud, J.-P., et al. (21 authors), 2004, A European aerosol phenomenology—2: chemical characteristics of particulate matter at kerbside, urban, rural and background sites in Europe. *Atmospheric Environment*, **38**, 2579-2595.

Putaud, J.-P., et al. (39 authors), 2010, A European aerosol phenomenology—3: Physical and chemical characteristics of particulate matter from 60 rural, urban, and kerbside sites across Europe. *Atmospheric Environment*, **44**, 1308-1320.

Putaud, J.P., F. Cavalli, S. Martins dos Santos, and A. Dell'Acqua, Long-term trends in aerosol optical characteristics in the Po Valley, Italy, Atmos. Chem. Phys., 14, 9129–9136, 2014.

Putaud J.P., Bergamaschi P., Bressi M, Cavalli F., Cescatti A., Daou D., Dell'Acqua A., Douglas K., Duerr M., Fumagalli I., Goded I., Grassi F., Gruening C., Hjorth J., Jensen N.R., Lagler F., Manca G., Martins Dos Santos S., Matteucci M., Passarella R., Pedroni V., Pokorska O., Roux D. JRC – Ispra Atmosphere – Biosphere – Climate Integrated monitoring Station. 2013 report, JRC report EUR 26995 EN, 2014.

Putaud J.P., Bergamaschi P., Cavalli F., Dell'Acqua A., Douglas K., Duerr M., Fumagalli I., Goded I., Grassi F., Gruening C., Jensen N.R., Lagler F., Manca G., Martins Dos Santos S., Matteucci M., Passarella R., Pedroni V., Pokorska O., Roux D. JRC – Ispra Atmosphere – Biosphere – Climate Integrated monitoring Station. 2015 report, JRC report EUR 28153 EN, 2017.

Russell, L.M.: Aerosol organic-mass-to-organic carbon ratio measurements, *Environ. Sci. Technol.*, **37**, 2982-2987, 2003.

Schmid, O., et al., Spectral light absorption by ambient aerosols influenced by biomass burning in the Amazon Basin I: comparison and field calibration of absorption measurements techniques, *Atmos. Chem. Phys.*, **6**, 3443-3462, 2006.

Stratmann, F., Wiedensohler, A. A new data inversion algorithm for DMPS-measurements. *J. Aerosol Sci.*, **27** (Suppl 1), 339-340, 1996.

Thoning, K.W., P.P. Tans, and W.D. Komhyr, Atmospheric carbon dioxide at Mauna Loa Observatory, 2. Analysis of the NOAA/GMCC data, 1974-1985., J. Geophys. Res., 94, 8549-8565, 1989.

Van Dingenen, R., et al. (28 authors), 2004, A European aerosol phenomenology −1: Physical characterization of particulate matter at kerbside, urban, rural and background sites in Europe, *Atmospheric Environment*, **38**, 2561-2577.

Weingartner, E., Saathoff, H., Schnaiter, M., Streit, N., Bitnar, B., and Baltensperger, U., Absorption of light by soot particles: determination of the absorption coefficient by means of aethalometers, *J. Aerosol Sci.*, **34**, 1445-1463, 2003.

Weitkamp, C. (editor), LIDAR Range-Resolved Optical Remote Sensing of the Atmosphere, *Springer*, New York, 2005.

WHO, Health risks of ozone from long-range transboundary air pollution, 2008.

WMO Greenhouse gas bulletin, The State of Greenhouse Gases in the Atmosphere Based on Global Observations through 2016, https://library.wmo.int/opac/doc_num.php?explnum_id=4022, 2017.Worthy D. E. F., Levin,I., Trivett N. B. A., Kuhlmann A.J., Hopper J. F., and Ernst M. K. Seven years of continuous methane observations at a remote boreal site in Ontario, Canada, J. Geophys. Res., 103 (D13), 15995-16007, 1998.

Worthy, D. E. F., I. Levin, N. B. A. Trivett, A. J. Kuhlmann, J. F. Hopper, and M. K. Ernst, Seven years of continuos methane observations at a remote boreal site in Ontario, Canada, J. Geophys. Res., 103 (D13), 15995-16007, 1998.

Zahorowski, W., S. D. Chambers, A. Henderson-Sellers, Ground based radon-222 observations and their application to atmospheric studies, J. Environm. Radioact., 76, 3-33, 2004.

# Links

ACTRIS, *www.actris.eu*

ARPA Lombardia, *ita.arpalombardia.it/ITA/qaria/doc_RichiestaDati.asp*

Calipso, *www.nasa.gov/mission_pages/calipso/main*

Chemical Co-ordinating Centre of EMEP, *www.nilu.no/projects/ccc*

CLRTAP, *www.unece.org/env/lrtap/welcome.html*

EARLINET, *www.earlinet.org*

EMEP, *www.emep.int*

EPTR*,* European Pollutant Release & Transfer Register*,* prtr.ec.europa.eu/MapSearch.aspx

European Committee for Standardisation (CEN), *www.cen.eu/cen/pages/default.aspx*

EUSAAR, *www.eusaar.net*

Global Atmosphere Watch (GAW), *www.wmo.int/pages/prog/arep/gaw*

*ICOS, www.icos-ri.eu*

*InGOS, www.ingos-infrastructure.eu*

WDCA, *www.gaw-wdca.org*

World Meteorological Organization (WMO), *www.wmo.int/pages/index_en.html.*

# List of figures

# List of tables

## JRC Mission

As the science and knowledge service of the European Commission, the Joint Research Centre's mission is to support EU policies with independent evidence throughout the whole policy cycle.

**EU Science Hub**
ec.europa.eu/jrc

@EU_ScienceHub

EU Science Hub - Joint Research Centre

Joint Research Centre

EU Science Hub

Publications Office